https://doi.org/10.35662/unine-thesis-3063

Faculté des Sciences
Institut de mathématiques
Rue Emile-Argand 11, CH-2000 Neuchâtel

A study of the Hill three-body problem by modern symplectic geometry

Thèse

présentée à la Faculté des Sciences
pour l'obtention du grade de docteur ès Sciences en mathématiques

par

Cengiz Aydin

Acceptée sur proposition du jury :

Prof. Felix Schlenk	Université de Neuchâtel, CH	directeur de thèse, rapporteur
Prof. Urs Frauenfelder	Universität Augsburg, DE	directeur de thèse, rapporteur
Prof. Bruno Colbois	Université de Neuchâtel, CH	expert interne
JProf. Agustin Moreno	Universität Heidelberg, DE	rapporteur

Soutenue le 29 avril 2023

unine
Université de Neuchâtel
Faculté des sciences

Rue Emile-Argand 11
CH-2000 Neuchâtel
doctorat.sciences@unine.ch

IMPRIMATUR POUR THESE DE DOCTORAT

La Faculté des sciences de l'Université de Neuchâtel autorise l'impression de la présente thèse soutenue par

Monsieur Cengiz AYDIN

Titre :

"A study of the Hill three-body problem by modern symplectic geometry"

sur le rapport des membres du jury composé comme suit :

- Prof. Felix Schlenk, directeur de thèse, Université de Neuchâtel, Suisse
- Prof. Bruno Colbois, Université de Neuchâtel, Suisse
- Prof. Urs Frauenfelder, Universität Augsburg, Allemagne
- Prof. junior Agustin Moreno, Universität Heidelberg, Allemagne

Neuchâtel, le 12 juin 2023

Le Doyen, Prof. R. Bshary

To my father İbrahim Aydın

Abstract

The Hill three-body problem is a limiting case of the restricted three-body problem, which was first proposed by Hill in 1878. His motivation was to describe the motion of the Moon - the companion of the Earth - in the Sun–Earth–Moon system.

The fundamental families of planar periodic orbits are those of direct (family g) and retrograde periodic orbits (family f). Since the spatial system is invariant under a symplectic involution, whose fixed point set corresponds to the planar problem, planar orbits have planar and spatial Floquet multipliers, and planar and spatial Conley–Zehnder indices. In order to determine their indices we examine analytically the scenario about the bifurcation of the family g and f from the Kepler problem for very low energies. Moreover, the specification of the Floquet multipliers is given by the orbit's invariance under a certain anti-symplectic involution, which leaves the system invariant as well. Why are all these constructions fantastic tools?

Hill found numerically a planar direct periodic orbit with the period of one synodic month of our Moon, which is about 29.53 days. Being elliptic, we can therefore assign to it planar and spatial rotation angles. Together with the indices, they have deep astronomical significance, because on the one hand the anomalistic month of our Moon, which is about 27.55 days, corresponds to the planar rotation angle and planar Conley–Zehnder index. On the other hand the draconitic month of our Moon, which is about 27.21 days, corresponds to the spatial rotation angle and spatial Conley–Zehnder index. These lunar months date back to the Babylonians until around 500 BCE.

For higher energies, we explore the interaction between the Conley–Zehnder index and bifurcation points of such invariant planar as well as spatial periodic orbits. When the Floquet multipliers move through a root of unity, new families of periodic orbits bifurcate and the index jumps by integers. By the numerical continuations of the family g and f, we determine the index of various families of planar and spatial periodic orbits bifurcating from g and f. Since these families can bifurcate again and meet each other, this procedure can get complicated. This index leads to a grading on local Floer homology. Since the local Floer homology and its Euler characteristic stay invariant under bifurcation, the index provides important information about the interconnectedness of such families, which we illustrate in form of bifurcation graphs.

Since the solutions of Hill's system may serve as orbits for space mission design or astronomical observations, our results promote the interaction between symplectic geometry and applied problems.

Keywords: three-body problem, Hill's lunar problem, symplectic geometry, Babylonian lunar periods, bifurcation, Conley–Zehnder index, symmetry

Résumé

Le problème à trois corps de Hill est un cas limite du problème à trois corps restreint qui a été proposé pour la première fois par Hill en 1878. Sa motivation était de décrire le mouvement de la Lune - le compagnon de la Terre - dans le système Soleil-Terre-Lune.

Les familles fondamentales d'orbites périodiques planaires sont celles des orbites périodiques directes (famille g) et rétrogrades (famille f). Puisque le système spatial est invariant sous une involution symplectique, dont l'ensemble des points fixes correspond au problème planaire, les orbites planaires ont des multiplicateurs de Floquet planaires et spatiaux, et des indices de Conley–Zehnder planaires et spatiaux. Afin de déterminer leurs indices, nous examinons analytiquement le scénario de bifurcation de la famille g et f du problème de Kepler pour les très basses énergies. De plus, la spécification des multiplicateurs de Floquet est donnée par l'invariance de l'orbite sous une certaine involution anti-symplectique qui laisse le système invariant également. Pourquoi toutes ces constructions sont-elles des outils fantastiques?

Hill a trouvé numériquement une orbite périodique directe planaire ayant la période d'un mois synodique de notre Lune, soit environ 29,53 jours. Comme elle est elliptique, nous pouvons lui attribuer des angles de rotation planaires et spatiaux. Avec les indices, ils ont une profonde signification astronomique, car d'une part le mois anormal de notre Lune, qui est d'environ 27,55 jours, correspond à l'angle de rotation planaire et à l'indice planaire de Conley–Zehnder. D'autre part, le mois draconitique de notre Lune, qui est d'environ 27,21 jours, correspond à l'angle de rotation spatial et à l'indice spatial de Conley–Zehnder. Ces mois lunaires remontent aux Babyloniens jusqu'à environ 500 ans avant notre ère.

Pour des énergies plus élevées, nous explorons l'interaction entre l'indice de Conley–Zehnder et les points de bifurcation de ces orbites invariantes planaires et spatiales périodiques. Lorsque les multiplicateurs de Floquet passent par une racine de l'unité, de nouvelles familles d'orbites périodiques bifurquent et l'indice passe change par un entier. Par des extensions numériques de la famille g et f, nous déterminons l'indice de diverses familles d'orbites périodiques planaires et spatiales bifurquant à partir de g et f. Comme ces familles peuvent bifurquer à nouveau et se rencontrer, cette procédure peut s'avérer compliquée. Cet indice conduit à une gradation de l'homologie locale de Floer. Comme l'homologie locale de Floer et sa caractéristique d'Euler restent invariantes en cas de bifurcation, l'indice fournit des informations importantes sur l'interconnexion de ces familles, que nous illustrons sous la forme de graphes de bifurcation.

Comme les solutions du système de Hill peuvent servir d'orbites pour la conception de missions spatiales ou d'observations astronomiques, nos résultats favorisent l'interaction entre la géométrie symplectique et des problèmes appliqués.

Mots-clés: problème à trois corps, problème lunaire de Hill, géométrie symplectique, périodes lunaires babyloniennes, bifurcation, indice de Conley–Zehnder, symétrie

Acknowledgment

First and foremost, I would like to thank my supervisor Felix Schlenk for his support and his continuous interest in my work. He approaches almost everything in a very geometrical way and explains mathematical techniques by reducing the central idea to what he calls "*Mickey Mouse examples*". Thank you for our discussions, your valuable feedback, and for carefully reviewing my works and providing constructive criticism. Your expertise has greatly influenced my way of thinking and my personal style. Thank you once again, Felix.

Another person I also owe thank is Urs Frauenfelder for suggesting the basic ideas of this project and his continuous support. He was the supervisor at the Universität Augsburg of my Master's thesis, on which my studies on the Hill three-body problem are based. I distinctly remember: In summer 2018 in his office in Augsburg, he told me that the Floquet multipliers of Hill's orbit should correspond to the Babylonian lunar periods. Only at that time I did not know much about the Conley–Zehnder index, Rabinowitz action functional, bifurcation out of a Morse–Bott component, etc. This was the beginning of my deep theoretical and numerical journey in the Hill jungle. Many thanks again, Urs.

Many thanks to Bruno Colbois and Agustin Moreno for completing the jury of my thesis and for their precious time.

I also want to thank the mathematical community at the Université de Neuchâtel, in particular my academic siblings Joé Brendel, Joel Schmitz and Johannes Hauber.

I am also thankful to Vassilis S. Kalantonis and Alexander Batkhin for providing the initial data for the spatial periodic orbits they have found in the spatial Hill's system.

Finally, I am deeply grateful to my mother, my sister, my brother and my lovely wife Seda for their continuous support during my PhD, in particular during the difficult time after the sudden death of my father İbrahim Aydın on December 8, 2019. May God be merciful to him.

Contents

1 Introduction

"*Celestial mechanics is the origin of dynamical systems, linear algebra, topology, variational calculus and symplectic geometry.*"

- V. I. Arnold in [6, p. 1] (2000)

1.1 Astronomical lunar overview and Babylonian lunar periods

In astronomy, one distinguishes two kinds of periodic orbits, "*retrograde*" and "*direct*" ones. The Sun rotates about its own axis. The planets circle around the Sun in the same direction, and all of them rotate about their own axis in this direction, except Venus and Uranus, which rotate about their own axis in the other direction. Usually, moons, which are the companions of the planet, move around the planet in the way the planet circles around the Sun. Such a periodic orbit of the moon is called a direct periodic orbit, and in the other case is a retrograde one, see Figure 1.1. For instance, Neptune's moon "*Triton*" is retrograde. Our Moon is direct.

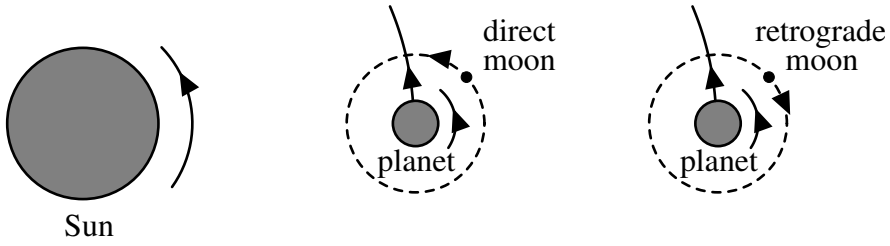

Figure 1.1: Direct and retrograde periodic orbit.

"*A most impressive achievement in Babylonian astronomy was the development of lunar theories that yielded very good results enabling the Babylonians to compute lunar eclipses with great success. Fundamental to these theories was the discovery of the periods for lunar motion (the sidereal, synodic, draconitic, and anomalistic months), and these periods had been accurately determined by about 500 B.C.*"

- B. R. Goldstein in [31, p. 1] (2002)

The **synodic month** is the period of the Moon's new moon phase. The Moon is new if the Sun and the Moon are in conjunction, relative to the line joining the Sun and the Earth, see Figure 1.2. The **lunarity** is defined as the average number of synodic months during a complete rotation of the Earth around the Sun.

The **sidereal month** of the Moon is a complete rotation around the Earth relative to fixed stars. In other words, the sidereal month is the time needed for a full rotation of the Earth–Moon vector, when viewed from the inertial frame provided by the fixed stars, see Figure 1.2. New moons occur when the Sun–Earth line (corresponding to the dashed lines in Figure 1.2) and the Earth–Moon vector are parallel. Since the Earth is also moving, one sidereal month is

not sufficient to yield one synodic month, hence the synodic month is longer than the sidereal month.

If the Moon is closer to the Earth, then its motion is faster, hence the speed of the Moon varies. The **anomalistic month** is the time the Moon takes from the closest point ("*perigee*") back to the closest point, or equivalently to return to the same speed.

The orbit of the Moon is inclined to the ecliptic by about 5°, and the **draconitic month** is the period from one intersection point with the ecliptic, called "*the nodes of the orbit*", back to itself. The line joining these two intersection points is known as "*the nodal line*". At one node the Moon moves from south of the ecliptic to north of it, i.e., the Moon crosses the ecliptic by going up. This node is called "the ascending node" and the other one, where the Moon crosses the ecliptic by going down, is called "*the descending node*". Therefore the draconitic month is the period for consecutive ascending (or descending) nodes.

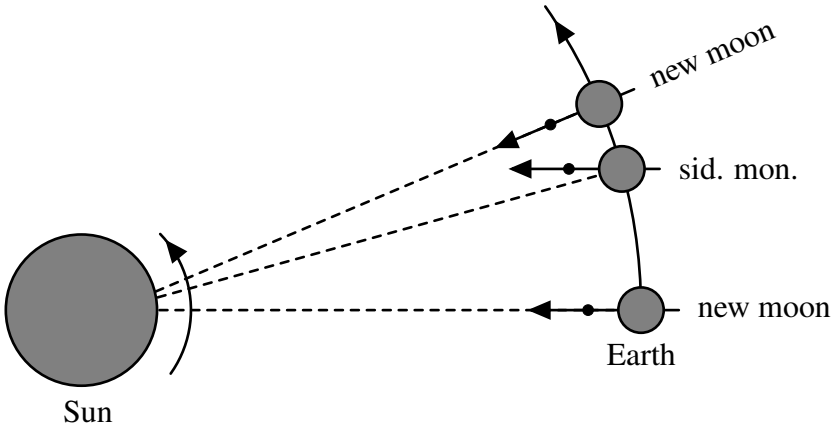

Figure 1.2: Synodic month vs. sidereal month.

The mean values of these periods were already known to the Babylonians around 500 BCE (see [31, p. 1]) and are also mentioned in Ptolemy's (c.100–c.175) Almagest (see [57]) which was one of the most influential works for scientists, in particular for those mentioned in the following quote from [46, p. xi]:

> "*Over the centuries, through the work of men such as Ptolemy, Ibn ash-Shāṭir, Copernicus, Tycho Brahe, Kepler, and Newton, models of the heavens came to reproduce the results of observations with greater and greater accuracy.*"

According to [52, pp. 310–311, p. 504], [55, p. 198] and [46, p. 58] the **Babylonian lunar periods** in the sexagesimal system are

1 syn. month	=	29;31,50,8,20 days
251 syn. months	=	269 anom. months
5458 syn. months	=	5923 drac. months
12;22,8 syn. months	=	1 Earth's sid. year
12 sid. months	=	5,27;51,20 days

and with the modern values from [45, p. 57, p. 30] and [54, p. 420] we deduce the Table 1.1.

	Babylonian value			modern value
1 syn. month	$29\frac{13753}{25920}$	$\approx$	29.530594 days	29.530589 days
1 anom. month	$27\frac{3866723}{6972480}$	$\approx$	27.554569 days	27.554551 days
1 drac. month	$27\frac{16290497}{76762080}$	$\approx$	27.212220 days	27.212220 days
1 sid. month	$27\frac{347}{1080}$	$\approx$	27.321296 days	27.321661 days
1 Earth's sid. year	$365\frac{1520039}{5832000}$	$\approx$	365.260637 days	365.25636 days
lunarity	$12\frac{83}{225}$	$\approx$	12.368888	12.368746

Table 1.1: Babylonian and modern values.

Notice that about 13.369081 (from Babylonian values) resp. 13.368746 (from modern values) sidereal months occur during one Earth's sidereal year, i.e., during one Earth's sidereal year the number of the Moon's sidereal months is one more than the number of synodic months.

1.2 Main results

1.2.1 Hill's orbit and Babylonian lunar periods

The Moon is a complex dynamical system. Indeed, it is attracted not only by the Earth but also with a comparable force by the Sun. To this complexity George William Hill (1838–1914) made a good first approximation to the Sun–Earth–Moon system in [38] (1878). His motivation was to describe the motion of the Moon. According to planetological data (see [53, pp. 52–53, 62]) we have Table 1.2.

	mass	mean distance to the Sun	mean distance to the Earth
Sun	1.989×10^{30} kg		
Earth	5.98×10^{24} kg	149.6×10^{6} km	
Moon	7.35×10^{22} kg		384000 km

Table 1.2: Planetological data.

We see that the mass of the Earth is about 0.0003% compared to the Sun and the one of the Moon is about 1.234% compared to the Earth. Moreover, the mean distance of the Moon to the Earth compared to the one between Earth and Sun is about 0.25668%. Given these extreme proportions, Hill's idea was to study a limit case which is a simplified model of the circular restricted three body problem.

In this limiting case the massless body is attracted by two primaries, one of which is infinitely much heavier than the second one. In Hill's original set-up the primaries are the Sun and the Earth. In rotating coordinates, one shifts the smaller primary to the origin and zooms in a region around it by pushing the huge primary off to infinity (see Figure 1.3).

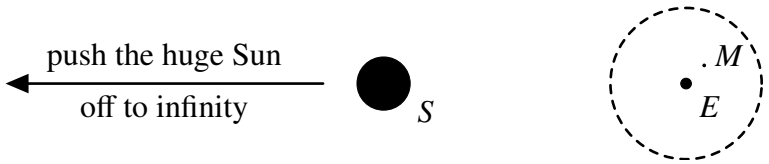

Figure 1.3: The Hill three-body problem, e.g., for the Sun–Earth–Moon system.

The goal is to understand the dynamics of the massless body, which is described by the Hamil-

tonian

$$H\colon T^*\big(\mathbb{R}^3 \setminus \{(0,0,0)\}\big) \to \mathbb{R}, \quad (q,p) \mapsto \underbrace{\frac{1}{2}|p|^2 - \frac{1}{|q|} + p_1q_2 - p_2q_1}_{\text{rotating Kepler problem}} - q_1^2 + \frac{1}{2}q_2^2 + \frac{1}{2}q_3^2, \quad (1.2.1)$$

consisting of the rotating Kepler problem (e.g., Earth–Moon) with a velocity independent gravitational perturbation produced by the massive body (e.g., Sun).

The synodic period. Hill's clever concept was that in his equation the true trajectory of the Moon must be close to a planar direct periodic orbit, which is centered at the Earth and has the correct period. This planar periodic orbit is called "*variational orbit*" or "*Hill's intermediate orbit*", i.e., perturbation theory to this orbit gives better and better approximations of the true orbit of the Moon, which is therefore almost periodic.

In Hill's work [38, p. 259] (1878) we read that he has found numerically in the ecliptic the variational orbit, denoted by q_{Hill}, of lunarity $12\frac{59}{160}$. By using its initial data for the traditional Jacobi integral $\Gamma = -2H = 6.50888$ and position $q_1(0) = 0.17610$, we plot the orbit in Figure 1.4 and calculate numerically the values

$$T_{q_{Hill}} = 0.507944, \quad \text{lunarity} = 12.369814, \quad T_s = 29.528039, \quad (1.2.2)$$

where $T_{q_{Hill}}$ is denoted for the first return time and T_s is denoted for the **synodic period**. Note that in view of the constellation in Hill's system, after the first return time we obtain the constellation for a synodic month. For the unit of time, 2π corresponds to a complete rotation of the Earth around the Sun. Therefore,

$$T_s = \frac{T_{q_{Hill}} \cdot 365.25636}{2\pi}.$$

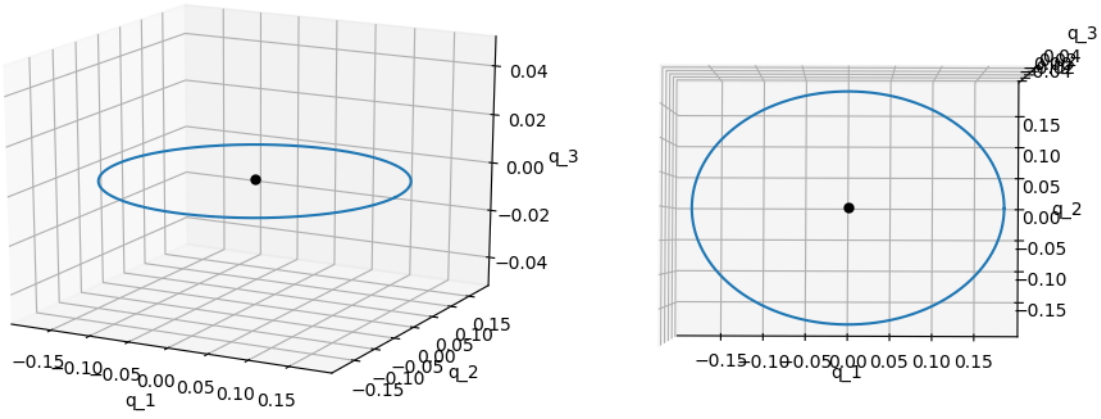

Figure 1.4: Hill's planar direct orbit q_{Hill} in the spatial system; left: from the side, right: from above.

The natural question to ponder is:

"*How can we relate Hill's orbit to the anomalistic and draconitic period?*"

Since Hill's planar direct periodic orbit obeys special symmetries in the spatial system, we study the symmetries next.

1.2.2 The linear symmetries

A **symmetry** ρ is, by definition, a symplectic or anti-symplectic involution of the phase space which leaves the Hamiltonian invariant, i.e.,

$$H \circ \rho = H, \quad \rho^2 = \mathrm{id}, \quad \rho^* \omega = \pm\omega.$$

Symmetries of the Hill three-body problem play an important role, since a natural class of periodic orbits are those that are invariant with respect to such involutions. In fact, linear symmetries are used traditionally for finding and studying invariant orbits; analytically by Birkhoff's "*shooting method*" [16] (1915) as well as numerically by Hill [38] (1878), by Hénon [34] (1969), [36] (1974) and by Michalodimitrakis [49] (1980).

The reflection at the ecliptic $\{q_3 = 0\}$ gives rise to the symplectic involution

$$\sigma\colon T^*\mathbb{R}^3 \to T^*\mathbb{R}^3, \quad (q_1, q_2, q_3, p_1, p_2, p_3) \mapsto (q_1, q_2, -q_3, p_1, p_2 - p_3) \tag{1.2.3}$$

which leaves the Hamiltonian (1.2.1) invariant. The planar system can be viewed as the restriction of this spatial problem to the fixed point set $\mathrm{Fix}(\sigma) = \{(q_1, q_2, 0, p_1, p_2, 0)\}$. Note that planar periodic orbits, such as Hill's orbit, are invariant under σ.

Other linear symplectic symmetries are $-\sigma$ and $\pm\mathrm{id}$, where $-\sigma$ corresponds to a rotation around the q_3-axis by π. Its fixed point set is $\mathrm{Fix}(-\sigma) = \{(0, 0, q_3, 0, 0, p_3)\}$, thus the q_3-axis is invariant under $-\sigma$. Four linear anti-symplectic symmetries are given in Table 1.3.

notation	underlying geometry
$\rho_1(q,p) = (q_1, -q_2, q_3, -p_1, p_2, -p_3)$	reflection at the q_1q_3-plane
$\rho_2(q,p) = (-q_1, q_2, q_3, p_1, -p_2, -p_3)$	reflection at the q_2q_3-plane
$\overline{\rho_1}(q,p) = (q_1, -q_2, -q_3, -p_1, p_2, p_3)$	rotation around the q_1-axis by π
$\overline{\rho_2}(q,p) = (-q_1, q_2, -q_3, p_1, -p_2, p_3)$	rotation around the q_2-axis by π

Table 1.3: Linear anti-symplectic symmetries.

These eight linear symmetries form a group, denoted by Σ_3, which provides already all linear symmetries.

Theorem 1.2.1. $\{\rho\colon T^*\mathbb{R}^3 \to T^*\mathbb{R}^3$ *linear* $\mid H\circ\rho = H$, $\rho^2 =$ *id and* $\rho^*\omega = \pm\omega\} = \Sigma_3$. *Moreover,* Σ_3 *is isomorphic to* $\mathbb{Z}_2 \times \mathbb{Z}_2 \times \mathbb{Z}_2$.

Since the maps $\sigma, \rho_1, \rho_2, \overline{\rho_1}$ and $\overline{\rho_2}$ leave $\mathrm{Fix}(\sigma)$ invariant, the two maps

$$\rho_1^p(q,p) := \rho_1|_{\mathrm{Fix}(\sigma)}(q,p) = \overline{\rho_1}|_{\mathrm{Fix}(\sigma)}(q,p) = (q_1, -q_2, 0, -p_1, p_2, 0)$$
$$\rho_2^p(q,p) := \rho_2|_{\mathrm{Fix}(\sigma)}(q,p) = \overline{\rho_2}|_{\mathrm{Fix}(\sigma)}(q,p) = (-q_1, q_2, 0, p_1, -p_2, 0)$$

are the two linear anti-symplectic involutions known from the planar problem. Their product is the symplectic symmetry $-\mathrm{id}$, and they correspond to the reflections about the q_1- resp. q_2-axes, i.e., it is not possible to say whether we are going to the Sun or away from it. Together with id, these four linear symmetries in the planar problem form a Klein four-group, i.e.,

$$\Sigma_2 := \langle \rho_1^p, \rho_2^p \mid (\rho_1^p)^2 = (\rho_2^p)^2 = (\rho_1^p \circ \rho_2^p)^2 = \mathrm{id}\rangle \cong \mathbb{Z}_2 \times \mathbb{Z}_2.$$

For the planar problem, these symmetries are already all linear symmetries.

Theorem 1.2.2. $\{\rho\colon T^*\mathbb{R}^3 \to T^*\mathbb{R}^3$ *linear* $\mid H|_{Fix(\sigma)}\circ\rho = H|_{Fix(\sigma)}$, $\rho^2 =$ *id and* $\rho^*\omega = \pm\omega\} = \Sigma_2$.

A remarkable property of the Hill three-body problem is that the spatial linear symmetries determine already the planar linear symmetries. To see this, consider the projection map given by the restriction to $\mathrm{Fix}(\sigma)$,

$$\pi\colon \Sigma_3 \to \Sigma_2, \quad \rho \mapsto \rho|_{\mathrm{Fix}(\sigma)}.$$

If $\rho \in \Sigma_3$ is symplectic or anti-symplectic, then $\rho|_{\mathrm{Fix}(\sigma)}$ is a linear symplectic or anti-symplectic involution on $\mathrm{Fix}(\sigma)$ as well, respectively. Moreover, $\rho|_{\mathrm{Fix}(\sigma)}$ leaves $H|_{\mathrm{Fix}(\sigma)}$ invariant. Therefore the map π is well-defined. While the map π is not injective (since $\pi(\rho_1) = \pi(\overline{\rho_1})$), it is surjective. To see that, let $\rho \in \Sigma_2$. If ρ is symplectic, then a symplectic extension is given by $q_3 \mapsto q_3$ and $p_3 \mapsto p_3$. If ρ is anti-symplectic, then an anti-symplectic extension is given by $q_3 \mapsto -q_3$ and $p_3 \mapsto p_3$. Theorem 1.2.2 thus follows from Theorem 1.2.1.

Remark 1.2.1. Hill's orbit is invariant under ρ_1 and ρ_2, i.e., it is invariant under the reflections about the q_1- and q_2-axis.

1.2.3 Symplectic splitting for planar periodic orbits

Let $q = (q, p) \in \mathrm{Fix}(\sigma)$ be a planar periodic orbit with $q_0 = \big(q(0), p(0)\big)$ and first return time T_q. Consider the time T_q map of the linearized Hamiltonian flow, which is a 6×6 symplectic matrix and called **monodromy**. Since q is invariant under σ, the Hamiltonian vector field X_H is invariant under σ as well, i.e., $\sigma^* X_H = X_H$. In other words, the differential of σ induces a symplectic involution commuting with the flow, i.e.,

$$d\sigma(q_0) \circ d\varphi_H^{T_q}(q_0) \circ d\sigma(q_0) = d\varphi_H^{T_q}(q_0). \tag{1.2.4}$$

Therefore the monodromy leaves the eigenspaces $T_{q_0}\mathrm{Fix}(\sigma)$ and $E_{-1}\big(d\sigma(q_0)\big)$ invariant. The first space is formed by 4-dimensional planar coordinates and the latter by 2-dimensional spatial coordinates. In particular, since these two eigenspaces are symplectically orthogonal, each of them is a symplectic vector space and the monodromy admits a symplectic decomposition

$$d\varphi_H^{T_q}(q_0)\colon T_{q_0}\mathrm{Fix}(\sigma) \oplus E_{-1}\big(d\sigma(q_0)\big) \to T_{q_0}\mathrm{Fix}(\sigma) \oplus E_{-1}\big(d\sigma(q_0)\big),$$

$$d\varphi_H^{T_q}(q_0) = \begin{pmatrix} A_p & 0 \\ 0 & A_s \end{pmatrix}, \quad A_p \in \mathrm{Sp}(2), \quad A_s \in \mathrm{Sp}(1) = \mathrm{SL}(2,\mathbb{R}),$$

where A_p is the monodromy of q viewed in the planar problem and A_s is a 2×2 symplectic matrix which arises by linearization only along the spatial components. The restriction to the 5-dimensional energy hypersurface Σ induces on the quotient by the line bundle $\ker\omega|_\Sigma = \langle X_H|_\Sigma\rangle \subset T\Sigma$ the **reduced monodromy**, whose eigenvalues are called **Floquet multipliers**. In view of the symplectic splitting of the induced 4-dimensional symplectic vector space into

$$T_{q_0}\Sigma/\ker\omega_{q_0} = \big(T_{q_0}\mathrm{Fix}(\sigma|_\Sigma)/\ker\omega_{q_0}\big) \oplus \Big(E_{-1}\big(d\sigma(q_0)\big)\Big),$$

the reduced monodromy is of the form

$$\overline{d\varphi_H^{T_q}|_\Sigma(q_0)} = \begin{pmatrix} \overline{A}_p & 0 \\ 0 & A_s \end{pmatrix}, \quad \overline{A}_p, A_s \in \mathrm{Sp}(1) = \mathrm{SL}(2,\mathbb{R}), \tag{1.2.5}$$

where $\overline{A}_p$ is the reduced monodromy of q viewed in the planar problem. Note that $\overline{A}_p$ and A_s are linear orientation area-preserving transformations of $\mathbb{R}^2$. In particular, we obtain the following two important properties.

i) The **Floquet multipliers** are determined by those of $\overline{A}_p$ and A_s, which are real or lie on the unit circle. Consequently, it is not possible that the Floquet multipliers are given by four different complex numbers of the form $\lambda, 1/\lambda, \overline{\lambda}$ and $1/\overline{\lambda}$.
ii) The transversal **Conley–Zehnder index** of q splits additively $\mu_{CZ} = \mu^p_{CZ} + \mu^s_{CZ}$, where μ^p_{CZ} and μ^s_{CZ} are the Conley–Zehnder indices of the path of symplectic matrices generated by the planar and spatial part of the linearized Hamiltonian flow, respectively. Roughly speaking, this index is a kind of a mean winding number for the linearized flow.

Geometrical interpretation in the elliptic case. Let us consider the case that the planar periodic orbit q is planar and spatial elliptic, which means that $|\mathrm{tr}(\overline{A}_p)| < 2$ and $|\mathrm{tr}(A_s)| < 2$. Then the Floquet multipliers are of the form $e^{\pm \mathrm{i}\theta_p}$ and $e^{\pm \mathrm{i}\theta_s}$, and each of $\overline{A}_p$ and A_s is conjugate to a rotation in $\mathbb{R}^2$ (see (1.2.7)). Consider each rotation function $\theta_p(t)$ and $\theta_s(t)$, starting at $\theta_p(0) = \theta_s(0) = 0$ and giving continuously each rotation angle at each time $t \in [0, T_q]$. The index measures the number of times that an eigenvalue crosses 1 during the first return time T_q, which is called **rotation number** and denoted by $\mathrm{rot}^p(q)$ and $\mathrm{rot}^s(q)$. Their relations are given by

$$\mu^p_{CZ} = 1 + 2 \cdot \mathrm{rot}^p(q) = 1 + 2 \cdot \lfloor \theta_p(T_q)/(2\pi) \rfloor, \quad \mu^s_{CZ} = 1 + 2 \cdot \mathrm{rot}^s(q) = 1 + 2 \cdot \lfloor \theta_s(T_q)/(2\pi) \rfloor,$$

i.e., for every complete rotation the index jumps by 2 and is odd. We define each **rotation angle** by

$$\varphi_p \equiv \theta_p(T_q) \bmod 2\pi, \quad \varphi_s \equiv \theta_p(T_q) \bmod 2\pi \tag{1.2.6}$$

and obtain

$$\overline{d\varphi_H^{T_q}|_\Sigma(q_0)} = \begin{pmatrix} \overline{A}_p & 0 \\ 0 & A_s \end{pmatrix} \sim \begin{pmatrix} \cos\varphi_p & -\sin\varphi_p & 0 & 0 \\ \sin\varphi_p & \cos\varphi_p & 0 & 0 \\ 0 & 0 & \cos\varphi_s & -\sin\varphi_s \\ 0 & 0 & \sin\varphi_s & \cos\varphi_s \end{pmatrix}. \tag{1.2.7}$$

Since the calculation of each Floquet multipliers yields two angles $\pm\theta_p$ and $\pm\theta_s$, it is not obvious which of them determines each rotation angle. Hence, **there are two fundamental questions:**

i) *How can we determine the index and thereby the rotation number?*
ii) *How can we decide if φ_p corresponds to θ_p or $-\theta_p$, resp. if φ_s corresponds to θ_s or $-\theta_s$?*

1.2.4 The Conley–Zehnder index for family g and f for very low energies

In order to determine the indices, one studies the birth of families of orbits, i.e., where and how do the families of orbits dynamically arise? One source of known periodic orbits in the Hill three-body problem is the rotating Kepler problem. For very low energies, one approaches the rotating Kepler problem which after regularization becomes the geodesic flow. For all sufficiently small energies up until an undetermined $\varepsilon_0 > 0$, we are able to prove analytically the following two theorems.

Theorem 1.2.3 (Planar problem). *From the circular direct and retrograde periodic orbit in the Kepler problem one family of periodic orbits bifurcates in each case, which are referred to as direct periodic orbits (family g) and retrograde periodic orbits (family f), respectively. These two orbits exist for all sufficiently low energies $\varepsilon \in (0, \varepsilon_0]$, and*

$$\mu^p_{CZ} = \begin{cases} 3 & \text{for family } g \\ 1 & \text{for family } f. \end{cases} \tag{1.2.8}$$

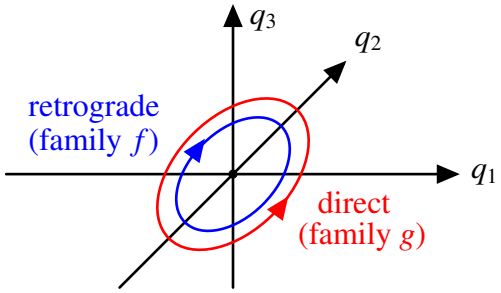

Figure 1.5: Direct and retrograde periodic orbits for very low energies.

The fundamental families of planar periodic orbits around the smaller primary located at the origin are those of direct and retrograde periodic orbits, which since the work of Elis Strömgren and his associates in the Copenhagen Observatory are traditionally called family g resp. f (see the Copenhagen category in [56, Chapter 9.4]). For low energy values, these two families begin with infinitesimal circular direct resp. retrograde periodic orbits, see Figure 1.5.

Theorem 1.2.4 (Spatial problem). *The planar families g and f, and two families of spatial collision periodic orbits bifurcate from the Kepler problem. These four orbits exist for all sufficiently low energies $\varepsilon \in (0, \varepsilon_0]$, and*

$$\mu_{CZ} = \begin{cases} 6 & \text{for family } g \text{ (planar)} \\ 4 & \text{for the one family of collision orbits bouncing back (spatial)} \\ 4 & \text{for the other family of collision orbits bouncing back (spatial)} \\ 2 & \text{for family } f \text{ (planar).} \end{cases} \tag{1.2.9}$$

Moreover, in view of $\mu_{CZ} = \mu^p_{CZ} + \mu^s_{CZ}$, by (1.2.8) and (1.2.9),

	family g (planar)	*family f (planar)*
$\mu_{CZ} / \mu^p_{CZ} / \mu^s_{CZ}$	6 / 3 / 3	2 / 1 / 1

Therefore,

$$\mathrm{rot}^p(q) = \mathrm{rot}^s(q) = \begin{cases} 1 & \text{for family } g \\ 0 & \text{for family } f. \end{cases} \tag{1.2.10}$$

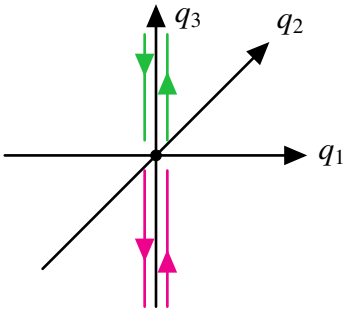

Figure 1.6: Spatial collision periodic orbits for very low energies.

The two families of spatial collision periodic orbits from Theorem 1.2.4 are illustrated in Figure 1.6. One collides with the origin from above (the green one) and the second one from below (the purple one). Note that these two families are in $\mathrm{Fix}(-\sigma) = \{(0, 0, q_3, 0, 0, p_3)\}$ and their orbits are known as "*polar orbits*" (see for instance [14]).

1.2.5 Symmetry specifies the Floquet multipliers

For this, the invariance under an anti-symplectic involution plays a key role. Let us consider a planar periodic orbit q which is invariant, e.g., under ρ_1. Contrary to (1.2.4), the Hamiltonian vector field X_H is anti-invariant under ρ_1, which means that

$$d\rho_1(q_0) \circ d\varphi_H^{T_q}(q_0) \circ d\rho_1(q_0) = \left(d\varphi_H^{T_q}(q_0)\right)^{-1}. \tag{1.2.11}$$

If we choose a symplectic basis, called **Lagrangian basis**, with respect to the Lagrangian splitting

$$T_{q_0}\mathrm{Fix}(\rho_1) \oplus E_{-1}\left(d\rho_1\,(q_0)\right),$$

meaning that the two eigenspaces are Lagrangian submanifolds, then the differential $d\rho_1\,(q_0)$ is represented by the standard anti-symplectic involution $\begin{pmatrix} I_3 & 0 \\ 0 & -I_3 \end{pmatrix}$. Since ρ_1 commutes with σ, in view of the symplectic splitting (1.2.5) and by using the identity (1.2.11), the reduced monodromy is of the form

$$\overline{d\varphi_H^{T_q}|_\Sigma(q_0)} = \begin{pmatrix} \overline{A}_p & 0 \\ 0 & A_s \end{pmatrix} = \begin{pmatrix} a & b & 0 & 0 \\ c & a & 0 & 0 \\ 0 & 0 & \tilde{a} & \tilde{b} \\ 0 & 0 & \tilde{c} & \tilde{a} \end{pmatrix}, \quad a^2 - bc = \tilde{a}^2 - \tilde{b}\tilde{c} = 1.$$

For each matrix, a change of basis, corresponding to a scaling on the Lagrangian, is given by the action

$$\begin{pmatrix} k & 0 \\ 0 & \frac{1}{k} \end{pmatrix} \begin{pmatrix} a & b \\ c & a \end{pmatrix} \begin{pmatrix} \frac{1}{k} & 0 \\ 0 & k \end{pmatrix} = \begin{pmatrix} a & k^2 b \\ \frac{1}{k^2} c & a \end{pmatrix}, \quad k \in \mathbb{R}^* = \mathrm{GL}(1, \mathbb{R}). \tag{1.2.12}$$

We immediately see that each trace and the **signatures of $b, c, \tilde{b}$ and $\tilde{c}$ are invariant** under a change of basis. Hence in the elliptic case, in view of (1.2.6) and (1.2.7), we have

$$\varphi_p = \begin{cases} \theta_p \in (0, \pi) & \text{if } b < 0 \\ 2\pi - \theta_p \in (\pi, 2\pi) & \text{if } b > 0, \end{cases} \qquad \varphi_s = \begin{cases} \theta_s \in (0, \pi) & \text{if } \tilde{b} < 0 \\ 2\pi - \theta_s \in (\pi, 2\pi) & \text{if } \tilde{b} > 0. \end{cases}$$

1.2.6 Back to Hill's orbit and Babylonian lunar periods

For elliptic planar periodic orbits, we define each of the

- **anomalistic**, denoted by T_a, and
- **draconitic period**, denoted by T_d,

as the **period for each complete rotation during T_s**. Recall that the number of each complete rotation is determined by the rotation numbers $\mathrm{rot}^p(q)$ and $\mathrm{rot}^s(q)$. Let us consider the mean angular velocity v_a of the anomaly given by $\theta_p(T_q)/T_s = (2\pi \cdot \mathrm{rot}^p(q) + \varphi_p)/T_s$. Then T_a is determined by $v_a \cdot T_a = 2\pi$. Doing the same procedure for T_d, we obtain

$$T_a = \frac{T_s}{\mathrm{rot}^p(q) + \varphi_p/(2\pi)}, \quad T_d = \frac{T_s}{\mathrm{rot}^s(q) + \varphi_s/(2\pi)}.$$

For Hill's orbit. Recall that Hill's orbit q_{Hill} is invariant under ρ_1. After choosing a Lagrangian basis with respect to ρ_1, our numerical approximation of the linearized flow yields

$$\overline{d\varphi_H^{T_{q_{Hill}}}|_\Sigma(q_{Hill_0})} = \begin{pmatrix} \overline{A}_p & 0 \\ 0 & A_s \end{pmatrix} = \begin{pmatrix} 0.900406 & -0.047407 & 0 & 0 \\ 3.988493 & 0.900147 & 0 & 0 \\ 0 & 0 & 0.860479 & -0.035351 \\ 0 & 0 & 7.343376 & 0.860451 \end{pmatrix},$$

$$\det(\overline{A}_p) = 0.999582, \quad \mathrm{tr}(\overline{A}_p) = 1.800554, \quad \det(A_s) = 1.000000, \quad \mathrm{tr}(A_s) = 1.720931.$$

We see that Hill's orbit is planar and spatial elliptic. In particular, in the case of our Moon the orbit has to be planar and spatial elliptic since otherwise our Moon would fly away. Moreover, the signatures of b and $\tilde{b}$ are both negative, hence each rotation angle is determined by

$$\varphi_p = \theta_p = 0.450390, \quad \varphi_s = \theta_s = 0.534613.$$

Based on the indices and rotation numbers for very low energies (see Theorem 1.2.3 and 1.2.4 and (1.2.10)), for Hill's orbit we also verified numerically that these do not change, i.e.,

$$\mathrm{rot}^p(q_{Hill}) = \mathrm{rot}^s(q_{Hill}) = 1 \quad \Rightarrow \quad T_a = \frac{T_s}{1+\varphi_p/(2\pi)}, \quad T_d = \frac{T_s}{1+\varphi_s/(2\pi)}. \tag{1.2.13}$$

Hence, each of the anomalistic and draconitic period is shorter than the synodic periodic. Furthermore, by using (1.2.2) and (1.2.13), for the **anomalistic** and **draconitic period** we compute

$$T_a = 27.552987, \quad T_d = 27.212616,$$

thus these computed values are a very good approximation to the experimentally measured data.

1.2.7 For higher energies: Numerical results and bifurcation graph

While the beginning of the families g and f for very low energies is analytical, their continuation is numerical. The crossing of the eigenvalue 1, via simple closed orbits or their multiple covers, generates bifurcations of new families.

On the one hand the Conley–Zehnder index jumps by integers when bifurcation points are crossed. The index jump depends on how the eigenvalue 1 is crossed, from above or from below, which is determined in view of the signatures of $b, c, \tilde{b}$ and $\tilde{c}$

On the other hand the Conley–Zehnder index leads to a grading on the **local Floer homology**. Since the local Floer homology and its Euler characteristic stays **invariant at a bifurcation point**, the Conley–Zehnder index provides important information about the interconnectedness of such families.

By using our techniques, we determine the index of the families in the Table 1.4. From the second row all the families arise through bifurcation from g and f, hence they can be traced back to the families g and f. Note that the orbits of the families g and f are doubly-symmetric with respect to ρ_1 and ρ_2, i.e., they are invariant under the reflection at the q_1- and q_2-axis.

from the articles by	family	remark
Hénon [34] (1969)	g, f	planar
	g'	planar (from μ^p_{CZ} jump from g)
Hénon [35] (1970), [37] (2003)	g_3	planar (from the 3rd cover of f)
Batkhin–Batkhina [13] (2009)	g_{2v}	spatial (from μ^s_{CZ} jump from g)
	g^{YOZ}_{1v}	spatial (from the 2nd cover of g)
Michalodimitrakis [49] (1980)	$g1v$	spatial (from the 2nd cover of g & g')
Kalantonis [44] (2020)	$f_g^{(2,3)}$, $f_g^{(2cut,3)}$	spatial (from the 3rd cover of g)
	$f_{g'}^{(2,3)}$, $f_{g'}^{(2cut,3)}$	spatial (from the 3rd cover of g')
	$f_g^{(1,4)}$, $f_g^{(1cut,4)}$	spatial (from the 4th cover of g)
	$f_{g'}^{(1,4)}$, $f_{g'}^{(1cut,4)}$	spatial (from the 4th cover of g')

Table 1.4: The families of planar and spatial periodic orbits in this thesis.

Note that the action given by (1.2.12) splits each of the positive and negative hyperbolic cases into two subcases, namely

	pos. hyperb. I	pos. hyperb. II	neg. hyperb. I	neg. hyperb. II
if	$a > 1, b < 0, c < 0$	$a > 1, b > 0, c > 0$	$a < -1, b > 0, c > 0$	$a < -1, b < 0, c < 0$

Family g. Our results of the family g are given in Table 1.5. Notice that $\Gamma = -2H$ corresponds to the traditional Jacobi integral.

energy values Γ	planar	spatial	μ^p_{CZ}	μ^s_{CZ}	μ_{CZ}
$(+\infty, 4.49999)$	elliptic	elliptic	3	3	6
$(4.49999, 1.3829)$	pos. hyperb. I	elliptic	2	3	5
$(1.3829, -\infty)$	pos. hyperb. I	pos. hyperb. II	2	4	6

Table 1.5: The family g.

Family g'. In view of Table 1.5, at the planar transition from elliptic to pos. hyperb. I, the planar index jumps from 3 to 2 (i.e., the eigenvalue 1 is crossed from above) and there bifurcates the family g', whose data are collected in Table 1.6. The orbits of the family g' are simply-symmetric with respect to the reflection at the q_1-axis, and by using the reflection at the q_2-axis one obtains its symmetric family, hence the family g' appears twice.

energy values Γ	planar	spatial	μ^p_{CZ}	μ^s_{CZ}	μ_{CZ}
$(4.49999, 4.2851)$	elliptic	elliptic	3	3	6
$(4.2851, 4.2806)$	elliptic	neg. hyperb. I	3	3	6
$(4.2806, 4.2714)$	elliptic	elliptic	3	3	6
$(4.2714, 3.3901)$	neg. hyperb. I	elliptic	3	3	6
$(3.3901, 0.4771)$	neg. hyperb. I	pos. hyperb. II	3	4	7
$(0.4771, -0.2195)$	neg. hyperb. I	elliptic	3	5	8
$(-0.2195, -4.6921)$	neg. hyperb. I	neg. hyperb. II	3	5	8
$(-4.6921, -4.7047)$	elliptic	neg. hyperb. II	3	5	8
$(-4.7047, -\infty)$	pos. hyperb. I	neg. hyperb. II	4	5	9

Table 1.6: The family g'.

Let us verify that this is in accordance with the Euler characteristics before and after bifurcation of g'. These are given in Table 1.7.

	before bifurcation	after bifurcation
planar problem	$(-1)^3 = -1$	$(-1)^2 + 2 \cdot (-1)^3 = -1$
spatial problem	$(-1)^6 = 1$	$(-1)^5 + 2 \cdot (-1)^6 = 1$

Table 1.7: Euler characteristics before and after the emergence of the family g'.

Family g_{2v}. In view of Table 1.5, at the spatial transition of the family g from elliptic to pos. hyperb. II, where μ^s_{CZ} jumps from 3 to 4 (i.e., the eigenvalue 1 is crossed from below), the family g_{2v} bifurcates, which appears twice by using σ. They have $\mu_{CZ} = 5$ and the Euler characteristics before and after bifurcation are $(-1)^5 = -1$ and $2 \cdot (-1)^5 + (-1)^6 = -1$.

Family f. Neither the planar ($\mu^p_{CZ} = 1$) nor the spatial index ($\mu^s_{CZ} = 1$) of the simple closed f-orbits jumps, i.e., they are planar and spatial elliptic for all times. The smallest cover of an f-orbit from which new families of spatial orbits bifurcate, is a 5-th cover. Furthermore, in

the limit case for very high energy values, we analytically show that these orbits converge to a degenerate planar retrograde periodic orbit where all three periods (i.e., the first return time and the planar and spatial rotation angles) becomes 2π, which corresponds to 365.25 days - the period of the Earth around the Sun.

The other families of planar and spatial orbits from Table 1.4 bifurcate from the respective iteration of the underlying planar periodic orbits. We illustrate their interconnectedness in form of a **bifurcation graph**. Moreover, we want to emphasize the following special bifurcation result, which is shown in Figure 1.7.

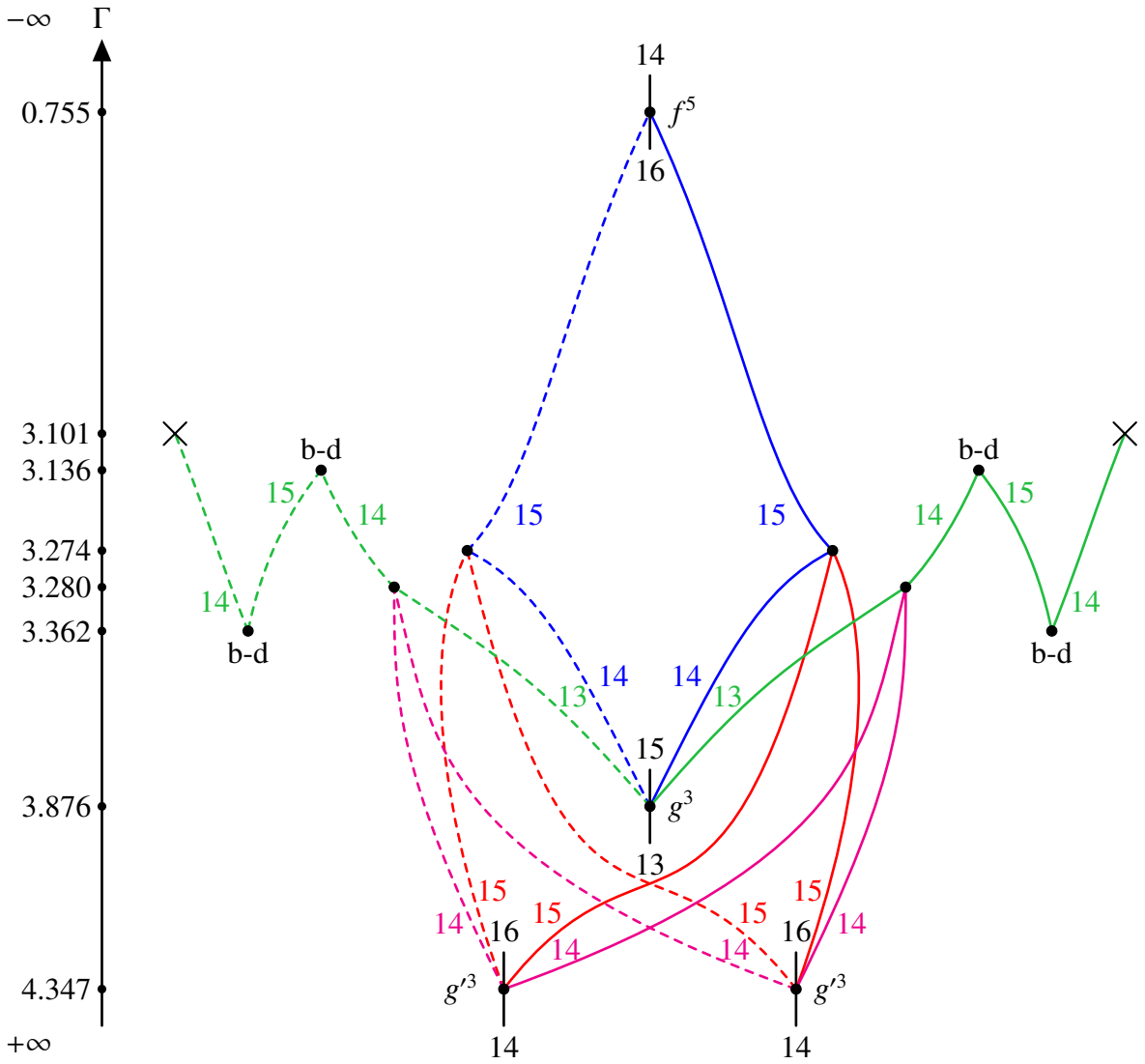

Figure 1.7: The bifurcation graph between the 3rd cover of g, the 3rd cover of g' and the 5th cover of f with the families $f_g^{(2,3)}$, $f_g^{(2cut,3)}$, $f_{g'}^{(2,3)}$ and $f_{g'}^{(2cut,3)}$.

The bifurcation graph is constructed as follows:

1) We draw from bottom to top in the direction of increasing energy. Each vertex corresponds to a degenerate periodic orbit and each edge to a family of periodic orbits with their (constant) Conley–Zehnder index. We distinguish two kinds of edges. The first kind corresponds to the underlying family of planar periodic orbits where the index jumps and the bifurcations happen. We draw these edges in black, vertically and shortly before and after the bifurcations. The second kind corresponds to a new family branching out from

the index jump. We draw such edges coloured, and every new family gets his own colour. If there is a symmetric family, then these edges are drawn in the same colour, but dashed.

2) The cross stands for collision and the term "b-d" for a periodic orbit of birth-death type. In general, a periodic orbit of birth-death type is a degenerate orbit from which two families bifurcate with an index difference of 1 and into the same energy direction. Its local Floer homology and its Euler characteristic are therefore zero.

To the Figure 1.7:

1) The branches (not dashed) correspond to the families $f_g^{(2,3)}$, $f_g^{(2cut,3)}$, $f_{g'}^{(2,3)}$ and $f_{g'}^{(2cut,3)}$ with their resp. colours. In view of the symmetry σ, these families give rise to a second bifurcation branch (dashed).
2) At $\Gamma = 3.876$ the index of the 3rd cover of the family g jumps from 13 to 15. At this transition the two families $f_g^{(2,3)}$ and $f_g^{(2cut,3)}$ bifurcate. Their indices are 14 and 13, respectively. The orbits of the first family are doubly-symmetric with respect to $\overline{\rho_1}$ and $\overline{\rho_2}$, hence they are invariant under $-\sigma$. They end at the value $\Gamma = 0.755$ at the 5th cover of f, and inbetween there is an index jump from 14 to 15. In the second family, the orbits are doubly-symmetric with respect to ρ_1 and ρ_2, thus they are invariant under $-\sigma$ as well. At the value $\Gamma = 3.280$ the index jumps from 13 to 14, and the orbits eventually undergo collision. Until then, this family consists of branches that bifurcate from a periodic orbit of birth-death type. The dashed branches are obtained by using σ. Note that the orbits of the symmetric family (dashed) of $f_g^{(2,3)}$ are doubly-symmetric with respect to ρ_1 and ρ_2, and the orbits of the symmetric family (dashed) of $f_g^{(2cut,3)}$ are doubly-symmetric with respect to $\overline{\rho_1}$ and $\overline{\rho_2}$.
3) Consider the family g', where at $\Gamma = 4.347$ the index of the 3rd cover jumps from 14 to 16. At this value of Γ the two families $f_{g'}^{(2,3)}$ and $f_{g'}^{(2cut,3)}$ bifurcate, with indices 15 resp. 14. According to Kalantonis [44, p. 11], the two families $f_{g'}^{(2,3)}$ and $f_{g'}^{(2cut,3)}$ terminate at the 3rd cover of the resp. planar orbit of g' which is symmetric to the planar orbit of g', from which they have bifurcated. These are the two not-dashed branches, respectively. We have a deeper insight:
   i) The orbits of the family $f_{g'}^{(2,3)}$ are simply-symmetric with respect to $\overline{\rho_1}$, and its two not-dashed branches are symmetric by $\overline{\rho_2}$. Recall that the orbits of $f_g^{(2,3)}$ are doubly-symmetric with respect to $\overline{\rho_1}$ and $\overline{\rho_2}$. Therefore, very close to the value $\Gamma = 3.274$, by comparing the initial data, and by using these symmetries and especially the indices, we conclude that the family $f_{g'}^{(2,3)}$ ends at the first index jump of the family $f_g^{(2,3)}$. This explains why they come together at the value $\Gamma = 3.274$.
   ii) The same happens for the family $f_{g'}^{(2cut,3)}$, namely its orbits are simply-symmetric with respect to ρ_1 and its two not-dashed branches are symmetric by ρ_2. Recall that the orbits of $f_g^{(2cut,3)}$ are doubly-symmetric with respect to ρ_1 and ρ_2. Hence very close to the value $\Gamma = 3.280$, by comparing the initial data, and by using these symmetries and especially the indices, we obtain that $f_{g'}^{(2cut,3)}$ ends at the first index jump of the family $f_g^{(2cut,3)}$ (at the value $\Gamma = 3.280$).
   iii) Each family yields the bifurcation of a second branch (dashed) by using σ. Furthermore, note that the symmetry properties of the orbits of the spatial families $f_{g'}^{(2,3)}$ compared to $f_g^{(2,3)}$, and of $f_{g'}^{(2cut,3)}$ compared to $f_g^{(2cut,3)}$, are similar to the symmetry properties of the orbits of the planar family g' compared to g.

In particular, the index provides an organized structure for the families, and the bifurcation

graph organizes the local bifurcations and thereby helps to check the Euler characteristics of the local Floer homology groups. For instance,

i) at the value $\Gamma = 3.876$ at g^3 it is $(-1)^{13} = -1$ before, and $2\cdot(-1)^{13}+2\cdot(-1)^{14}+(-1)^{15} = -1$ after bifurcation.
ii) At the value $\Gamma = 0.755$ at f^5 it is $2 \cdot (-1)^{15} + (-1)^{16} = -1$ before, and $(-1)^{14} = 1$ after bifurcation. Here we see that at this bifurcation point there are still undiscovered families branching out from f^5.

1.3 Outline of the thesis

The main results of this PhD thesis consist of the four papers [8], [9], [10], [11] during my PhD at the Université de Neuchâtel under the supervision of Felix Schlenk and the continuous support of Urs Frauenfelder. Now we give a chapter by chapter outline of this thesis.

Chapter 2 is written for readers not familiar with this kind of flow language or the reduced monodromy in terms of symplectic geometry. Furthermore, in the case of $\mathrm{Sp}(1) = \mathrm{SL}(2,\mathbb{R})$, we discuss the relation between the stability, the Floquet multipliers and the transversal Conley–Zehnder index of periodic orbits.

In order to discuss the symplectic decomposition in a more general and more conceptual way, we introduce in **Chapter** 3 the concept of Hamiltonian manifold, which generalizes energy hypersurfaces. The general statement on the symplectic splitting is formulated in the Theorem 3.1.13.

In **Chapter** 4 we introduce a general construction of the special symmetrical form of the monodromy and reduced monodromy with respect to the invariance under symplectic and anti-symplectic symmetries. Furthermore, we generalize the invariance of the signatures of b, c, $\tilde{b}$ and $\tilde{c}$, and show concretely how to determine the index jump at a bifurcation point.

The subject of **Chapter** 5 is to discuss the Hamiltonian (1.2.1), prove Theorem 1.2.1 and show how to calculate the monodromy and reduced monodromy of special symmetrical form for planar and spatial symmetric periodic orbits.

The goal of **Chapter** 6 is to prove Theorem 1.2.3 and 1.2.4, based on "*the averaging method*" described in [27, Chapter 8] for the bifurcation scenario for the planar problem. We use and extend this technique to the spatial problem and prove the existence of two additional (spatial collision) periodic orbits. Furthermore, by an explicit calculation of Morse–Bott indices, we determine their Conley–Zehnder indices.

In **Chapter** 7 we briefly sketch the local Floer homology and its Euler characteristics associated to good and bad orbits, which stay invariant before and after bifurcation.

In **Chapter** 8 we present the data for our numerical results for all the families from Table 1.4. They consist of all relevant data such as the initial data, the Floquet multipliers, the signatures, the indices and the periods. We also plot these periodic orbits in the configuration space and give overviews in form of bifurcation graphs such as in the Figure 1.7.

Some of our numerical computations for planar and spatial symmetric periodic orbits, including explicit Python codes, can be found on arXiv:2206.07803.

1.4 Further interesting things to know

Compared to Hill and Adams. For the "*motion of the lunar perigee*" (i.e., the analysis of anomalistic period) Hill arrived in [39], by transforming his equations to an infinite set of homogeneous linear equations, at an infinite determinant, which corresponds to these equations written in power series. He was the first who attacked such a problem. In 1877 John Couch Adams (1819–1892) used exactly the same method in [2] to study the "*motion of the lunar node*" (i.e., the analysis of draconitic period). Since the determinant is infinite, it was not obvious that it converges. In 1881, according to [59, p. 116], Poincaré, who was greatly influenced by Hill's approach, proved the relevant theorem, namely that an infinite determinant converges if and only if the non-diagonal elements have finite sum and the product of the elements on the diagonal is finite. We refer to [32] and [59] for more details with a lot of history.

Nowadays nobody makes use of their huge computations. In contrast to this computational approach by Hill and Adams, our geometrical way leads us to a much less computational approximation of their periods in terms of the Floquet multipliers of the linearized spatial Hill equation and their Conley–Zehnder indices.

Hill–Brown–Eckert. The famous work "*Tables of the motion of the moon*" [19] (1919) by Ernest William Brown (1866–1938) about lunar ephemeris is based on an extension of Hill's work. Near the end of Brown's life, Wallace John Eckert (1902–1971) verified numerically the accuracy of Brown's computation, and further developments by Eckert and his collaborators led to the computational basis for the Apollo program. We refer the curious reader to [32] and [59] for much more about the Hill–Brown–Eckert theory and their lives.

Can we find Hill's variational orbit analytically? Establishing this orbit analytically is still an open problem, that was addressed already by George David Birkhoff (1884–1944). Birkhoff gave in [16] from 1915 an analytical proof for the existence of a planar retrograde periodic orbit, with the same symmetries as Hill's variational orbit, for energy level sets below the unique critical value $-(3^{4/3})/2$ (the traditional one is $3^{4/3}$). In the same work he asked if the retrograde orbit spans a disk-like global surface of section. By applying Brouwer's translation theorem to the Poincaré return map one can find a fixed point which should correspond to a direct one. This question is still an open problem and nowadays modern methods of symplectic geometry are developed to find an answer. We refer to [27] for a profound discussion.

2 Periodic orbits of Hamiltonian systems

"*Hamiltonian mechanics cannot be understood without differential forms.*"

- V. I. Arnold in [5, p. 163] (1989)

2.1 Periodic orbits, monodromy and reduced monodromy

Let (M, ω) be a $2n$ dimensional symplectic manifold, i.e., $\omega \in \Omega^2(M)$ is a 2-form, called "*symplectic form*" on M, which is closed, i.e., $d\omega = 0$, and non-degenerate.

Example 2.1.1 (**Cotangent bundles**)**.** The archetypical example is the cotangent bundle T^*Q of a n dimensional smooth manifold Q. In classical mechanics T^*Q corresponds to phase space and Q to configuration space. In canonical coordinates $(q, p) = (q_1, ..., q_n, p_1, ..., p_n) \in T^*Q$, where q is a point in configuration space and $p \in T_q^*Q$ its momentum in the fiber, the cotangent bundle is endowed with a coordinate-independent 1-form, the so-called "*Liouville one-form*", defined by $\lambda_{\text{can}} = \sum_{i=1}^n p_i dq_i$. The canonical symplectic form on T^*Q is $\omega_{\text{can}} = -d\lambda_{\text{can}} = \sum_{i=1}^n dq_i \wedge dp_i$.

Remark 2.1.2. The first analytical condition of a symplectic form forces that all symplectic manifolds locally look like the Euclidean space $\mathbb{R}^{2n}$ equipped with the standard symplectic form (Darboux's theorem, see for instance [42, pp. 10–11] for details). For the second algebraic condition: Since $\omega \in \Omega^2(M)$, we get for each point $x \in M$ an alternating multilinear map

$$\omega_x \colon T_xM \times T_xM \to \mathbb{R}. \tag{2.1.1}$$

Non-degeneracy means that for all $x \in M$ and for all $0 \neq v \in T_xM$ there exists $0 \neq w \in T_xM$ such that $\omega_x(v, w) \neq 0$. Equivalently, if $\omega_x(v, w) = 0$ for all $v \in T_xM$, then $w = 0$. Moreover, this condition implies that the top exterior power $\omega^{\wedge n} = \omega \wedge ... \wedge \omega \neq 0$ is a volume form, hence symplectic manifolds are necessarily even-dimensional and orientable. Furthermore, (2.1.1) defines a map

$$T_xM \to T_x^*M, \quad v \mapsto \omega_x(v, \cdot). \tag{2.1.2}$$

Being non-degenerate is equivalent to (2.1.2) being an isomorphism.

Let $H \in C^\infty(M, \mathbb{R})$ be an autonomous Hamiltonian function and X_H the Hamiltonian vector field, which is uniquely defined by

$$dH(\cdot) = \omega(X_H, \cdot). \tag{2.1.3}$$

We call $\gamma \in C^\infty(\mathbb{R}, M)$ a **periodic orbit** of H if it is a solution to the first order ODE

$$\dot{\gamma}(t) = X_H\big(\gamma(t)\big), \quad t \in \mathbb{R} \tag{2.1.4}$$

such that there exists a period $T > 0$ with $\gamma(t + T) = \gamma(t)$ for all $t \in \mathbb{R}$, see Figure 2.1. Trivial periodic orbits are critical points of H. For a non-trivial periodic orbit γ we denote the **first return time** by T_γ which is the minimum of the set $\{T \geq 0 \mid \gamma(T) = \gamma(0)\}$, hence for every

period T we obtain $T = n \cdot T_\gamma$ for some $n \in \mathbb{Z}$. Since H is autonomous, there are no self-intersections, i.e., for $\tau \in (0, T_\gamma)$ it holds that $\gamma(0) \neq \gamma(\tau)$.

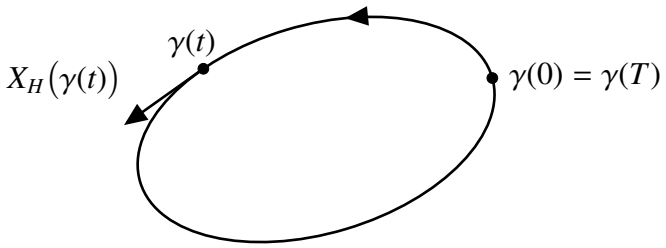

Figure 2.1: Periodic orbit.

The solutions of (2.1.4) generate the family of Hamiltonian flows $\varphi_H^t \colon M \to M$ of X_H via

$$\varphi_H^0 = \mathrm{id}_M, \quad \frac{d}{dt}\varphi_H^t(x) = X_H\big(\varphi_H^t(x)\big), \quad t \in \mathbb{R}, \quad x \in M.$$

Note that for $t, s \in \mathbb{R}$ it holds that $\varphi_H^{t+s} = \varphi_H^s \circ \varphi_H^t$ and $\varphi_H^{-t} \circ \varphi_H^t = \varphi_H^0 = \mathrm{id}_M$.

Remark 2.1.3. Take $Q = \mathbb{R}^n$ as configuration space and as phase space its trivial cotangent bundle $T^*\mathbb{R}^n = \mathbb{R}^n \times \mathbb{R}^n$ with the canonical symplectic form. We have $dH = \sum_{i=1}^n \left(\frac{\partial H}{\partial q_i} dq_i + \frac{\partial H}{\partial p_i} dp_i \right)$ and $X_H = \sum_{i=1}^n \left(\frac{\partial H}{\partial p_i} \frac{\partial}{\partial q_i} - \frac{\partial H}{\partial q_i} \frac{\partial}{\partial p_i} \right)$, since the equation (2.1.3) is satisfied by X_H,

$$\begin{aligned} \sum_{i=1}^n dq_i \wedge dp_i(X_H, \cdot) &= \sum_{i=1}^n \Big(dq_i(X_H) dp_i(\cdot) - dq_i(\cdot) dp_i(X_H) \Big) \\ &= \sum_{i=1}^n \left(\frac{\partial H}{\partial p_i} dp_i(\cdot) - dq_i(\cdot) \Big(- \frac{\partial H}{\partial q_i} \Big) \right) \\ &= dH(\cdot). \end{aligned}$$

Therefore (2.1.4) is equivalent to the Hamiltonian equation of motion

$$\frac{dq_i}{dt} = \frac{\partial H}{\partial p_i}, \quad \frac{dp_i}{dt} = -\frac{\partial H}{\partial q_i}.$$

Lemma 2.1.4 (Preservation of energy). The Hamiltonian flow preserves the Hamiltonian H.

Proof. The total time derivative of H equals

$$\begin{aligned} \frac{d}{dt} H\left(\varphi_H^t(x)\right) &= dH\left(\varphi_H^t(x)\right) \frac{d}{dt}\varphi_H^t(x) \\ &= dH\left(\varphi_H^t(x)\right) X_H\left(\varphi_H^t(x)\right) \\ &= \omega(X_H, X_H)\left(\varphi_H^t(x)\right) \\ &= 0, \end{aligned}$$

where the last equality follows by the anti-symmetry of ω. Therefore

$$H\left(\varphi_H^t(x)\right) = H\left(\varphi_H^0(x)\right) = H(x).$$

□

Lemma 2.1.5. The Hamiltonian flow preserves the symplectic form, i.e., $(\varphi_H^t)^*\omega = \omega$.

Proof. By using Cartan's identity for the Lie derivative of the symplectic form with respect to the Hamiltonian vector field we calculate

$$\begin{aligned}
\frac{d}{dt}(\varphi_H^t)^*\omega &= \left.\frac{d}{ds}\right|_{s=0} (\varphi_H^{t+s})^*\omega \\
&= \left.\frac{d}{ds}\right|_{s=0} (\varphi_H^s\varphi_H^t)^*\omega \\
&= \left.\frac{d}{ds}\right|_{s=0} (\varphi_H^t)^*(\varphi_H^s)^*\omega \\
&= (\varphi_H^t)^* \left.\frac{d}{ds}\right|_{s=0} (\varphi_H^s)^*\omega \\
&= (\varphi_H^t)^* \mathcal{L}_{X_H}\omega \\
&= (\varphi_H^t)^* (d \underbrace{\iota_{X_H}\omega}_{\omega(X_H,\cdot)} + \iota_{X_H} \underbrace{d\omega}_{=0}) \\
&= (\varphi_H^t)^* (d^2 H) \\
&= 0.
\end{aligned}$$

Therefore $(\varphi_H^t)^*\omega = (\varphi_H^0)^*\omega = \omega$. □

Remark 2.1.6. Since the pullback commutes with the wedge product, the flow is volume preserving as well, meaning that $(\varphi_H^t)^*\omega^{\wedge n} = \omega^{\wedge n}$.

Now let γ be a non-trivial periodic orbit with first return time T_γ, then we characterize it by $\gamma(t) = \varphi_H^{tT_\gamma}(\gamma(0))$, for $t \in S^1 = \mathbb{R}/\mathbb{Z}$. Since $(\varphi_H^t)^*\omega = \omega$, by its linearized flow we obtain the linear symplectic map

$$d\varphi_H^{T_\gamma}(\gamma(0)) : (T_{\gamma(0)}M, \omega_{\gamma(0)}) \to (T_{\gamma(0)}M, \omega_{\gamma(0)}) \tag{2.1.5}$$

which is called the **monodromy**.

Lemma 2.1.7. For two different points $x_1, x_2 \in M$ on γ the two monodromy matrices $d\varphi_H^{T_\gamma}(x_1)$ and $d\varphi_H^{T_\gamma}(x_2)$ are symplectically conjugated.

Proof. Let $x_1, x_2 \in M$ be different points on γ, then there exists t_0 such that $\varphi_H^{t_0}(x_1) = x_2$. By differentiation the equation $\varphi_H^t\left(\varphi_H^{t_0}(x_1)\right) = \varphi_H^{t_0}\left(\varphi_H^t(x_1)\right)$ we calculate

$$d\varphi_H^t\left(\varphi_H^{t_0}(x_1)\right) d\varphi_H^{t_0}(x_1) = d\varphi_H^{t_0}\left(\varphi_H^t(x_1)\right) d\varphi_H^t(x_1).$$

For $t = 1$ we obtain $d\varphi_H^{T_\gamma}(x_2)d\varphi_H^{t_0}(x_1) = d\varphi_H^{t_0}(x_1)d\varphi_H^{T_\gamma}(x_1)$, and since $d\varphi_H^{t_0}(x_1)$ is a linear symplectomorphism, the assertion follows. □

Remark 2.1.8. As a consequence of Lemma 2.1.7 the eigenvalues of the monodromy (2.1.5) are independent of the choice of the starting point of γ.

Moreover, we compute

$$X_H(\gamma(0)) = \frac{d}{dt}\varphi_H^t(\gamma(0)) = \frac{d}{dt}\varphi_H^{T_\gamma}\left(\varphi_H^t(\gamma(0))\right) = d\varphi_H^{T_\gamma}(\gamma(0))\, X_H(\gamma(0)). \tag{2.1.6}$$

Since γ is not trivial, $X_H(\gamma(0))$ does not vanish. Hence $X_H(\gamma(0))$ is an eigenvector of the monodromy (2.1.5) with eigenvalue 1. This trivial eigenvalue exists always double, since in general, if λ is an eigenvalue of a symplectic matrix, then so are $1/\lambda, \overline{\lambda}$ and $1/\overline{\lambda}$ (see Figure 2.2 and [27, pp. 124–125] for details).

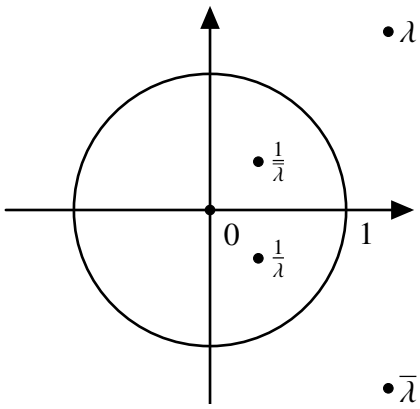

Figure 2.2: Eigenvalues of a symplectic matrix occur in quadruples.

In view of Lemma 2.1.4 we can assign the energy value $c = H(\gamma)$ to the periodic orbit. For a regular value c of H we know that $dH(x) \neq 0$ which by (2.1.3) is equivalent to $X_H(x) \neq 0$, for all points $x \in H^{-1}(c)$. Therefore the level set

$$\Sigma := \Sigma_c := H^{-1}(c) \subset M \tag{2.1.7}$$

is a codimension one energy hypersurface that is invariant under the Hamiltonian flow φ_H^t. Its tangent space at a point $x \in \Sigma \subset M$ is given by

$$T_x\Sigma = \{\xi \in T_xM : dH(x)\xi = 0\} = \ker\big(dH(x)\big).$$

By taking any Riemannian metric on M, the gradient of H with respect to this metric does not vanish, and we obtain the following decomposition of the $2n$ dimensional symplectic vector space

$$T_xM = T_x\Sigma \oplus \langle \nabla H(x) \rangle, \tag{2.1.8}$$

see Figure 2.3. Recall that a symplectic manifold is orientable via the volume form $\omega^{\wedge n}$. Let denote the normal space at $x \in \Sigma$ by $N_x\Sigma := \langle \nabla H(x) \rangle$. Since the normal bundle $N\Sigma$ of Σ is also orientable, by the splitting (2.1.8) the energy hypersurface Σ is orientable.

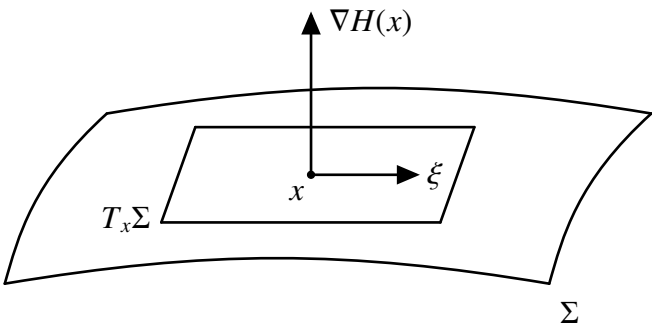

Figure 2.3: The tangent space of the energy hypersurface Σ and the gradient of H.

By Definition (2.1.3) of X_H and by the anti-symmetry of ω, we have

$$dH(x)X_H(x) = \omega_x\left(X_H(x), X_H(x)\right) = 0.$$

Hence X_H is tangent to the level sets Σ of H. In other words, X_H defines a non-vanishing vector field on Σ, i.e.,

$$X_H(x) \in T_x\Sigma \setminus \{0\}.$$

Furthermore, we consider the subspace

$$\ker\omega_x = \{v \in T_x\Sigma : \omega_x(v, w) = 0, \forall w \in T_x\Sigma\} \subset T_x\Sigma$$

and compute for $\xi \in T_x\Sigma$ that

$$\omega_x\big(X_H(x), \xi\big) = dH(x)\xi = 0,$$

meaning that $X_H(x) \in \ker\omega_x$. By the non-degeneracy of ω,

$$\ker\omega_x = \langle X_H(x)\rangle \subset T_x\Sigma. \tag{2.1.9}$$

Thus $\ker\omega|_\Sigma \subset T\Sigma$ is a one-dimensional distribution, i.e., $(\ker\omega|_\Sigma, \pi_{\ker\omega|_\Sigma}, \Sigma)$ is a line subbundle of the tangent bundle $(T\Sigma, \pi, \Sigma)$, and the line bundle $\ker\omega_{|\Sigma}$ is known as the **characteristic line bundle**. Notice that since it has the non-vanishing section $X_H|_\Sigma$, i.e., a smooth map $X_H|_\Sigma : \Sigma \to \ker\omega|_\Sigma$ such that $\pi_{\ker\omega|_\Sigma} \circ X_H|_\Sigma = \mathrm{id}_\Sigma$, it is orientable.

Remark 2.1.9. We have a foliation on Σ (see Figure 2.4) where a leaf $L \subset \Sigma$ of the foliation is a one-dimensional submanifold such that $T_xL = \ker\omega_x$, for all $x \in L$. Indeed, a leaf trough x corresponds to a trajectory of the flow, i.e., $L_x = \{\varphi_H^t(x) : t \in \mathbb{R}\}$. Therefore, the periodic orbits are in one-to-one correspondence with closed characteristics of Σ, which are diffeomorphic to S^1. Non-compact leaves are diffeomorphic to $\mathbb{R}$, hence non-periodic orbits. Describing the leaves instead of the flow is somewhat easier, since one does not care about time. Therefore, to understand the foliation on Σ means to understand the dynamics of $X_H|_\Sigma$ up to time-parametrization.

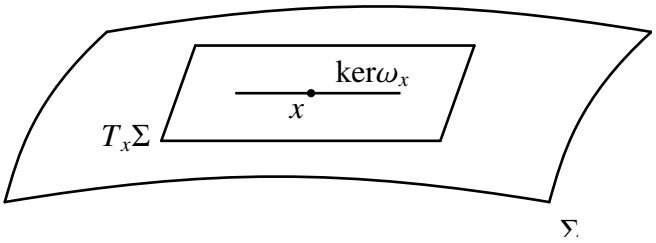

Figure 2.4: The characteristic foliation on Σ.

Back to the monodromy (2.1.5). Because of (2.1.6), the restriction to the energy hypersurface $d\varphi_H^{T_\gamma}|_\Sigma$ leaves the characteristic line bundle $\ker\omega|_\Sigma \subset T\Sigma$ invariant. This induces a symplectic bundle map $\overline{d\varphi_H^{T_\gamma}|_\Sigma}$, which is characterized by the commutative diagram

$$\begin{array}{ccc} T\Sigma & \xrightarrow{d\varphi_H^{T_\gamma}|_\Sigma} & T\Sigma \\ \pi\downarrow & & \downarrow\pi \\ T\Sigma/(\ker\omega|_\Sigma) & \xrightarrow{\overline{d\varphi_H^{T_\gamma}|_\Sigma}} & T\Sigma/(\ker\omega|_\Sigma) \end{array}$$

Notice that $T\Sigma/(\ker\omega|_\Sigma)$ is a symplectic vector bundle over Σ of rank $2n-2$. The induced map

$$A := \overline{d\varphi_H^{T_\gamma}|_\Sigma(\gamma(0))}\colon T_{\gamma(0)}\Sigma/(\ker\omega_{\gamma(0)}|_{T_{\gamma(0)}\Sigma}) \to T_{\gamma(0)}\Sigma/(\ker\omega_{\gamma(0)}|_{T_{\gamma(0)}\Sigma}) \tag{2.1.10}$$

is called **reduced monodromy** which is a symplectomorphism of the $2n-2$ dimensional symplectic vector space $T_{x_0}\Sigma/(\ker\omega_{\gamma(0)}|_{T_{\gamma(0)}\Sigma})$. Moreover, the **Floquet multipliers** are defined as the eigenvalues of (2.1.10) and we call the periodic orbit γ **non-degenerate** if 1 is not a Floquet multiplier, which is equivalent to $\ker(A-\mathrm{id}) = \{0\}$. Note that the eigenvalues of the monodromy and the reduced monodromy differ by the double trivial eigenvalue 1 from (2.1.6).

2.2 In the case of $\mathrm{Sp}(1) = \mathrm{SL}(2,\mathbb{R})$: Stability, Floquet multipliers and Conley–Zehnder index

We consider the case that the reduced monodromy (2.1.10) is a symplectomorphism in

$$\mathrm{Sp}(1) = \mathrm{SL}(2,\mathbb{R}) = \{\Psi\colon \mathbb{R}^2 \to \mathbb{R}^2 \text{ linear} \mid \det\Psi = 1\},$$

where linear symplectomorphisms are exactly the linear orientation area-preserving transformations of $\mathbb{R}^2$. The Floquet multipliers are the zeros of the polynomial

$$\lambda^2 - \lambda\mathrm{tr}(A) + 1.$$

If $|\mathrm{tr}(A)| < 2$, then the eigenvalues are on the unit circle, so of the form $e^{\pm i\theta}$, and if $|\mathrm{tr}(A)| > 2$, then they are real and of the form $\lambda, 1/\lambda$ (see Figure 2.5). In particular, they are given respectively by

$$\frac{1}{2}\mathrm{tr}(A) \pm i\frac{1}{2}\sqrt{4-\big(\mathrm{tr}(A)\big)^2}, \quad \frac{1}{2}\mathrm{tr}(A) \pm \frac{1}{2}\sqrt{\big(\mathrm{tr}(A)\big)^2-4}.$$

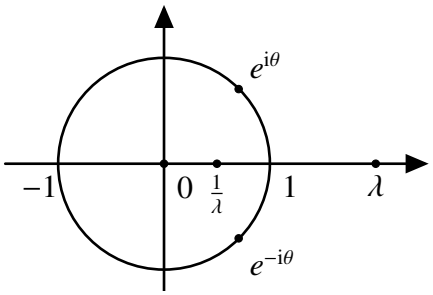

Figure 2.5: Eigenvalues of a 2×2 symplectic matrix.

In 1984, Charles Conley and Eduard Zehnder [22] defined an index theory, which generalizes the usual Morse index for closed geodesics on a Riemannian manifold. We refer the reader for details on Morse Theory to the books of Milnor [50], Banyaga–Hurtubise [12], Audin–Damian [7] and for Morse–Bott Theory, which is a generalization, to the articles of Bott [17], Banyaga–Hurtubise [12] and Frauenfelder [23, Appendix].

One can roughly describe the Conley–Zehnder index as a mean winding number for the linearized Hamiltonian flow along the orbit γ or the number of times that an eigenvalue crosses 1. It roughly measures how often neighboring orbits of the same energy wind round the orbit γ. Since we treat the reduced monodromy (2.1.10) in Sp(1), we consider the transversal

Conley–Zehnder index with standard normalization or counter-clockwise normalization for non-degenerate paths, as defined by Hofer–Wysocki–Zehnder [41, Appendix], [40, Section 3] where the details can be seen. Explicitly, it is given in the following way.

Let $b_1(0), b_2(0)$ and $X_H|_\Sigma(\gamma(0))$ be a basis for the 3-dimensional vector space $T_{\gamma(0)}\Sigma$ such that

$$T_{\gamma(0)}\Sigma = \langle b_1(0), b_2(0)\rangle_{\mathbb{R}} \oplus \langle X_H|_\Sigma(\gamma(0))\rangle_{\mathbb{R}}, \quad \omega_{\gamma(0)}\big(b_1(0), b_2(0)\big) = 1.$$

Note that $\omega_{\gamma(0)}\big(b_i(0), X_H|_\Sigma(\gamma(0))\big) = 0$, for $i = 1, 2$. The first two basis vectors induce a symplectic basis for the 2 dimensional symplectic vector space $T_{\gamma(0)}\Sigma/(\ker\omega_{\gamma(0)}|_{T_{\gamma(0)}\Sigma})$ and we denote by $P := \langle b_1(0), b_2(0)\rangle_{\mathbb{R}}$ the 2-plane.

We choose a smooth disc map $\overline{\gamma} \in C^\infty(\mathbb{D}, \Sigma)$, where $\mathbb{D} = \{z \in \mathbb{C} \mid |z| \le 1\}$, such that on the boundary it satisfies $\overline{\gamma}(e^{2\pi i t/T_\gamma}) = \gamma(t)$. Furthermore, we fix a symplectic trivialization for the pullback bundle $\tau\colon \mathbb{D}\times\mathbb{R}^2 \to \overline{\gamma}^*T\Sigma/\ker\omega|_\Sigma$. For details about such trivializations we refer to [47, Section 2.6]. With respect to these choices, the linearized flow along γ generates a path $\Phi_\gamma\colon [0, T_\gamma] \to \mathrm{Sp}(1)$ of symplectic matrices in $\mathbb{R}^2$ defined by

$$\begin{array}{ccc} \mathbb{R}^2 & \xrightarrow{\Phi_\gamma(t)} & \mathbb{R}^2 \\ {\scriptstyle \left(\tau(1)\right)^{-1}}\downarrow & & \uparrow{\scriptstyle \tau(e^{2\pi i t/T_\gamma})} \\ T_{\gamma(0)}\Sigma/(\ker\omega_{\gamma(0)}|_{T_{\gamma(0)}\Sigma}) & \xrightarrow{\overline{d\varphi_H^t|_\Sigma(\gamma(0))}} & T_{\gamma(t)}\Sigma/(\ker\omega_{\gamma(t)}|_{T_{\gamma(t)}\Sigma}) \end{array}$$

This path starts at $\Phi_\gamma(0) = \mathrm{id}$ and has a well-defined Conley–Zehnder index, and the transversal Conley–Zehnder index of γ is the Conley–Zehnder index of this path, which we denote by μ_{CZ}. Now the periodic orbit γ is partitioned into three classes, depending on the trace of A.

a) **Elliptic:** $|\mathrm{tr}(A)| < 2$ and the eigenvalues are on the unit circle and of the form $e^{\pm i\theta}$. Then A is conjugate to a rotation in $\mathbb{R}^2$ and the 2-plane P was rotated by an angle. Consider the rotation function $\theta(t)$ which gives the rotation angle of the 2-plane P at each time $t \in [0, T_\gamma]$. Note that $\theta(0) = 0$ and $\theta(t)$ is continuous in t. Then

$$\mu_{CZ} = 1 + 2\cdot \mathrm{rot}(\gamma),$$

where

$$\mathrm{rot}(\gamma) := \lfloor \theta(T_\gamma)/(2\pi)\rfloor = \frac{1}{2}(\mu_{CZ} - 1) \in \mathbb{Z}$$

is the number of complete rotations of the neighboring orbits during T_γ. Therefore for every complete rotation the index jumps by 2 and is odd.

b) **Positive hyperbolic:** $\mathrm{tr}(A) > 2$ and the eigenvalues are positive real and of the form λ, $1/\lambda$. Then the 2-plane P was rotated by $m\pi$ for an integer m and

$$\mu_{CZ} = m \in 2\mathbb{Z}.$$

If the orbit changes its stability from elliptic to positive hyperbolic, or vice versa, then the eigenvalue 1 is crossed and the index jumps by ± 1. If the rotation angle moves through 0 to positive hyperbolic, then μ_{CZ} jumps by -1 and if it goes through 2π to positive hyperbolic, then μ_{CZ} jumps by $+1$. For the other way, the change of index is exactly backwards (see Figure 2.6).

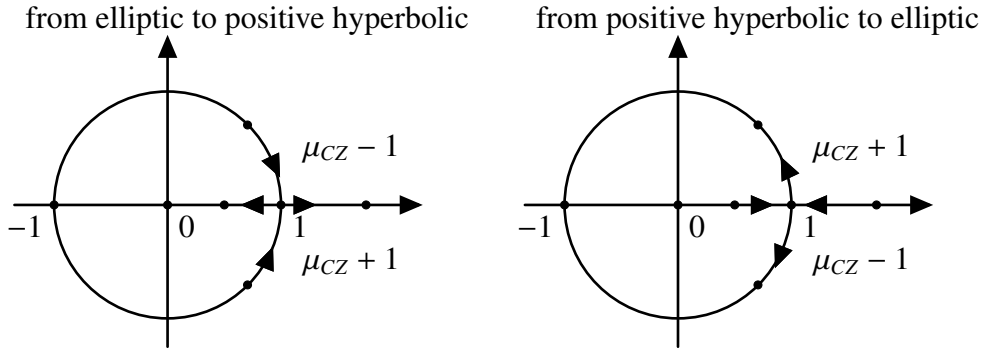

Figure 2.6: The index jump by ±1 in the elliptic and positive hyperbolic transitions.

c) **Negative hyperbolic:** $\mathrm{tr}(A) < 2$ and the eigenvalues are negative real and of the form λ, $1/\lambda$. Then the 2-plane P was rotated again by $m\pi$ for an integer m and

$$\mu_{CZ} = m \in 2\mathbb{Z} + 1.$$

For the cases from elliptic to negative hyperbolic, or vice versa, the index does not change, i.e., in the negative hyperbolic case the index is odd as well.

Remark 2.2.1. Geometrically, elliptic periodic orbits have the property that orbits starting sufficiently close to γ, i.e., neighboring orbits of the same energy, remain near γ for a long time, while for hyperbolic orbits they may fly away. Furthermore, by the implicit function theorem, non-degenerate periodic orbits always come in a smooth family of periodic orbits and hence form a smooth orbit cylinder (see Figure 2.7 and [48, p. 202] for details). Moreover, all periodic orbits on the orbit cylinder have the same index, since they are connected by a path of non-degenerate orbits.

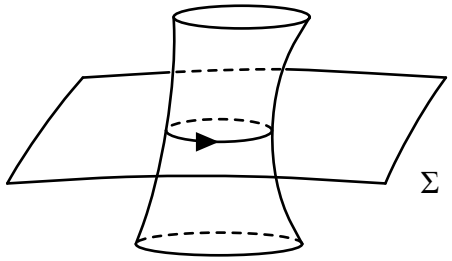

Figure 2.7: Orbit cylinder.

Let γ^n be the n times iteration of γ with first return time nT_γ, $n \geq 1$. We call γ^n the "*n-th cover of* γ". Assume that γ^n is non-degenerate for all $n \geq 1$, then the index iteration (we refer to [41, p. 249] for details) is given by the Table 2.1.

γ	Conley–Zehnder index of γ^n
pos. / neg. hyperbolic	$n \cdot \mu_{CZ}$
elliptic	$1 + 2\lfloor n \cdot \theta(T_\gamma)/(2\pi) \rfloor$

Table 2.1: Index iteration.

Recall that for the cases from elliptic to negative hyperbolic, or vice versa, the index does not change. Nevertheless, its double cover crosses the eigenvalue 1 and the index of its double cover

jumps by ± 1. Notice that the double cover of a negative hyperbolic periodic orbits is positive hyperbolic. In the elliptic case, if the rotation angle is a $\tilde{k}$-th root of unity, for $\tilde{k} \geq 3$ the $\tilde{k}$-th cover is still elliptic and goes through the eigenvalue 1, thus its index jumps by ± 2.

Question: *How can we determine the index jump?*

In Section 4.5 we see for periodic orbits, which are invariant under an anti-symplectic involution, how the index jump is determined.

3 Hamiltonian manifolds

"*A Hamiltonian manifold is the odd-dimensional analog of a symplectic manifold.*"

- U. Frauenfelder and O. van Koert in [27, p. 20] (2018)

3.1 Involutive Hamiltonian manifolds and Symplectic Splitting

The archetypical examples of Hamiltonian manifolds are energy hypersurfaces, see (2.1.7).

Definition 3.1.1. A **Hamiltonian manifold** is a pair (Σ, ω) where Σ is a $2n-1$ dimensional manifold and $\omega \in \Omega^2(\Sigma)$ a closed 2-form such that $\ker\omega \subset T\Sigma$ is a one-dimensional distribution. The 2-form ω is called a **Hamiltonian structure** on Σ.

Definition 3.1.2. A **Hamiltonian vector field** X on a Hamiltonian manifold is a non-vanishing section of the line bundle $\ker\omega$.

Remark 3.1.3. Since the Lie derivative vanishes by Cartan's identity, $\mathcal{L}_X\omega = d\iota_X\omega + \iota_X d\omega = 0$, the Hamiltonian structure is preserved under the flow of X for all times $t \in \mathbb{R}$, i.e., $(\varphi_X^t)^*\omega = \omega$.

Remark 3.1.4. As seen before in the case of energy hypersurfaces (2.1.7), a Hamiltonian manifold comes with a foliation on Σ (see Figure 2.4), whose leaves $L \subset \Sigma$ are the one-dimensional submanifolds such that $T_xL = \ker\omega_x$, for all $x \in L$. Compact leaves are diffeomorphic to S^1 and non compact ones are diffeomorphic to $\mathbb{R}$.

Definition 3.1.5. A **symplectic involution** σ on a Hamiltonian manifold (Σ, ω) is a diffeomorphism $\sigma : \Sigma \to \Sigma$ such that

$$\sigma^2 = \mathrm{id}_\Sigma, \quad \sigma^*\omega = \omega.$$

We next study the properties of the linear isomorphism

$$d\sigma(x) : T_x\Sigma \to T_{\sigma(x)}\Sigma, \quad x \in \Sigma. \tag{3.1.1}$$

Lemma 3.1.6. The one-dimensional distribution is invariant under $d\sigma(x)$, i.e., if $\xi \in \ker\omega_x$, then

$$d\sigma(x)\xi \in \ker\omega_{\sigma(x)}.$$

Proof. Let $\xi \in \ker\omega_x$, i.e.,

$$\omega_x(\xi, \eta) = 0, \quad \text{for all } \eta \in T_x\Sigma.$$

By (3.1.1) we know that for all $\eta' \in T_{\sigma(x)}\Sigma$ there exists a unique element $\eta \in T_x\Sigma$ such that $d\sigma(x)\eta = \eta'$. Using $\sigma^*\omega = \omega$ we compute for all $\eta' \in T_{\sigma(x)}\Sigma$ that

$$\omega_{\sigma(x)}\big(d\sigma(x)\xi, \eta'\big) = \omega_{\sigma(x)}\big(d\sigma(x)\xi, d\sigma(x)\eta\big) = \omega_x(\xi, \eta) = 0. \qquad \square$$

Let $x \in \mathrm{Fix}(\sigma) = \{x \in \Sigma \mid \sigma(x) = x\}$. By choosing a Riemannian metric on Σ which is σ-invariant, we can parametrize $\mathrm{Fix}(\sigma)$, locally around x, by the restriction of the exponential map to $E_1\big(d\sigma(x)\big)$. Thus $\mathrm{Fix}(\sigma)$ is a submanifold of Σ and

$$T_x\mathrm{Fix}(\sigma) = E_1\big(d\sigma(x)\big) = \ker\big(d\sigma(x) - \mathrm{id}\big).$$

Furthermore, the eigenvalues of $d\sigma(x)$ are ± 1 and we obtain the two eigenspaces

$$E_1\big(d\sigma(x)\big) = \{\xi \in T_x\Sigma : d\sigma(x)\xi = \xi\} = \ker\big(d\sigma(x) - \mathrm{id}\big) \subset T_x\Sigma$$

and

$$E_{-1}\big(d\sigma(x)\big) = \{\eta \in T_x\Sigma : d\sigma(x)\eta = -\eta\} = \ker\big(d\sigma(x) + \mathrm{id}\big) \subset T_x\Sigma.$$

In particular, the tangent space splits into the direct sum of the eigenspaces, i.e.,

$$T_x\Sigma = E_1\big(d\sigma(x)\big) \oplus E_{-1}\big(d\sigma(x)\big).$$

Remark 3.1.7. We recall from linear symplectic geometry: Let (V, ω) be a symplectic vector space and $W \subset V$ a linear subspace. The "*symplectic complement*" W^ω of W is defined as the subspace

$$W^\omega := \{v \in V \mid \omega(v, w) = 0, \forall w \in W\}.$$

Furthermore W is called "*symplectic*" if $\omega|_W$ is symplectic. Equivalently,

$$W \cap W^\omega = \{0\},$$

i.e., W and W^ω are "*symplectically orthogonal*". In addition, for any subspace W it holds that

$$\dim V = \dim W + \dim W^\omega, \quad (W^\omega)^\omega = W.$$

The non-degeneracy of ω implies that for a symplectic subspace $W \subset V$ we obtain

$$V = W \oplus W^\omega$$

and the symplectic complement $W^\omega \subset V$ is also symplectic. Finally, if V_1 and V_2 are sub-vector spaces of V that are symplectically orthogonal, then V_1 and V_2 are symplectic.

Definition 3.1.8. Let $S \subset T_x\Sigma$ be a linear subspace. The **symplectic complement** of S is defined as the linear subspace $\{\xi \in T_x\Sigma \mid \omega_x(\xi, \eta) = 0, \forall \eta \in S\}$. We call two subspaces $S_1, S_2 \subset T_x\Sigma$ **symplectically orthogonal** if

$$\omega_x(\xi, \eta) = 0, \quad \text{for all } \xi \in S_1,\ \eta \in S_2.$$

Lemma 3.1.9. Let $x \in \mathrm{Fix}(\sigma)$. Then the eigenspaces $E_1\big(d\sigma(x)\big)$ and $E_{-1}\big(d\sigma(x)\big)$ are symplectically orthogonal.

Proof. Since $\sigma^*\omega = \omega$ we obtain for all $\xi \in E_1\big(d\sigma(x)\big)$ that

$$\omega_x(\xi, \eta) = \omega_{\sigma(x)}\big(d\sigma(x)\xi, d\sigma(x)\eta\big) = \omega_x(\xi, -\eta) = -\omega_x(\xi, \eta)$$

for all $\eta \in E_{-1}\big(d\sigma(x)\big)$. □

Lemma 3.1.10. Let $x \in \mathrm{Fix}(\sigma)$, and assume that X is a non-vanishing section of the line bundle $\ker\omega$ such that X is invariant under σ, i.e., σ and the flow of X commute. Then $\varphi_X^t(x) \in \mathrm{Fix}(\sigma)$ and the linearized flow map

$$d\varphi_X^t(x)\colon T_x\Sigma \to T_{\varphi_X^t(x)}\Sigma$$

leaves the two decompositions

$$T_x\Sigma = E_1\left(d\sigma(x)\right) \oplus E_{-1}\left(d\sigma(x)\right), \quad T_{\varphi_X^t(x)}\Sigma = E_1\Big(d\sigma\big(\varphi_X^t(x)\big)\Big) \oplus E_{-1}\Big(d\sigma\big(\varphi_X^t(x)\big)\Big)$$

invariant, meaning that for $\xi \in E_{\pm1}\big(d\sigma(x)\big)$ we have that $d\varphi_X^t(x)\xi \in E_{\pm1}\Big(d\sigma\big(\varphi_X^t(x)\big)\Big)$.

Proof. Since $x \in \mathrm{Fix}(\sigma)$ and σ commutes with φ_X^t, we have

$$\varphi_X^t(x) = \varphi_X^t\left(\sigma(x)\right) = \sigma\left(\varphi_X^t(x)\right),$$

which means that $\varphi_X^t(x) \in \mathrm{Fix}(\sigma)$. Moreover, for $\xi \in E_{\pm1}\big(d\sigma(x)\big)$ we calculate

$$d\varphi_X^t(x)\xi = \pm d\varphi_X^t(x)\big(d\sigma(x)\xi\big) = \pm d\sigma\big(\varphi_X^t(x)\big)\big(d\varphi_X^t(x)\xi\big),$$

and therefore

$$d\sigma\big(\varphi_X^t(x)\big)\big(d\varphi_X^t(x)\xi\big) = \pm d\sigma^2\big(\varphi_X^t(x)\big)\big(d\varphi_X^t(x)\xi\big) = \pm d\varphi_X^t(x)\xi. \qquad \square$$

Furthermore, we obtain an induced $2n-2$ dimensional symplectic vector space

$$T_x\Sigma/\ker\omega_x$$

and a quotient bundle $T\Sigma/\ker\omega$ over Σ which is a symplectic vector bundle of rank $2n-2$. Therefore, if the Hamiltonian manifold (Σ,ω) is orientable, then the line bundle $\ker\omega$ is also orientable. This motivates the next definition and lemma.

Definition 3.1.11. An **involutive Hamiltonian manifold** is a triple (Σ,ω,σ), where (Σ,ω) is an oriented Hamiltonian manifold and σ a symplectic involution which preserves the orientation of the line bundle $\ker\omega$.

Corollary 3.1.12. Let (Σ,ω,σ) be an involutive Hamiltonian manifold and $x \in \mathrm{Fix}(\sigma)$. Then

$$\ker\omega_x \subset E_1\big(d\sigma(x)\big) = T_x\mathrm{Fix}(\sigma).$$

Proof. In view of Lemma 3.1.6 we obtain for $\xi \in \ker\omega_x$ that $d\sigma(x)\xi = \pm\xi$, and in fact $+\xi$ since σ is orientation preserving. $\square$

Theorem 3.1.13 (Symplectic Splitting). *Let (Σ,ω,σ) be an involutive Hamiltonian manifold and $x \in \mathrm{Fix}(\sigma)$. Then:*

1) *The induced $2n-2$ dimensional symplectic vector space at x splits into two symplectic vector spaces,*

$$T_x\Sigma/\ker\omega_x = \Big(E_1\big(d\sigma(x)\big)/\ker\omega_x\Big) \oplus \Big(E_{-1}\big(d\sigma(x)\big)\Big).$$

2) *Let X be a non-vanishing section of the line bundle* $\ker\omega$ *such that X is invariant under the symplectic involution σ. Then the induced linearized flow map*

$$\overline{d\varphi_X^t(x)}\colon T_x\Sigma/\ker\omega_x \to T_{\varphi_X^t(x)}\Sigma/\ker\omega_{\varphi_X^t(x)}$$

is a $(2n-2)\times(2n-2)$ symplectic matrix that splits into two symplectic maps. More precisely,

$$\overline{d\varphi_X^t(x)} = \begin{pmatrix} A_1 & 0 \\ 0 & A_2 \end{pmatrix},$$

where

$$A_1\colon T_x\mathrm{Fix}(\sigma)/\ker\omega_x \to T_{\varphi_X^t(x)}\mathrm{Fix}(\sigma)/\ker\omega_{\varphi_X^t(x)}$$
$$A_2\colon E_{-1}\big(d\sigma(x)\big) \to E_{-1}\big(d\sigma(\varphi_X^t(x))\big)$$

are symplectic matrices.

Proof. By Lemma 3.1.9, the two eigenspaces of the decomposition

$$T_x\Sigma = E_1\big(d\sigma(x)\big) \oplus E_{-1}\big(d\sigma(x)\big)$$

are symplectically orthogonal. By Corollary 3.1.12 we know that $\ker\omega_x \subset E_1\big(d\sigma(x)\big) = T_x\mathrm{Fix}(\sigma)$, which implies the first statement. The matrix form of the induced linearized flow consists of four block matrices,

$$\overline{d\varphi_X^t(x)} = \begin{pmatrix} A_1 & B_1 \\ B_2 & A_2 \end{pmatrix},$$

where

$$A_1\colon T_x\mathrm{Fix}(\sigma)/\ker\omega_x \to T_{\varphi_X^t(x)}\mathrm{Fix}(\sigma)/\ker\omega_{\varphi_X^t(x)}$$
$$A_2\colon E_{-1}\big(d\sigma(x)\big) \to E_{-1}\big(d\sigma(\varphi_X^t(x))\big)$$

and where

$$B_1\colon E_{-1}\big(d\sigma(x)\big) \to T_{\varphi_X^t(x)}\mathrm{Fix}(\sigma)/\ker\omega_{\varphi_X^t(x)}$$
$$B_2\colon T_x\mathrm{Fix}(\sigma)/\ker\omega_x \to E_{-1}\big(d\sigma(\varphi_X^t(x))\big)$$

are zero maps by Lemma 3.1.10. It now follows that A_1 and A_2 are symplectic. □

Remark 3.1.14. The dimensions of $\big(T_x\mathrm{Fix}(\sigma)/\ker\omega_x\big)$ and $\Big(E_{-1}\big(d\sigma(x)\big)\Big)$ are even, since they are symplectic vector spaces. Moreover, they are determined by the fixed point set $\mathrm{Fix}(\sigma)$, which is odd-dimensional. In particular,

	dimension
$T_x\mathrm{Fix}(\sigma)/\ker\omega_x$	$\dim(\mathrm{Fix}(\sigma)) - 1$
$E_{-1}\big(d\sigma(x)\big)$	$2n - 1 - \dim(\mathrm{Fix}(\sigma))$

Remark 3.1.15. Consequently, the eigenvalues of $\overline{d\varphi_X^t(x)}$ are given by those of A_1 and A_2. Recall that if $A_1, A_2 \in \mathrm{Sp}(1) = \mathrm{SL}(2,\mathbb{R})$ then the eigenvalues are real or lie on the unit circle, hence it is not possible that they are given by four different complex numbers $\lambda, 1/\lambda, \overline{\lambda}$ and $1/\overline{\lambda}$.

3.2 Every contact manifold is a Hamiltonian manifold

Let (Σ, λ) be a contact manifold, i.e., Σ is a $2n-1$ dimensional manifold and λ a 1-form on Σ, called "*contact form on* Σ", such that $\lambda \wedge (d\lambda)^{\wedge(n-1)}$ is a volume form on Σ. The "*Reeb vector field*" R on Σ is defined by the conditions $\lambda(R) = 1$ and $\iota_R d\lambda = 0$. Then $\omega := d\lambda$ is a Hamiltonian structure on Σ, i.e., the tuple $(\Sigma, \omega = d\lambda)$ is a Hamiltonian manifold. Namely, for $x \in \Sigma$ the Reeb vector field is a non-vanishing section of the line bundle $\ker d\lambda = \ker\omega \subset T\Sigma$ and

$$\ker\omega_x = \langle R(x)\rangle. \tag{3.2.2}$$

The "*hyperplane distribution*" is defined as $\xi := \ker\lambda \subset T\Sigma$, it is also called "*contact structure on* Σ". This leads to the decomposition

$$T\Sigma = \xi \oplus \langle R\rangle. \tag{3.2.3}$$

The restriction of $\omega = d\lambda$ to ξ makes ξ a symplectic vector bundle of rank $2n-2$ over Σ, i.e., for $x \in \Sigma$ the space $(\xi_x, \omega|_{\xi_x} = d\lambda|_{\xi_x})$ is a symplectic vector space. The contact structure $\xi = \ker\lambda$ is determined by the contact form λ, but the converse is not true: For every positive smooth function f, the 1-form $f\lambda$ is also a contact form that gives the same contact structure, i.e.,

$$\xi = \ker\lambda = \ker f\lambda,$$

but in general, the Reeb vector fields of λ and $f\lambda$ are not parallel. Therefore we cannot obtain the Hamiltonian structure $\omega = d\lambda$ from the contact structure $\xi = \ker\lambda$. Since the Hamiltonian structure $\omega = d\lambda$ determines the dynamics up to time reparametrization, our major attention is on $\omega = d\lambda$.

Remark 3.2.1. If contact manifolds arise as energy hypersurfaces (2.1.7), then by (2.1.9) and (3.2.2), i.e., by

$$\langle X_H(x)\rangle = \ker\omega_x = \langle R(x)\rangle,$$

the restriction of the Hamiltonian vector field $X_H|_\Sigma$ and the Reeb vector field are parallel, i.e., up to time reparametrization their flows coincide. In view of (3.2.3), for a periodic orbit γ with first return time T_γ the reduced monodromy (2.1.10) corresponds to the transverse linearized Reeb flow

$$d\varphi_R^{T_\gamma}(\gamma(0))|_{\xi_{\gamma(0)}} : \xi_{\gamma(0)} \to \xi_{\gamma(0)}.$$

Definition 3.2.2. A **contact form** on a Hamiltonian manifold (Σ, ω) is a 1-form λ on Σ such that $d\lambda = \omega$ and $\lambda \wedge \omega^{\wedge(n-1)} > 0$.

Remark 3.2.3. Every Hamiltonian manifold (Σ, ω) with a contact form λ is orientable via the volume form $\lambda \wedge \omega^{\wedge(n-1)} > 0$. Not every Hamiltonian manifold has a contact form. The next lemma gives a condition.

Lemma 3.2.4. Let (Σ, ω) be an oriented Hamiltonian manifold which is simply connected. If there exists a closed leaf $L \subset \Sigma$ with filling disk $D \subset \Sigma$ (i.e., $\partial D = L$) such that $\int_D \omega \leq 0$, then (Σ, ω) has no contact form.

Proof. Assume that (Σ, ω) has a contact form λ and there is a closed leaf $L \subset \Sigma$ with filling disk $D \subset \Sigma$, which is a periodic orbit of the Reeb vector field R. Then there exists $T > 0$ and a smooth

map $x : [0,T] \to \Sigma$, which is injective on $[0,T)$ and such that $\dot{x}(t) = R\big(x(t)\big)$, $x(T) = x(0)$ and $\mathrm{im}(x) = L$ (see Figure 3.1). By Stokes' theorem and the definition of R we obtain

$$\int_D \omega = \int_D d\lambda = \int_{\partial D = L} \lambda = \int_0^T \lambda\big(x(t)\big) \underbrace{\dot{x}(t)}_{R\left(x(t)\right)} dt = \int_0^T 1 dt = T > 0.$$

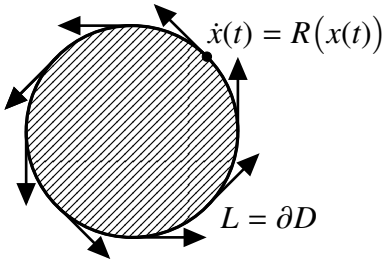

Figure 3.1: Periodic orbit of Reeb vector field with filling disk.

□

In the following let $(\Sigma, \omega = d\lambda, \sigma)$ be an involutive Hamiltonian manifold, i.e., λ is a contact form on (Σ, ω) and σ is a symplectic involution which preserves the orientation of the line bundle $\ker\omega = \ker d\lambda$.

Remark 3.2.5. For $x \in \Sigma$, as in (3.2.2) and (3.2.3), consider the decomposition

$$T_x\Sigma = \ker\omega_x \oplus \xi_x.$$

Since σ preserves the orientation of the line bundle, the orientation of $T\Sigma$ is σ-invariant.

Remark 3.2.6. For $x \in \mathrm{Fix}(\sigma)$ we obtain by Corollary 3.1.12 that

$$\langle R(x)\rangle \subset E_1\big(\sigma(x)\big) = T_x\mathrm{Fix}(\sigma).$$

Moreover, by the first part of the Symplectic Splitting Theorem 3.1.13 the $2n-2$ dimensional symplectic vector space ξ_x splits into two symplectic spaces, namely

$$\xi_x = \big(T_x\mathrm{Fix}(\sigma)/\langle R(x)\rangle\big) \oplus \Big(E_{-1}\big(d\sigma(x)\big)\Big) = T_x\Sigma/\langle R(x)\rangle. \tag{3.2.4}$$

Lemma 3.2.7. The restriction of λ to the fixed point set $\mathrm{Fix}(\sigma)$ is preserved under σ and a contact form on $\mathrm{Fix}(\sigma)$.

Proof. Since $\sigma^*\omega = \omega$ and the pullback commutes with the exterior derivative, we have

$$d\lambda = \omega = \sigma^*\omega = \sigma^* d\lambda = d\sigma^*\lambda.$$

Hence there is a closed 1-form λ' on Σ such that

$$\sigma^*\lambda = \lambda + \lambda'.$$

Therefore for all $\eta \in T_x\mathrm{Fix}(\sigma)$ we obtain

$$\lambda_x(\eta) = \lambda_x\big(d\sigma(x)\eta\big) = \lambda_x(\eta) + \lambda'_x(\eta),$$

i.e., λ' vanishes on $T_x\mathrm{Fix}(\sigma)$. Thus $\lambda_F := \lambda|_{T\mathrm{Fix}(\sigma)}$ is preserved under σ. We next show that λ_F is a volume form. For $x \in \mathrm{Fix}(\sigma)$ consider the symplectic splitting

$$\ker\lambda_x = \xi_x = \big(T_x\mathrm{Fix}(\sigma)/\langle R(x)\rangle\big) \oplus \Big(E_{-1}\big(d\sigma(x)\big)\Big) = T_x\Sigma/\langle R(x)\rangle$$

from (3.2.4). Since $E_1' := T_x\mathrm{Fix}(\sigma)/\langle R(x)\rangle$ is symplectic, for a basis $v_1, ..., v_{2k}$ of E_1' we have

$$(\omega_F)_x(v_1, ..., v_{2k}) \neq 0.$$

Then on the basis $R, v_1, ..., v_{2k}$ of $T_x\mathrm{Fix}(\sigma)$ we obtain

$$\lambda_F(x) \wedge \big(\omega_F(x)\big)^{\wedge k}(R, v_1, ..., v_{2k}) = \lambda_x(R) \cdot (\omega_x)^{\wedge k}(v_1, ..., v_{2k}) \neq 0. \qquad \square$$

Remark 3.2.8. As in the spatial Hill three-body problem, the reflection at the ecliptic in the spatial CR3BP (circular restricted three-body problem) gives rise to a symplectic involution whose fixed point set corresponds to the planar CR3BP. In [4] it was proved that the regularized planar CR3BP is of contact type for energies below and also slightly above the first critical value. In [20] it was shown that the regularized spatial CR3BP has also the contact property. Now Lemma 3.2.7 together with the result from [20] implies the result from [4].

In the previous lemma it was not necessary that λ is preserved by σ. In the next lemma and corollary we show that the average $\frac{1}{2}(\lambda + \sigma^*\lambda)$ is always a contact form which is preserved under σ.

Lemma 3.2.9. $\sigma^*\lambda$ is a contact form on (Σ, ω).

Proof. It holds that

$$d\sigma^*\lambda = \sigma^* d\lambda = \sigma^*\omega = \omega.$$

By using $\lambda \wedge \omega^{\wedge(n-1)} > 0$ and Remark 3.2.5 we have that

$$\sigma^*\lambda \wedge \omega^{\wedge(n-1)} = \sigma^*\lambda \wedge (\sigma^*\omega)^{\wedge(n-1)} = \sigma^*(\lambda \wedge \omega^{\wedge(n-1)}) > 0. \tag{3.2.5}$$

$\square$

Corollary 3.2.10. $\frac{1}{2}(\lambda + \sigma^*\lambda)$ is a contact form on (Σ, ω) which is preserved by σ.

Proof. We denote the average by $\tilde{\lambda} := \frac{1}{2}(\lambda + \sigma^*\lambda)$. It is easy to see that $d\tilde{\lambda} = \omega$. By taking the sum of $\lambda \wedge \omega^{\wedge(n-1)} > 0$ and (3.2.5) we obtain that $\tilde{\lambda} \wedge \omega^{\wedge(n-1)} > 0$, hence $\tilde{\lambda}$ is a contact form on (Σ, ω). Since σ is an involution, it is obvious that $\sigma^*\tilde{\lambda} = \tilde{\lambda}$. $\square$

4 On monodromy with respect to the invariance under symmetries

"Beauty is bound up with symmetry."

- H. Weyl in [58, p. 3] (1952)

Let (M, ω) be a $2n$ dimensional symplectic manifold and $H \in C^\infty(M, \mathbb{R})$ be an autonomous Hamiltonian function. Moreover, let γ be a periodic orbit of X_H and T_γ be its first return time.

4.1 Symmetries of Hamiltonian systems

A **symmetry** ρ is a symplectic or anti-symplectic involution on (M, ω) which leaves H invariant, meaning that $\rho\colon M \to M$ is a diffeomorphism satisfying

$$H \circ \rho = H, \quad \rho^2 = \mathrm{id}_M, \quad \rho^*\omega = \pm\omega.$$

We call γ **symmetric** with respect to ρ if γ is invariant under ρ. Depending on if γ is invariant under a symplectic or an anti-symplectic symmetry, there are different consequences for γ.

a) Let σ be a symplectic symmetry which leaves γ invariant. Then in view of definition (2.1.3) of X_H we obtain

$$\omega(X_H, \cdot) = \omega(X_{H\circ\sigma}, \cdot) = d(H \circ \sigma)(\cdot) = \sigma^*\big(dH(\cdot)\big) = \sigma^*\big(\omega(X_H, \cdot)\big) = \underbrace{\sigma^*\omega}_{\omega}(\sigma^* X_H, \cdot).$$

Since ω is non-degenerate, X_H is therefore invariant under σ, i.e.,

$$\sigma^* X_H = X_H.$$

In other words, its flow and σ commute, i.e.,

$$\varphi_H^t \circ \sigma = \sigma \circ \varphi_H^t, \tag{4.1.1}$$

and therefore

$$\gamma \in \mathrm{Fix}(\sigma).$$

b) Let ρ be an anti-symplectic symmetry which leaves γ invariant. Then we have

$$\rho^* X_H = -X_H,$$

which means that X_H is anti-invariant under ρ. Equivalently,

$$\varphi_H^t \circ \rho = \rho \circ \varphi_H^{-t}, \tag{4.1.2}$$

hence

$$\gamma(t) = \rho\big(\gamma(-t)\big), \quad t \in [0, T_\gamma], \qquad \gamma(0), \gamma(T_\gamma/2) \in \mathrm{Fix}(\rho).$$

Remark 4.1.1. Consider the standard symplectic vector space $(\mathbb{R}^{2n}, \omega_0)$ with

$$\omega_0(v, w) := \langle Jv, w\rangle = v^T J^T w = \langle v, J^T w\rangle, \qquad \text{for all } v, w \in \mathbb{R}^{2n},$$

where $J = \begin{pmatrix} 0 & I_n \\ -I_n & 0 \end{pmatrix}$ with respect to the splitting $\mathbb{R}^{2n} = \mathbb{R}^n \times \mathbb{R}^n$. Note that $J^2 = -I_{2n}$ and $J^T = J^{-1} = -J$. A linear isomorphism Ψ of $(\mathbb{R}^{2n}, \omega_0)$ is called symplectic if $\omega_0(\Psi v, \Psi w) = \omega_0(v, w)$, for all $v, w \in \mathbb{R}^{2n}$, which is equivalent to $\Psi^T J \Psi = J$. The set of symplectic matrices in $\mathbb{R}^{2n}$ is denoted by

$$\mathrm{Sp}(n) = \{\Psi \colon (\mathbb{R}^{2n}, \omega_0) \to (\mathbb{R}^{2n}, \omega_0) \text{ linear isomorphism} \mid \Psi^T J \Psi = J\}.$$

It is easy to show that if $\Psi, \Phi \in \mathrm{Sp}(n)$, then $\Psi\Phi, \Psi^{-1}, \Psi^T \in \mathrm{Sp}(n)$ and also $J \in \mathrm{Sp}(n)$. In particular, $\mathrm{Sp}(n)$ is a group under matrix multiplication. Moreover, a $2n \times 2n$ matrix which is written as

$$\begin{pmatrix} A & B \\ C & D \end{pmatrix} \tag{4.1.3}$$

with respect to the splitting $\mathbb{R}^{2n} = \mathbb{R}^n \times \mathbb{R}^n$, is symplectic if and only if

$$A^T C, B^T D \text{ are symmetric and } A^T D - C^T B = I_n. \tag{4.1.4}$$

Its inverse is given by $\begin{pmatrix} D^T & -B^T \\ -C^T & A^T \end{pmatrix}$.
The set of anti-symplectic matrices in $\mathbb{R}^{2n}$ we denote by

$$\mathrm{Sp}^-(n) = \{\Psi \colon (\mathbb{R}^{2n}, \omega_0) \to (\mathbb{R}^{2n}, \omega_0) \text{ linear isomorphism} \mid \Psi^T J \Psi = -J\},$$

which is not a group, since for $\Psi, \Phi \in \mathrm{Sp}^-(n)$ the multiplication $\Psi\Phi$ is symplectic. Nevertheless $\Psi^{-1}, \Psi^T \in \mathrm{Sp}^-(n)$ and $-J \in \mathrm{Sp}^-(n)$. A $2n \times 2n$ matrix given in the block form (4.1.3) is anti-symplectic if and only if

$$A^T C, B^T D \text{ are symmetric and } A^T D - C^T B = -I_n. \tag{4.1.5}$$

The inverse matrix is given by $\begin{pmatrix} -D^T & B^T \\ C^T & -A^T \end{pmatrix}$.

4.2 Monodromy with respect to the invariance under symplectic symmetries

Let γ be symmetric with respect to a symplectic symmetry σ. Then the differential

$$d\sigma(\gamma(0)) : T_{\gamma(0)}M \to T_{\gamma(0)}M$$

is a linear symplectic involution on the symplectic vector space $(T_{\gamma(0)}M, \omega_{\gamma(0)})$. Since the two eigenspaces $E_{\pm 1}\big(d\sigma(\gamma(0))\big)$ are symplectically orthogonal, we have the symplectic decomposition

$$T_{\gamma(0)}M = E_1\big(d\sigma(\gamma(0))\big) \oplus E_{-1}\big(d\sigma(\gamma(0))\big) = T_{\gamma(0)}\mathrm{Fix}(\sigma) \oplus E_{-1}\big(d\sigma(\gamma(0))\big).$$

Moreover, because of (4.1.1), the monodromy

$$d\varphi_H^{T_\gamma}(\gamma(0)) : T_{\gamma(0)}M \to T_{\gamma(0)}M$$

leaves the two eigenspaces invariant. Therefore the **monodromy** is of the form

$$d\varphi_H^{T_\gamma}(\gamma(0)) = \begin{pmatrix} A_1 & 0 \\ 0 & A_2 \end{pmatrix},$$

where

$$A_1 : T_{\gamma(0)}\mathrm{Fix}(\sigma) \to T_{\gamma(0)}\mathrm{Fix}(\sigma), \quad A_2 : E_{-1}\big(d\sigma(\gamma(0))\big) \to E_{-1}\big(d\sigma(\gamma(0))\big)$$

are symplectic matrices. Recall from (2.1.6) that $X_H(x_0)$ is an eigenvector of the monodromy to the double trivial eigenvalue 1, hence

$$X_H(\gamma(0)) \in T_{\gamma(0)}\mathrm{Fix}(\sigma).$$

On energy level sets Σ, which are orientable by (2.1.8), $\sigma|_\Sigma$ preserves the orientation of the line bundle $\ker\omega|_\Sigma = \langle X_H|_\Sigma\rangle$, which means that the triple $(\Sigma, \omega|_\Sigma, \sigma|_\Sigma)$ is an involutive Hamiltonian manifold. Note that

$$\dim\big(T_{\gamma(0)}\mathrm{Fix}(\sigma) \cap T_{\gamma(0)}\Sigma\big) = \dim\big(\mathrm{Fix}(\sigma)\big) - 1, \quad E_{-1}\big(d\sigma|_\Sigma(\gamma(0))\big) = E_{-1}\big(d\sigma(\gamma(0))\big).$$

Since $\gamma \in \mathrm{Fix}(\sigma|_\Sigma)$, by the Symplectic Splitting Theorem 3.1.13, we have the symplectic decomposition of the $2n-2$ dimensional symplectic vector space

$$T_{\gamma(0)}\Sigma/(\ker\omega_{\gamma(0)}|_{T_{\gamma(0)}\Sigma}) = \big(T_{\gamma(0)}\mathrm{Fix}(\sigma|_\Sigma)/(\ker\omega_{\gamma(0)}|_{T_{\gamma(0)}\Sigma})\big) \oplus \Big(E_{-1}\big(d\sigma(\gamma(0))\big)\Big),$$

and the **reduced monodromy** is of the form $\overline{d\varphi_H^{T_\gamma}|_\Sigma(\gamma(0))} = \begin{pmatrix} \overline{A}_1 & 0 \\ 0 & A_2 \end{pmatrix}$, where

$$\overline{A}_1 : T_{\gamma(0)}\mathrm{Fix}(\sigma|_\Sigma)/(\ker\omega_{\gamma(0)}|_{T_{\gamma(0)}\Sigma}) \to T_{\gamma(0)}\mathrm{Fix}(\sigma|_\Sigma)/(\ker\omega_{\gamma(0)}|_{T_{\gamma(0)}\Sigma})$$

is a linear symplectic map. Thus the Floquet multipliers are given by those of $\overline{A}_1$ and A_2. Recall that in the special case of $\overline{A}_1, A_2 \in \mathrm{Sp}(1) = \mathrm{SL}(2,\mathbb{R})$ it is not possible that the Floquet multipliers are given by four different complex numbers $\lambda, 1/\lambda, \overline{\lambda}$ and $1/\overline{\lambda}$.

4.3 Monodromy with respect to the invariance under anti-symplectic symmetries

The concept of this section is mainly based on [25].

4.3.1 Monodromy

Let γ be symmetric with respect to an anti-symplectic symmetry ρ. Then the differential

$$d\rho(\gamma(0)) : T_{\gamma(0)}M \to T_{\gamma(0)}M$$

is a linear anti-symplectic involution on the symplectic vector space $(T_{\gamma(0)}M, \omega_{\gamma(0)})$.

Lemma 4.3.1. The decomposition

$$T_{\gamma(0)}M = T_{\gamma(0)}\mathrm{Fix}(\rho) \oplus E_{-1}\big(d\rho\,(\gamma(0))\big) \tag{4.3.6}$$

is a Lagrangian splitting, meaning that the two eigenspaces are Lagrangian submanifolds, i.e., their respective dimensions are $\frac{1}{2}\dim(M) = n$ and ω vanishes on the respective tangent bundles.

Proof. Their dimensions are n in view of the isomorphism

$$T_{\gamma(0)}\mathrm{Fix}(\rho) \to E_{-1}\big(d\rho\,(\gamma(0))\big), \quad \xi + d\rho\,(\gamma(0))\,\xi \mapsto \xi - d\rho\,(\gamma(0))\,\xi$$

and the decomposition

$$T_{\gamma(0)}M \to T_{\gamma(0)}\mathrm{Fix}(\rho) \oplus E_{-1}\big(d\rho\,(\gamma(0))\big), \quad \xi \mapsto \frac{1}{2}\big(\xi + d\rho\,(\gamma(0))\,\xi\big) + \frac{1}{2}\big(\xi - d\rho\,(\gamma(0))\,\xi\big).$$

Moreover, for all $\xi, \eta \in T_{\gamma(0)}\mathrm{Fix}(\rho)$ we have

$$\omega_{\gamma(0)}(\xi,\eta) = -(\rho^*\omega)_{\gamma(0)}(\xi,\eta) = -\omega_{\rho(\gamma(0))}\big(d\rho\,(\gamma(0))\,\xi, d\rho\,(\gamma(0))\,\eta\big) = -\omega_{\gamma(0)}(\xi,\eta),$$

hence $\omega_{\gamma(0)}(\xi,\eta) = 0$. The same holds for all $\xi, \eta \in E_{-1}\big(d\rho\,(\gamma(0))\big)$. □

The existence of a symplectic (or canonical) basis for a symplectic vector space is given by a skew-symmetric version of the Gram–Schmidt process (see for instance [42, pp. 3–4]). Similarly, in view of the Lagrangian splitting (4.3.6), there exist bases

$$\{v_1, ..., v_n\} \text{ of } T_{\gamma(0)}\mathrm{Fix}(\rho), \quad \{w_1, ..., w_n\} \text{ of } E_{-1}\big(d\rho\,(\gamma(0))\big) \tag{4.3.7}$$

such that

$$\omega_{x_0}(v_i, w_j) = \delta_{ij}, \quad \text{for } i, j = 1, ..., n,$$

and $\{v_1, ..., v_n, w_1, ..., w_n\}$ is a symplectic basis of $T_{\gamma(0)}M$ (see for instance [3, pp. 532–533]). We refer to this kind of basis as **Lagrangian basis**. With respect to this basis the differential $d\rho\,(\gamma(0))$ is represented by the standard anti-symplectic involution $\rho_0 = \begin{pmatrix} I_n & 0 \\ 0 & -I_n \end{pmatrix}$.

Proposition 4.3.2 (The monodromy). The monodromy, with respect to a Lagrangian basis, written in block form (4.1.3) has the form

$$d\varphi_H^{T_\gamma}(\gamma(0)) = \begin{pmatrix} A & B \\ C & A^T \end{pmatrix}, \tag{4.3.8}$$

where

$$B, C, CA, AB \text{ are symmetric and } A^2 - BC = I_n. \tag{4.3.9}$$

Proof. In view of (4.1.2) we get

$$d\rho\,(\gamma(0)) \circ d\varphi_H^{T_\gamma}(\gamma(0)) \circ d\rho\,(\gamma(0)) = \big(d\varphi_H^{T_\gamma}(\gamma(0))\big)^{-1}, \tag{4.3.10}$$

which means that the monodromy is conjugated to its inverse by the linear anti-symplectic involution. With respect to the choice of a Lagrangian basis (4.3.7) and the monodromy written

in block form (4.1.3), the equation (4.3.10) becomes

$$\begin{pmatrix} I_n & 0 \\ 0 & -I_n \end{pmatrix} \begin{pmatrix} A & B \\ C & D \end{pmatrix} \begin{pmatrix} I_n & 0 \\ 0 & -I_n \end{pmatrix} = \begin{pmatrix} D^T & -B^T \\ -C^T & A^T \end{pmatrix} \quad \Leftrightarrow \quad \begin{pmatrix} A & -B \\ -C & D \end{pmatrix} = \begin{pmatrix} D^T & -B^T \\ -C^T & A^T \end{pmatrix}.$$

Now the statement follows by (4.1.4). □

Lemma 4.3.3. All linear anti-symplectic involutions are symplectically conjugated to each other.

Proof. Let ρ_1, ρ_2 be linear anti-symplectic involutions, $\{v_1, ..., v_n, w_1, ...w_n\}$ and $\{\tilde{v}_1, ..., \tilde{v}_n, \tilde{w}_1, ...\tilde{w}_n\}$ be Lagrangian bases, respectively. Then the basis change is given by the linear symplectic map

$$v_i \mapsto \tilde{v}_i, \quad w_i \mapsto \tilde{w}_i, \quad i = 1, ..., n.$$ □

Corollary 4.3.4. Every linear anti-symplectic involution is symplectically conjugated to the standard anti-symplectic involution ρ_0.

We denote the set of symplectic matrices of the form (4.3.8) satisfying (4.3.9) by

$$\widetilde{\mathrm{Sp}}(n) = \left\{ \begin{pmatrix} A & B \\ C & A^T \end{pmatrix} : B, C, CA, AB \text{ are symmetric and } A^2 - BC = I_n \right\}.$$

The next lemma generalizes Proposition 4.3.2.

Lemma 4.3.5. Every symplectic matrix $\Psi \in \mathrm{Sp}(n)$ is symplectically conjugated to a symplectic matrix from $\widetilde{\mathrm{Sp}}(n)$.

Proof. By a theorem of Wonenburger [60], every $\Psi \in \mathrm{Sp}(n)$ is the product of two linear anti-symplectic involutions, i.e.,

$$\Psi = \rho_1 \rho_2,$$

where ρ_1, ρ_2 are linear anti-symplectic involutions. Hence

$$\Psi^{-1} = \rho_2 \rho_1 = \rho_1 \Psi \rho_1,$$

which is a general form of the equation (4.3.10). By Corollary 4.3.4, there exists $\Psi_1 \in \mathrm{Sp}(n)$ such that

$$\Psi_1^{-1} \rho_1 \Psi_1 = \rho_0.$$

This implies

$$\Psi_1^{-1} \Psi \Psi_1 = \Psi_1^{-1} (\rho_1 \rho_2) \Psi_1 = \Psi_1^{-1} (\Psi_1 \rho_0 \Psi_1^{-1}) \rho_2 \Psi_1 = \rho_0 \Psi_1^{-1} \rho_2 \Psi_1. \tag{4.3.11}$$

One readily checks that $\Psi_1^{-1} \rho_2 \Psi_1$ is a linear anti-symplectic involution, thus Ψ is symplectically conjugated to the product of two linear anti-symplectic involutions as well. In addition, the equation (4.3.11) implies

$$(\Psi_1^{-1} \Psi \Psi_1)^{-1} = \Psi_1^{-1} \rho_2 \Psi_1 \rho_0 = \rho_0 (\Psi_1^{-1} \Psi \Psi_1) \rho_0,$$

i.e., the symplectic conjugacy $\Psi_1^{-1} \Psi \Psi_1$ is conjugated to its inverse by the standard anti-symplectic involution ρ_0. Therefore by the same steps as in the proof of Proposition 4.3.2, we have

$$\Psi_1^{-1} \Psi \Psi_1 \in \widetilde{\mathrm{Sp}}(n).$$ □

Remark 4.3.6 (**The reduced monodromy**). Since X_H is anti-invariant under ρ, we have

$$X_H(\gamma(0)) \in E_{-1}\big(d\rho(\gamma(0))\big).$$

On energy level sets Σ, the restriction $T_{\gamma(0)}\mathrm{Fix}(\rho|_\Sigma)$ is $n-1$ dimensional, and on the quotient by the line bundle $\ker\omega|_\Sigma = \langle X_H|_\Sigma\rangle$ we obtain the splitting

$$T_{\gamma(0)}\Sigma/(\ker\omega_{\gamma(0)}|_{T_{\gamma(0)}\Sigma}) = \big(T_{\gamma(0)}\mathrm{Fix}(\rho|_\Sigma)\big) \oplus \Big(E_{-1}\big(d\rho|_\Sigma(\gamma(0))\big)/(\ker\omega_{\gamma(0)}|_{T_{\gamma(0)}\Sigma})\Big).$$

By using the Lagrangian basis $\{v_1,...,v_n,w_1,...,w_n\}$ from (4.3.7), $n-1$ basis vectors of the first vector space are determined by $\{v_1,...,v_n\}$ and the energy condition. We denote them by $\{\tilde v_1,...,\tilde v_{n-1}\}$. By the Steinitz exchange lemma on $\{w_1,...,w_n\}$ and $X_H|_\Sigma(\gamma(0))$ we choose $\{\tilde w_1,...,\tilde w_{n-1}\}$ such that $\omega_{x_0}(\tilde v_i,\tilde w_j)=\delta_{ij}$, for $i,j=1,...,n-1$, and

$$T_{x_0}\Sigma = \langle \tilde v_1,...,\tilde v_{n-1}\rangle_{\mathbb{R}} \oplus \langle \tilde w_1,...,\tilde w_{n-1}, X_H|_\Sigma(x_0)\rangle_{\mathbb{R}}.$$

With respect to this basis, the reduced monodromy is an element from $\widetilde{\mathrm{Sp}}(n-1)$.

4.3.2 The signatures of a symmetric periodic orbit

Let the monodromy be a symplectic matrix from $\widetilde{\mathrm{Sp}}(n)$, then the following lemma shows that its spectrum is determined by the spectrum of A.

Lemma 4.3.7. The characteristic polynomial of the monodromy equals

$$\lambda^n \det\big(-2A-(-\lambda-\frac{1}{\lambda})I_n\big),$$

i.e., $\lambda^n\chi_{-2A}(-\lambda-\frac{1}{\lambda})$.

Proof. The decomposition

$$\begin{pmatrix} A-\lambda I_n & B \\ C & A^T-\lambda I_n\end{pmatrix}\begin{pmatrix} A-\lambda I_n & 0 \\ -C & I_n\end{pmatrix} = \begin{pmatrix} \lambda^2 I_n - 2\lambda A + I_n & B \\ 0 & A^T-\lambda I_n\end{pmatrix}$$

implies that the characteristic polynomial of the monodromy is given by

$$\det(\lambda^2 I_n - 2\lambda A + I_n),$$

which is equivalent to $\lambda^n\det\big(-2A-(-\lambda-\frac{1}{\lambda})I_n\big)$. □

Remark 4.3.8. In the case $n=1$, i.e.,

$$d\varphi_H^{T_x}(x_0) = \begin{pmatrix} a & b \\ c & a\end{pmatrix}, \quad a^2-bc=1,$$

where $a,b,c\in\mathbb{R}$, we have for its characteristic polynomial,

$$\lambda^2 - 2a\lambda + 1.$$

Note that a is the half of its trace. For the case $n=2$ we obtain

$$\lambda^4 - 2\mathrm{tr}A\lambda^3 + (2+4\det A)\lambda^2 - 2\mathrm{tr}A\lambda + 1.$$

Remark 4.3.9 (**Change of basis**). If a Lagrangian basis (4.3.7) is given, then $R \in \mathrm{GL}(n,\mathbb{R})$ acts on $\widetilde{\mathrm{Sp}}(n)$ by conjugation

$$\begin{pmatrix} R & 0 \\ 0 & (R^{-1})^T \end{pmatrix} \begin{pmatrix} A & B \\ C & A^T \end{pmatrix} \begin{pmatrix} R^{-1} & 0 \\ 0 & R^T \end{pmatrix} = \begin{pmatrix} RAR^{-1} & RBR^T \\ (R^{-1})^T C R^{-1} & (RAR^{-1})^T \end{pmatrix}.$$

Notice that the matrix A transforms as linear maps, and the matrices B and C transform as bilinear forms. Moreover, this basis change is symplectic, since

$$\begin{pmatrix} R^T & 0 \\ 0 & R^{-1} \end{pmatrix} \begin{pmatrix} 0 & I_n \\ -I_n & 0 \end{pmatrix} \begin{pmatrix} R & 0 \\ 0 & (R^{-1})^T \end{pmatrix} = \begin{pmatrix} 0 & I_n \\ -I_n & 0 \end{pmatrix}.$$

Definition 4.3.10. Let λ be an eigenvalue of A of multiplicity 1, v an eigenvector of A and $\tilde{v}$ an eigenvector of A^T to the eigenvalue λ. The ***C*-signature** of γ is defined as the signature of $v^T C v$ and the ***B*-signature** of γ as the signature of $\tilde{v}^T B \tilde{v}$. We denote them by

$$\mathrm{sign}_C(\lambda) = \mathrm{sign}(v^T C v), \quad \mathrm{sign}_B(\lambda) = \mathrm{sign}(\tilde{v}^T B \tilde{v}),$$

respectively.

Remark 4.3.11. Neither of the signatures depends on the resp. eigenvectors, since for a constant $k \in \mathbb{R}^*$,

$$\mathrm{sign}\big((kv)^T C (kv)\big) = k^2 \mathrm{sign}(v^T C v) = \mathrm{sign}(v^T C v) = \mathrm{sign}_C(\lambda).$$

Proposition 4.3.12 (**Invariance of signature**). Both signatures of γ are invariant under the change of basis given in Remark 4.3.9 , i.e., they are independent of the choice of the Lagrangian basis.

Proof. For the invariance of $\mathrm{sign}_C(\lambda)$ we consider the identity

$$AR^{-1}Rv = Av = \lambda v,$$

thus

$$RAR^{-1}Rv = \lambda Rv,$$

meaning that Rv is an eigenvector of RAR^{-1} to the eigenvalue λ. In view of the transformations

$$C \mapsto (R^{-1})^T C R^{-1}, \quad A \mapsto RAR^{-1}, \quad v \mapsto Rv,$$

we have

$$\mathrm{sign}\big((Rv)^T (R^{-1})^T C R^{-1} (Rv)\big) = \mathrm{sign}(v^T C v) = \mathrm{sign}_C(\lambda).$$

For $\mathrm{sign}_B(\lambda)$ we consider

$$A^T R^T (R^{-1})^T \tilde{v} = A^T \tilde{v} = \lambda \tilde{v}$$

and therefore

$$(R^{-1})^T A^T R^T (R^{-1})^T \tilde{v} = \lambda (R^{-1})^T \tilde{v},$$

which means that $(R^{-1})^T \tilde{v}$ is an eigenvector of $(R^{-1})^T A^T R^T$ to the eigenvalue λ. In view of

$$B \mapsto RBR^T, \quad A^T \mapsto (R^T)^{-1} A^T R^T, \quad \tilde{v} \mapsto (R^{-1})^T \tilde{v},$$

we obtain

$$\mathrm{sign}\Big(\big((R^{-1})^T \tilde{v}\big)^T RBR^T (R^{-1})^T \tilde{v}\Big) = \mathrm{sign}(\tilde{v}^T B \tilde{v}) = \mathrm{sign}_B(\lambda). \qquad \square$$

Remark 4.3.13. In the case $n = 1$, scaling on the Lagrangian yields

$$\begin{pmatrix} k & 0 \\ 0 & \frac{1}{k} \end{pmatrix} \begin{pmatrix} a & b \\ c & a \end{pmatrix} \begin{pmatrix} \frac{1}{k} & 0 \\ 0 & k \end{pmatrix} = \begin{pmatrix} a & k^2 b \\ \frac{1}{k^2} c & a \end{pmatrix}, \quad k \in \mathbb{R}^* = \mathrm{GL}(1, \mathbb{R}).$$

Note that the trace is invariant as well under conjugation.

4.4 Monodromy if the symplectic & anti-symplectic symmetries commute

Let γ be symmetric with respect to a symplectic symmetry σ and an anti-symplectic symmetry ρ, then recall that

$$\gamma \in \mathrm{Fix}(\sigma), \quad \gamma(0) \in \mathrm{Fix}(\rho).$$

Assume that

$$\sigma \circ \rho = \rho \circ \sigma$$

and consider the symplectic decomposition

$$T_{\gamma(0)} M = T_{\gamma(0)} \mathrm{Fix}(\sigma) \oplus E_{-1}\big(d\sigma(\gamma(0))\big).$$

Moreover, let

$$\dim\big(T_{\gamma(0)} \mathrm{Fix}(\sigma)\big) = 2k, \quad \dim\Big(E_{-1}\big(d\sigma(\gamma(0))\big)\Big) = 2\tilde{k}, \quad 2k + 2\tilde{k} = 2n.$$

Lemma 4.4.1. The monodromy is of the form

$$d\varphi_H^{T_\gamma}(\gamma(0)) = \begin{pmatrix} A_1 & 0 \\ 0 & A_2 \end{pmatrix},$$

where

$$\begin{aligned} &A_1 \colon T_{\gamma(0)} \mathrm{Fix}(\sigma) \to T_{\gamma(0)} \mathrm{Fix}(\sigma), && A_1 \in \widetilde{\mathrm{Sp}}(k), \\ &A_2 \colon E_{-1}\big(d\sigma(\gamma(0))\big) \to E_{-1}\big(d\sigma(\gamma(0))\big), && A_2 \in \widetilde{\mathrm{Sp}}(\tilde{k}). \end{aligned}$$

Proof. Since σ and ρ commute, the linear anti-symplectic involution

$$d\rho(\gamma(0)) : T_{\gamma(0)} M \to T_{\gamma(0)} M$$

leaves the symplectic decomposition

$$T_{\gamma(0)} M = T_{\gamma(0)} \mathrm{Fix}(\sigma) \oplus E_{-1}\big(d\sigma(\gamma(0))\big)$$

invariant. If we denote

$$E_1^{d\sigma} := T_{\gamma(0)} \mathrm{Fix}(\sigma), \quad E_{-1}^{d\sigma} := E_{-1}\big(d\sigma(\gamma(0))\big),$$

this invariance implies that each of the restriction

$$d\rho|_{E_1^{d\sigma}}(\gamma(0)) : E_1^{d\sigma} \to E_1^{d\sigma}, \quad d\rho|_{E_{-1}^{d\sigma}}(\gamma(0)) : E_{-1}^{d\sigma} \to E_{-1}^{d\sigma}$$

is a linear anti-symplectic involution. Hence the symplectic decomposition splits into two Lagrangian splittings, meaning that

$$T_{\gamma(0)}\mathrm{Fix}(\sigma) = E_1^{d\sigma} = \Big(E_1\big(d\rho|_{E_1^{d\sigma}}(\gamma(0))\big) \oplus E_{-1}\big(d\rho|_{E_1^{d\sigma}}(\gamma(0))\big)\Big)$$
$$E_{-1}\big(d\sigma(\gamma(0))\big) = E_{-1}^{d\sigma} = \Big(E_1\big(d\rho|_{E_{-1}^{d\sigma}}(\gamma(0))\big) \oplus E_{-1}\big(d\rho|_{E_{-1}^{d\sigma}}(\gamma(0))\big)\Big),$$

with Lagrangian bases $\{v_1, ..., v_k, w_1, ..., w_k\}$ resp. $\{\tilde{v}_1, ..., \tilde{v}_{\tilde{k}}, \tilde{w}_1, ..., \tilde{w}_{\tilde{k}}\}$. In view of Section 4.3.1, this proves the lemma. □

Remark 4.4.2. The two Lagrangian bases from the proof give a Lagrangian basis

$$\{v_1, ..., v_k, \tilde{v}_1, ..., \tilde{v}_{\tilde{k}}, w_1, ..., w_k, \tilde{w}_1, ..., \tilde{w}_{\tilde{k}}\}$$

on $T_{\gamma(0)}M$ with respect to the Lagrangian splitting

$$T_{\gamma(0)}M = T_{\gamma(0)}\mathrm{Fix}(\rho) \oplus E_{-1}\big(d\rho(\gamma(0))\big),$$

where

$$T_{\gamma(0)}\mathrm{Fix}(\rho) = \Big(E_1\big(d\rho|_{E_1^{d\sigma}}(\gamma(0))\big) \oplus E_1\big(d\rho|_{E_{-1}^{d\sigma}}(\gamma(0))\big)\Big)$$
$$E_{-1}\big(d\rho(\gamma(0))\big) = \Big(E_{-1}\big(d\rho|_{E_1^{d\sigma}}(\gamma(0))\big) \oplus E_{-1}\big(d\rho|_{E_{-1}^{d\sigma}}(\gamma(0))\big)\Big).$$

Remark 4.4.3. In view of Remark 4.3.6, the reduced monodromy is of the form

$$\overline{d\varphi_H^{T_\gamma}|_\Sigma(\gamma(0))} = \begin{pmatrix} \overline{A}_1 & 0 \\ 0 & A_2 \end{pmatrix},$$

where $\overline{A}_1$ is a linear symplectic map on $T_{\gamma(0)}\mathrm{Fix}(\sigma|_\Sigma)/(\ker\omega_{\gamma(0)}|_{T_{\gamma(0)}\Sigma})$ with $\overline{A}_1 \in \widetilde{\mathrm{Sp}}(k-1)$.

4.5 GIT quotient specifies Floquet multipliers, stability and index

Let G be a Lie group, i.e., G is a group and a smooth manifold such that

$$G \to G, \quad g \mapsto g^{-1}, \qquad G \times G \to G, \quad (g,h) \mapsto gh$$

are smooth. Let G act on a manifold M, meaning that there is a group homomorphism $\psi\colon G \to \mathrm{Diff}(M)$ such that

$$G \times M \to M, \quad (g,m) \mapsto \psi(g)(m) =: g_*m$$

is smooth. For any $m \in M$ the orbit through m is the set

$$Gm = \{g_*m \mid g \in G\}.$$

If m and n lie in the same orbit, then $Gm = Gn$. Moreover, M can be written as the disjoint union of orbits and the space of orbits is the quotient space M/G which is in general not a Hausdorff space. To ensure the Hausdorff property we consider the orbit closure relation on M which is

defined by

$$m \sim n \quad :\Leftrightarrow \quad \overline{Gm} \cap \overline{Gn} \neq \emptyset,$$

meaning that m is related to n if the closure of the orbits through m and n intersect. It is clear that this relation is reflexive and symmetric, but it is not necessarily transitive. If it is an equivalence relation, then the **GIT quotient** (geometric invariant theory quotient) is defined as

$$M//G := M/\sim .$$

Example 4.5.1. Let $\mathbb{R}_{>0}$ acting on $\mathbb{R}$ by multiplication, then there are exactly the three orbits $\mathbb{R}^-, \{0\}$ and $\mathbb{R}^+$. It is easy to verify that on the one hand the orbit space is not Hausdorff, but on the other hand the GIT quotient is

$$\mathbb{R}//\mathbb{R}_{>0} = \{\text{pt.}\}.$$

Example 4.5.2. Let $\mathrm{GL}(n,\mathbb{R})$ act on $\mathrm{Mat}(n,\mathbb{R})$ by conjugation. The GIT quotient avoids Jordan factors, therefore two matrices A, B are equivalent if and only if their characteristic polynomials are the same (see [25, Appendix A] for details). For a matrix A let $\chi_A(\lambda) = \lambda^n + a_{n-1}\lambda^{n-1} + ... + a_0$ be its characteristic polynomial. Then a homeomorphism is given by

$$\mathrm{Mat}(n,\mathbb{R})//\mathrm{GL}(n,\mathbb{R}) \to \mathbb{R}^n, \quad [A] \mapsto (a_{n-1}, ..., a_0).$$

Example 4.5.3. For this paper the relevant GIT quotient is

$$\widetilde{\mathrm{Sp}}(1)//\mathrm{GL}(1,\mathbb{R}),$$

which is well studied in [61, pp. 25–28]. Let $A \in \widetilde{\mathrm{Sp}}(1)$, i.e., $A = \begin{pmatrix} a & b \\ c & a \end{pmatrix}$, $a^2 - bc = 1$, and recall from Section 2.2 that the eigenvalues in the elliptic and hyperbolic case are resp. given by

$$a \pm \mathrm{i}\sqrt{(1-a^2)}, \quad a \pm \sqrt{(a^2-1)}.$$

Each of the positive and negative hyperbolic cases consists of two subcases, namely

pos. hyperb. I	pos. hyperb. II	neg. hyperb. I	neg. hyperb. II
$\begin{pmatrix} a>1 & b<0 \\ c<0 & a>1 \end{pmatrix}$	$\begin{pmatrix} a>1 & b>0 \\ c>0 & a>1 \end{pmatrix}$	$\begin{pmatrix} a<-1 & b>0 \\ c>0 & a<-1 \end{pmatrix}$	$\begin{pmatrix} a<-1 & b<0 \\ c<0 & a<-1 \end{pmatrix}$

Furthermore, recall from Remark 4.3.13 that the action is given by

$$k_*A := \begin{pmatrix} a & k^2 b \\ \frac{1}{k^2}c & a \end{pmatrix}, \quad k \in \mathbb{R}^*.$$

Note that $A_1, A_2 \in \widetilde{\mathrm{Sp}}(1)$ are equivalent in the GIT quotient if and only if $\overline{k_*A_1} \cap \overline{k_*A_2} \neq \emptyset$.

If A is non-degenerate, i.e., 1 is not an eigenvalue, and $b \neq 0, c \neq 0$, then one can always choose k such that $k^2 b = \pm\frac{1}{k^2}c$.

If A is elliptic, then A is equivalent to a rotation of $\mathbb{R}^2$ of the form $\begin{pmatrix} \cos\theta & -\sin\theta \\ \sin\theta & \cos\theta \end{pmatrix}$.

If A is hyperbolic, then A is equivalent to

$$\begin{pmatrix} a & \pm\sqrt{(a^2-1)} \\ \pm\sqrt{(a^2-1)} & a \end{pmatrix}, \quad a > 1 \text{ or } a < -1.$$

Obviously, the identity matrix lies in the closure of the orbits of

$$\begin{pmatrix} 1 & \pm b \\ 0 & 1 \end{pmatrix}, \quad \begin{pmatrix} 1 & 0 \\ \pm b & 1 \end{pmatrix}, \quad b > 0,$$

hence these three matrices are equivalent in the GIT quotient and identified to the single point $\{+1\}$.

The same holds for the matrices replacing 1 in the diagonals by -1, which we identify to the single point $\{-1\}$.

Topologically, the GIT quotient $\widetilde{\mathrm{Sp}}(1)//\mathrm{GL}(1,\mathbb{R})$ is isomorphic to a circle with four spikes (see Figure 4.1). Geometrically, the unit circle $\{z \in \mathbb{C} \mid |z| = 1\}\backslash\{\pm 1\}$ corresponds to equivalence classes of elliptic matrices, and each spike minus $\{\pm 1\}$ represents a hyperbolic subcase.

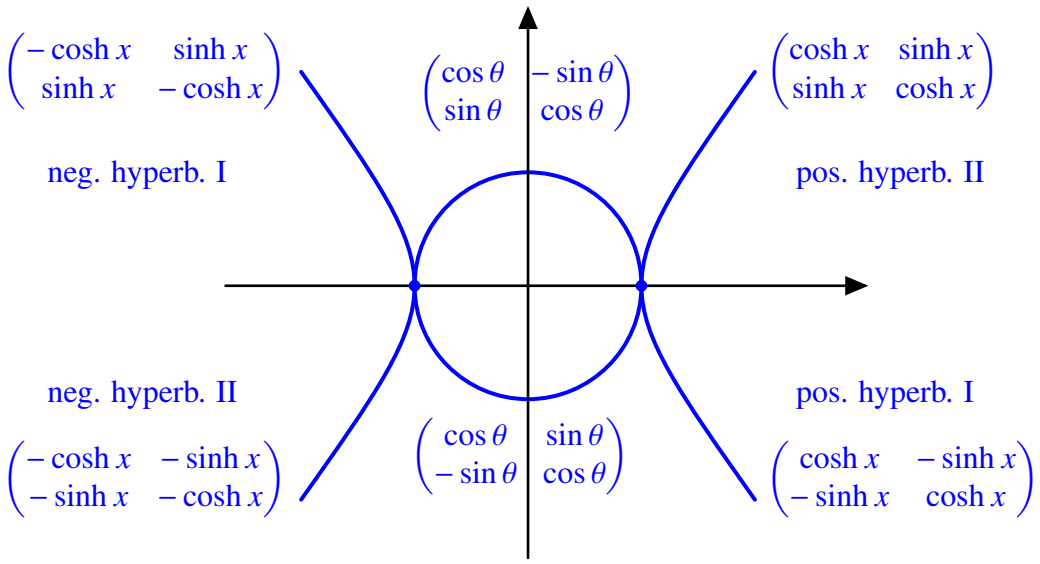

Figure 4.1: Topology of $\widetilde{\mathrm{Sp}}(1)//\mathrm{GL}(1,\mathbb{R})$.

Note that

a) the eigenvalues of the hyperbolic matrices are $e^{\pm x}$ for the pos. hyperb. and $-e^{\pm x}$ for the neg. hyperb. cases, which equal the Floquet multipliers λ and $1/\lambda$.
b) In the elliptic case, if $b < 0$, then the rotation is by $\theta \in (0,\pi)$ and if $b > 0$, then it is by $-\theta$, so the rotation angle equals $2\pi - \theta \in (\pi, 2\pi)$.
c) In view of Figure 2.6, we can decide in stability transitions how the index jumps (i.e., how the eigenvalue 1 is crossed, from above or from below), by using a Lagrangian basis for the monodromy and calculating the Floquet multipliers and its signatures.

5 On the spatial Hill three-body problem

"*It is an interesting evidence of the appreciation of Hill's abilities that when Professor R. S. Woodward introduced him to Poincaré the first words the latter said as he took his hand were "You are the one man I came to America to see." "*

- J. Ginsburg and D. E. Smith in [28, pp. 130–131] (1934)

5.1 The Hamiltonian

In the restricted three-body problem one considers two bodies, which we call Sun and Earth, and a massless body, called Moon, which does not influence the two bodies and is attracted by them according to Newton's law of gravitation. Note that this assumption is a good approximation of the actual system in view of the relations given in Table 1.2. The goal is to understand the dynamics of the Moon.

Denote by Δ the set of positions at which the Moon can collide with. Then the configuration space is $\mathbb{R}^3 \setminus \Delta$ and the phase space is the trivial cotangent bundle $T^*\left(\mathbb{R}^3 \setminus \Delta\right) = \left(\mathbb{R}^3 \setminus \Delta\right) \times \mathbb{R}^3$ with the canonical symplectic form $\omega = \sum dq_i \wedge dp_i$. Let $q = (q_1, q_2, q_3)$ denote the position of the Moon and $p = (p_1, p_2, p_3)$ its momentum in the fiber. Furthermore, the total mass is normalized to unity, i.e., the mass of the Earth is $\mu \in [0, 1]$ and that of the Sun is $1 - \mu$. The two bodies, denoted by $s(t)$ and $e(t)$, move on circles in the ecliptic (see Figure 5.1) with common center of mass with coordinates

$$s(t) = -\mu(\cos t, \sin t, 0), \quad e(t) = (1 - \mu)(\cos t, \sin t, 0).$$

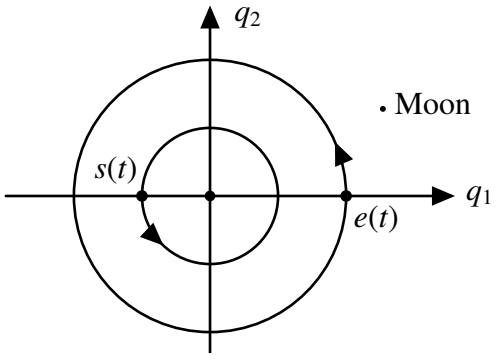

Figure 5.1: Planar circular restricted three body problem.

Denote by E the Hamiltonian in the inertial frame of the Moon, which is given by the kinetic energy and Newton's potential. Since E depends on time, the energy is not preserved by the Hamiltonian flow. Therefore we consider the angular momentum

$$L\colon T^*\mathbb{R}^3 \to \mathbb{R}, \quad (q, p) \mapsto p_1 q_2 - p_2 q_1 \tag{5.1.1}$$

whose vector field X_L generates a clockwise rotation of the ecliptic and its flow leaves E invariant. Hence the Hamiltonian

$$L(q, p) + E\left((\varphi_L^t)^{-1}(q, p)\right),$$

which reads

$$T^*\left(\mathbb{R}^3 \setminus \Delta\right) \to \mathbb{R}, \quad (q,p) \mapsto \frac{1}{2}|p|^2 - \frac{1-\mu}{|q-s|} - \frac{\mu}{|q-e|} + p_1q_2 - p_2q_1,$$

is autonomous and thus preserved along its flow. Note that its flow equals $\varphi_L^t \circ \varphi_E^t$ (see [27, pp. 59–60] for details). In this new coordinate system, we now have a uniform counterclockwise rotation of the coordinate system such that the sun and the earth are fixed at

$$s = (-\mu, 0, 0), \quad e = (1-\mu, 0, 0)$$

on the q_1-axis in the rotating frame. This first integral is due to Jacobi. In the limit case of Hill's system the Sun has a much bigger mass than the Earth and the Earth a much bigger mass than the Moon. In addition, the Moon moves very close to the Earth. The goal is to shift the Earth into the origin, blow up the coordinates around it and and let its mass μ tend to zero. Therefore we zoom into a region around the Earth by pushing the huge Sun off to infinity (see Figure 1.3).

The symplectic change of coordinates and momenta

$$T^*\mathbb{R}^3 \to T^*\mathbb{R}^3, \quad (q,p) \mapsto (q_1 - 1 + \mu, q_2, q_3, p_1, p_2 - 1 + \mu, p_3)$$

puts the Earth to the origin and the Sun to $(-1,0,0)$. For simplicity of notation, we denote the new coordinates again by (q,p). By adding the constant $\frac{(1-\mu)^2}{2}$, which does not change the Hamiltonian vector field, we obtain the new Hamiltonian $\widetilde{H}$ on $T^*\left(\mathbb{R}^3 \setminus \{(-1,0,0),(0,0,0)\}\right)$,

$$\begin{aligned}\widetilde{H}(q,p) &= \frac{1}{2}\left(p_1^2 + (p_2+1-\mu)^2 + p_3^2\right) - \frac{1-\mu}{\sqrt{(q_1+1)^2+q_2^2+q_3^2}} - \frac{\mu}{q_1^2+q_2^2+q_3^2} \\ &\quad + p_1q_2 - (p_2+1-\mu)(q_1+1-\mu) + \frac{(1-\mu)^2}{2} \\ &= \frac{1}{2}|p|^2 - \frac{\mu}{|q|} - (1-\mu)\left(\frac{1}{\sqrt{(q_1+1)^2+q_2^2+q_3^2}} + q_1\right) + p_1q_2 - p_2q_1.\end{aligned}$$

Now consider the conformally symplectic scaling (the blow up)

$$\phi_\mu \colon T^*\mathbb{R}^3 \to T^*\mathbb{R}^3, \quad (q,p) \mapsto (\mu^{\frac{1}{3}}q, \mu^{\frac{1}{3}}p)$$

by the constant conformal factor $\mu^{\frac{2}{3}}$, i.e., $\phi_\mu^*\omega = \mu^{\frac{2}{3}}\omega$. We define the family of Hamiltonians

$$H^\mu \colon T^*\left(\mathbb{R}^3 \setminus \{(-\mu^{-\frac{1}{3}},0,0),(0,0,0)\}\right) \to \mathbb{R}, \quad (q,p) \mapsto \mu^{-\frac{2}{3}}\left((\tilde{H}\circ\phi_\mu)(q,p) + 1 - \mu\right).$$

Then $\phi_\mu^* X_{\widetilde{H}} = X_{H^\mu}$ and, in explicit form,

$$H^\mu(q,p) = \frac{1}{2}|p|^2 - \frac{1}{|q|} + p_1q_2 - p_2q_1 - \frac{1-\mu}{\mu^{\frac{2}{3}}}\left(\frac{1}{\sqrt{1+2\mu^{\frac{1}{3}}q_1+\mu^{\frac{2}{3}}|q|^2}} + \mu^{\frac{1}{3}}q_1 - 1\right).$$

We simplify H^μ by using the second order Taylor expansion of the function

$$\frac{1}{\sqrt{1+x}} = 1 - \frac{x}{2} + \frac{3x^2}{8} + O(x^3)$$

for $|x| < 1$. By setting $x = 2\mu^{\frac{1}{3}} q_1 + \mu^{\frac{2}{3}}|q|^2$, we obtain

$$H^\mu(q,p) = \frac{1}{2}|p|^2 - \frac{1}{|q|} + p_1 q_2 - p_2 q_1 - \left(-\frac{1}{2}|q|^2 + \frac{3}{2}q_1^2 + O(\mu) \right).$$

For $\mu \to 0$, H^μ converges uniformly in the C^∞-topology on each compact subset to the following Hamiltonian H, which is the **Hamiltonian of the spatial Hill three-body problem** given by

$$H\colon T^*\big(\mathbb{R}^3 \setminus \{(0,0,0)\}\big) \to \mathbb{R}, \quad (q,p) \mapsto \underbrace{\frac{1}{2}|p|^2 - \frac{1}{|q|} + p_1 q_2 - p_2 q_1}_{\text{rotating Kepler problem}} - q_1^2 + \frac{1}{2}q_2^2 + \frac{1}{2}q_3^2. \quad (5.1.2)$$

Recall that the restriction of the spatial system to $\{q_3 = p_3 = 0\}$ gives the planar problem. To understand the physics, we complete the squares and obtain

$$H\colon T^*\big(\mathbb{R}^3 \setminus \{(0,0,0)\}\big) \to \mathbb{R}, \quad (q,p) \mapsto \frac{1}{2}\big((p_1+q_2)^2 + (p_2-q_1)^2 + p_3^2\big) + V(q), \quad (5.1.3)$$

where the effective potential only depends on the position and is defined as

$$V\colon \mathbb{R}^3 \setminus \{(0,0,0)\} \to \mathbb{R}, \quad q \mapsto -\frac{1}{|q|} - \frac{3}{2}q_1^2 + \frac{1}{2}q_3^2.$$

We see that the Hamiltonian (5.1.2) consists of the rotating Kepler problem (Earth–Moon) with a velocity independent gravitational perturbation produced by the massive body (Sun). In view of (5.1.3), in the kinetic part is a twist corresponding to the Coriolis force, which depends on the velocity. The effective potential consists of the Newtonian potential for the Earth and the term $-\frac{3}{2}q_1^2 + \frac{1}{2}q_3^2$. The term $-\frac{3}{2}q_1^2$ is what is left in the limit of the gravitational force and the centrifugal force by the huge Sun infinitely far away. The spatial term $\frac{1}{2}q_3^2$ is the left over of the gravitational force of the Sun, which is a strong attraction back to the ecliptic.

Since we work with symplectic coordinates, we treat the spatial Hill equation in (q,p)-coordinates given by

$$\begin{cases} \dot{q}_1 = p_1 + q_2, & \dot{p}_1 = p_2 - q_1 - \dfrac{\partial V}{\partial q_1}, \\ \dot{q}_2 = p_2 - q_1, & \dot{p}_2 = -p_1 - q_2 - \dfrac{\partial V}{\partial q_2}, \\ \dot{q}_3 = p_3, & \dot{p}_3 = -\dfrac{\partial V}{\partial q_3}. \end{cases} \quad (5.1.4)$$

The equation (5.1.4) is equivalent, via the transformations $\ddot{q}_1 = \dot{p}_1 + \dot{q}_2, \ddot{q}_2 = \dot{p}_2 - \dot{q}_1, \ddot{q}_3 = \dot{p}_3$, to the equation in $(q,\dot{q})$-coordinates given by

$$\begin{pmatrix} \ddot{q}_1 \\ \ddot{q}_2 \\ \ddot{q}_3 \end{pmatrix} + 2 \begin{pmatrix} 0 & -1 & 0 \\ 1 & 0 & 0 \\ 0 & 0 & 0 \end{pmatrix} \cdot \begin{pmatrix} \dot{q}_1 \\ \dot{q}_2 \\ \dot{q}_3 \end{pmatrix} + \nabla V(q) = 0 \quad \Leftrightarrow \quad \begin{cases} \ddot{q}_1 = 2\dot{q}_2 + 3q_1 - \dfrac{q_1}{|q|^3} \\ \ddot{q}_2 = -2\dot{q}_1 - \dfrac{q_2}{|q|^3} \\ \ddot{q}_3 = -q_3\left(\dfrac{1}{|q|^3} + 1\right) \end{cases}$$

To compute the monodromy we linearize the equation (5.1.4) along a periodic orbit, i.e., we

expand $(q+\Delta q, p+\Delta p)$ near (q,p) and obtain the linearized equation

$$\begin{cases} \Delta\dot{q}_1 = \Delta p_1 + \Delta q_2, & \Delta\dot{p}_1 = \Delta p_2 - \Delta q_1 - (\mathrm{H}_V(q)\cdot\Delta q)_1\,, \\ \Delta\dot{q}_2 = \Delta p_2 - \Delta q_1, & \Delta\dot{p}_2 = -\Delta p_1 - \Delta q_2 - (\mathrm{H}_V(q)\cdot\Delta q)_2\,, \\ \Delta\dot{q}_3 = \Delta p_3, & \Delta\dot{p}_3 = -(\mathrm{H}_V(q)\cdot\Delta q)_3\,, \end{cases}$$

which reads for planar periodic orbits

$$\begin{cases} \Delta\dot{q}_1 = \Delta p_1 + \Delta q_2, & \Delta\dot{p}_1 = \Delta p_2 - \Delta q_1 + \left(\dfrac{2q_1^2 - q_2^2}{|q|^5} + 3\right)\Delta q_1 + \dfrac{3q_1q_2}{|q|^5}\Delta q_2, \\ \Delta\dot{q}_2 = \Delta p_2 - \Delta q_1, & \Delta\dot{p}_2 = -\Delta p_1 - \Delta q_2 + \dfrac{3q_1q_2}{|q|^5}\Delta q_1 + \dfrac{2q_2^2 - q_1^2}{|q|^5}\Delta q_2, \\ \Delta\dot{q}_3 = \Delta p_3, & \Delta\dot{p}_3 = -\left(\dfrac{1}{|q|^3} + 1\right)\Delta q_3. \end{cases}$$

5.2 Proof of Theorem 1.2.1

In the introduction we discussed all the linear symmetries. Now we prove Theorem 1.2.1.

Proof of Theorem 1.2.1. Let ρ be a linear symmetry. We prove the theorem in three steps where the first one is obvious.

Step 1. *The Hamiltonian (5.1.2) is the sum of*

$$H_2(q,p) = \frac{1}{2}|p|^2 + p_1q_2 - p_2q_1 - q_1^2 + \frac{1}{2}q_2^2 + \frac{1}{2}q_3^2 \quad \text{and} \quad H_{-1}(q,p) = -\frac{1}{|q|},$$

where H_2 is homogeneous of degree 2 and H_{-1} is homogeneous of degree -1. Hence

$$H_2 \circ \rho = H_2, \quad H_{-1}\circ\rho = H_{-1}.$$

Step 2. *The matrix form of ρ with respect to the splitting $\mathbb{R}^6 = \mathbb{R}^3 \times \mathbb{R}^3$ and to the coordinates $(q_1,q_2,q_3,p_1,p_2,p_3)$ is*

$$\begin{cases} \begin{pmatrix} A & 0 \\ C & A \end{pmatrix}, \quad A \in O(3), \quad A = A^T, \quad C = -C^T, \quad AC = -CA, & \text{if } \rho \text{ is symplectic} \\ \begin{pmatrix} A & 0 \\ C & -A \end{pmatrix}, \quad A \in O(3), \quad A = A^T, \quad C = C^T, \quad AC = CA, & \text{if } \rho \text{ is anti-symplectic.} \end{cases}$$

To see that, we write ρ in matrix form

$$\begin{pmatrix} A & B \\ C & D \end{pmatrix},$$

with respect to the coordinates $(q_1,q_2,q_3,p_1,p_2,p_3)$, where $A,B,C,D \in \mathrm{Mat}(3,\mathbb{R})$. The ρ-invariance of H_{-1} yields

$$|Aq + Bp| = |q|, \quad \forall q,p.$$

For fixed p we take q with $|q|$ very small and find $Bp = 0$. Hence

$$B = 0, \quad A \in O(3).$$

Next, the ρ-invariance of H_2 yields for $q = 0$

$$|Dp| = |p|, \quad \forall p,$$

whence also $D \in O(3)$. Since ρ is an involution, we obtain

$$\rho \circ \rho = \begin{pmatrix} A^2 & 0 \\ CA + DC & D^2 \end{pmatrix} = \begin{pmatrix} I_3 & 0 \\ 0 & I_3 \end{pmatrix},$$

and with $AA^T = DD^T = I_3$, we obtain

$$A = A^T, \quad D = D^T, \quad CA + DC = 0. \tag{5.2.5}$$

If ρ is symplectic, then (5.2.5) and the linear symplectic relations (4.1.4) imply

$$AC = A^T C = C^T A, \quad A^T D = AD = I_3.$$

With $A^2 = I_3$ we have

$$D = A,$$

and therefore

$$0 = CA + DC = CA + AC = CA + C^T A = (C + C^T)A.$$

Since $\det(A) = \pm 1$, the matrix C is skew-symmetric and this proves the first assertion of the second step.

If ρ is anti-symplectic, then by (5.2.5) and the linear anti-symplectic conditions (4.1.5) we obtain

$$AC = A^T C = C^T A, \quad A^T D = AD = -I_3,$$

hence

$$D = -A,$$

and

$$0 = CA + DC = CA - AC = CA - C^T A = (C - C^T)A.$$

Therefore the matrix C is symmetric and the second assertion follows.

Step 3. *In both cases, the matrix C is the zero matrix and*

$$\begin{cases} \rho \in \{\pm\sigma, \pm id\}, & \text{if } \rho \text{ is symplectic} \\ \rho \in \{\rho_1, \rho_2\overline{\rho_1}, \overline{\rho_2}\}, & \text{if } \rho \text{ is anti-symplectic.} \end{cases}$$

In both cases, A is of the form

$$A = \begin{pmatrix} a & d & e \\ d & b & f \\ e & f & c \end{pmatrix}.$$

Since $A^2 = I_3$ and $A \in O(3)$, we have

$$A^2 = \begin{pmatrix} a^2+d^2+e^2 & ad+bd+ef & ae+df+ce \\ ad+bd+ef & d^2+b^2+f^2 & de+bf+cf \\ ae+df+ce & de+bf+cf & e^2+f^2+c^2 \end{pmatrix} = \begin{pmatrix} 1 & 0 & 0 \\ 0 & 1 & 0 \\ 0 & 0 & 1 \end{pmatrix} \tag{5.2.6}$$

and

$$\det(A) = abc + 2def - af^2 - be^2 - cd^2 = \pm 1.$$

If ρ is symplectic, then $\rho(q,p)$ is of the form

$$\begin{pmatrix} a & d & e & 0 & 0 & 0 \\ d & b & f & 0 & 0 & 0 \\ e & f & c & 0 & 0 & 0 \\ 0 & c_1 & c_2 & a & d & e \\ -c_1 & 0 & c_3 & d & b & f \\ -c_2 & -c_3 & 0 & e & f & c \end{pmatrix} \cdot \begin{pmatrix} q_1 \\ q_2 \\ q_3 \\ p_1 \\ p_2 \\ p_3 \end{pmatrix} = \begin{pmatrix} aq_1 + dq_2 + eq_3 \\ dq_1 + bq_2 + fq_3 \\ eq_1 + fq_2 + cq_3 \\ c_1q_2 + c_2q_3 + ap_1 + dp_2 + ep_3 \\ -c_1q_1 + c_3q_3 + dp_1 + bp_2 + fp_3 \\ -c_2q_1 - c_3q_2 + ep_1 + fp_2 + cp_3 \end{pmatrix}.$$

The equation $AC = -CA$ yields

$$\begin{pmatrix} -dc_1 - ec_2 & ac_1 - ec_3 & ac_2 + dc_3 \\ -bc_1 - fc_2 & dc_1 - fc_3 & dc_2 + bc_3 \\ -fc_1 - cc_2 & ec_1 - cc_3 & ec_2 + fc_3 \end{pmatrix} = \begin{pmatrix} -dc_1 - ec_2 & -bc_1 - fc_2 & -fc_1 - cc_2 \\ ac_1 - ec_2 & dc_1 - fc_3 & ec_1 - cc_3 \\ ac_2 + dc_3 & dc_2 + bc_3 & ec_2 + fc_3 \end{pmatrix}, \tag{5.2.7}$$

and therefore

$$ac_1 - ec_3 = -bc_1 - fc_2, \quad ac_2 + dc_3 = -fc_1 - cc_2, \quad dc_2 + bc_3 = ec_1 - cc_3. \tag{5.2.8}$$

In view of the ρ-invariance of H_2 we compare

$$H_2(q,p) = \frac{1}{2}|p|^2 + p_1q_2 - p_2q_1 - q_1^2 + \frac{1}{2}q_2^2 + \frac{1}{2}q_3^2$$

with $H_2\big(\rho(q,p)\big)$, which is

$$\begin{aligned} &\frac{1}{2}|p|^2 + p_1q_2\left(ac_1 - ec_3 + ab - d^2\right) - p_2q_1\left(bc_1 + fc_2 + ab - d^2\right) \\ &- q_1^2\left(\frac{1}{2}\left(-c_1^2 - c_2^2 - d^2 - e^2\right) - ac_1 + a^2\right) \\ &+ \frac{1}{2}q_2^2\left(c_1^2 + c_3^2 + 2bc_1 - 2d^2 + b^2 + f^2\right) \\ &+ \frac{1}{2}q_3^2\left(c_2^2 + c_3^2 + 2fc_2 - 2ec_3 - 2e^2 + f^2 + c^2\right) \\ &+ p_1q_1\left(-dc_1 - ec_2\right) + p_2q_2\left(dc_1 - fc_3\right) + p_3q_3\left(ec_2 + fc_3\right) \\ &+ p_1q_3\left(ac_2 + dc_3 + af - de\right) + p_3q_1\left(-fc_1 - cc_2 + de - af\right) \\ &+ p_2q_3\left(dc_2 + bc_3 + df - be\right) + p_3q_2\left(ec_1 - cc_3 + be - df\right) \\ &+ q_1q_2\left(c_2c_3 + 2dc_1 - 2ad + bd + ef\right) \\ &+ q_1q_3\left(-c_1c_3 + dc_2 + ec_1 - ac_3 - 2ae + df + ce\right) \\ &+ q_2q_3\left(c_1c_2 + fc_1 + bc_2 - dc_3 - 2de + bf + cf\right). \end{aligned}$$

By the coefficients of p_iq_i, for $i = 1, 2, 3$, we immediately have that the diagonal entries of AC in (5.2.7) are all zero. To see that the other entries of AC are also all zero, we set equal the coefficients of p_1q_2 with p_2q_1, of p_1q_3 with p_3q_1, of p_2q_3 with p_3q_2, and use (5.2.8), which imply

$$ac_1 - ec_3 = -bc_1 - fc_2 = 0, \quad ac_2 + dc_3 = -fc_1 - cc_2 = 0, \quad dc_2 + bc_3 = ec_1 - cc_3 = 0.$$

Hence $AC = 0$ and thus $C = 0$. By the coefficients of p_1q_2 and p_2q_1,

$$ab - d^2 = 1,$$

which means that $a \neq 0$ and $b \neq 0$. In view of $A^2 = I_3$ in (5.2.6) the two equations $ad+bd+ef = 0$ and $ae + df + ce = 0$ together with the coefficients of q_1q_2 and q_1q_3 imply $ad = ae = 0$. Since $a \neq 0$ we obtain

$$d = e = 0.$$

Furthermore, by the coefficient of p_1q_3 we have $af = de = 0$, hence $f = 0$. Together with the coefficients from the second until the fourth lines, we obtain

$$ab = 1, \quad a^2 = b^2 = c^2 = 1,$$

which correspond to $\pm\sigma$, $\pm\mathrm{id}$.

If ρ is anti-symplectic, then $\rho(q, p)$ is of the form

$$\begin{pmatrix} a & d & e & 0 & 0 & 0 \\ d & b & f & 0 & 0 & 0 \\ e & f & c & 0 & 0 & 0 \\ c_1 & c_2 & c_3 & -a & -d & -e \\ c_2 & c_4 & c_5 & -d & -b & -f \\ c_3 & c_5 & c_6 & -e & -f & -c \end{pmatrix} \cdot \begin{pmatrix} q_1 \\ q_2 \\ q_3 \\ p_1 \\ p_2 \\ p_3 \end{pmatrix} = \begin{pmatrix} aq_1 + dq_2 + eq_3 \\ dq_1 + bq_2 + fq_3 \\ eq_1 + fq_2 + cq_3 \\ c_1q_1 + c_2q_2 + c_3q_3 - ap_1 - dp_2 - ep_3 \\ c_2q_1 + c_4q_2 + c_5q_3 - dp_1 - bp_2 - fp_3 \\ c_3q_1 + c_5q_2 + c_6q_3 - ep_1 - fp_2 - cp_3 \end{pmatrix}.$$

The equation $AC = CA$ yields that

$$\begin{pmatrix} ac_1 + dc_2 + ec_3 & ac_2 + dc_4 + ec_5 & ac_3 + dc_5 + ec_6 \\ dc_1 + bc_2 + fc_3 & dc_2 + bc_4 + fc_5 & dc_3 + bc_5 + fc_6 \\ ec_1 + fc_2 + cc_3 & ec_2 + fc_4 + cc_5 & ec_3 + fc_5 + cc_6 \end{pmatrix}$$

equals

$$\begin{pmatrix} ac_1 + dc_2 + ec_3 & dc_1 + bc_2 + fc_3 & ec_1 + fc_2 + cc_3 \\ ac_2 + dc_4 + ec_5 & dc_2 + bc_4 + fc_5 & ec_2 + fc_4 + cc_5 \\ ac_3 + dc_5 + ec_6 & dc_3 + bc_5 + fc_6 & ec_3 + fc_5 + cc_6 \end{pmatrix}.$$

Therefore

$$\begin{aligned} ac_2 + dc_4 + ec_5 &= dc_1 + bc_2 + fc_3, \\ ac_3 + dc_5 + ec_6 &= ec_1 + fc_2 + cc_3, \\ dc_3 + bc_5 + fc_6 &= ec_2 + fc_4 + cc_5. \end{aligned}$$

Now $H_2\big(\rho(q,p)\big)$ is

$$\begin{aligned}
&\frac{1}{2}|p|^2 + p_1q_2\left(-ac_2 - dc_4 - ec_5 + d^2 - ab\right) - p_2q_1\left(dc_1 + bc_2 + fc_3 + d^2 - ab\right)\\
&- q_1^2\left(\frac{1}{2}\left(-c_1^2 - c_2^2 - d^2 - e^2\right) - dc_1 + ac_2 + a^2\right)\\
&+ \frac{1}{2}q_2^2\left(c_2^2 + c_4^2 + c_5^2 + 2bc_2 - 2dc_4 - 2d^2 + b^2 + f^2\right)\\
&+ \frac{1}{2}q_3^2\left(c_3^2 + c_5^2 + c_6^2 + 2fc_3 - 2ec_5 - 2e^2 + f^2 + c^2\right)\\
&+ p_1q_1\left(-ac_1 - dc_2 - ec_3\right) + p_2q_2\left(-dc_2 - bc_4 - fc_5\right) + p_3q_3\left(-ec_3 - fc_5 - cc_6\right)\\
&+ p_1q_3\left(-ac_3 - dc_5 - ec_6 + de - af\right) + p_3q_1\left(-ec_1 - fc_2 - cc_3 + af - de\right)\\
&+ p_2q_3\left(-dc_3 - bc_5 - fc_6 + be - df\right) + p_3q_2\left(-ec_2 - fc_4 - cc_5 + df - be\right)\\
&+ q_1q_2\left(c_1c_2 + c_2c_4 + c_3c_5 + bc_1 - ac_4 - 2ad + bd + ef\right)\\
&+ q_1q_3\left(c_1c_3 + c_2c_5 + c_3c_6 + fc_1 + dc_3 - ec_2 - ac_5 - 2ae + df + ce\right)\\
&+ q_2q_3\left(c_2c_3 + c_4c_5 + c_5c_6 + fc_2 + bc_3 - ec_4 - dc_5 - 2de + bf + cf\right).
\end{aligned}$$

In a similar way to the symplectic case we find that $C = 0$. In view of $A^2 = I_3$ in (5.2.6) the three equations $ad + bd + ef = 0$, $ae + df + ce = 0$ and $de + bf + cf = 0$ together with the coefficients of q_1q_2, q_1q_3, q_2q_3 imply $ad = ae = de = 0$. Since the coefficients of p_1q_3 and p_3q_1 yield $de = af$, we have

$$ad = ae = af = 0.$$

Suppose that $a = 0$, then in view of the coefficients of q_1^2 we see that $d^2 + e^2 = -2$ which is a contradiction. Hence

$$a \neq 0, \quad d = e = f = 0.$$

By the first four lines we obtain

$$ab = -1, \quad a^2 = b^2 = c^2 = 1,$$

which correspond to $\rho_1, \rho_2, \overline{\rho_1}$ and $\overline{\rho_2}$.

Group structure. The group structure is given by Table 5.1.

$\circ$	id	$-$id	$-\sigma$	σ	ρ_1	ρ_2	$\overline{\rho_1}$	$\overline{\rho_2}$
id	id	$-$id	$-\sigma$	σ	ρ_1	ρ_2	$\overline{\rho_1}$	$\overline{\rho_2}$
$-$id	$-$id	id	σ	$-\sigma$	$\overline{\rho_2}$	$\overline{\rho_1}$	ρ_2	ρ_1
$-\sigma$	$-\sigma$	σ	id	$-$id	ρ_2	ρ_1	$\overline{\rho_2}$	$\overline{\rho_1}$
σ	σ	$-\sigma$	$-$id	id	$\overline{\rho_1}$	$\overline{\rho_2}$	ρ_1	ρ_2
ρ_1	ρ_1	$\overline{\rho_2}$	ρ_2	$\overline{\rho_1}$	id	$-\sigma$	σ	$-$id
ρ_2	ρ_2	$\overline{\rho_1}$	ρ_1	$\overline{\rho_2}$	$-\sigma$	id	$-$id	σ
$\overline{\rho_1}$	$\overline{\rho_1}$	ρ_2	$\overline{\rho_2}$	ρ_1	σ	$-$id	id	$-\sigma$
$\overline{\rho_2}$	$\overline{\rho_2}$	ρ_1	$\overline{\rho_1}$	ρ_2	$-$id	σ	$-\sigma$	id

Table 5.1: Group structure of Σ_3.

This group is generated by $\{\rho_1, \rho_2, \sigma\}$, and

$$\Sigma_3 \cong \mathbb{Z}_2 \times \mathbb{Z}_2 \times \mathbb{Z}_2. \qquad \square$$

Table 5.1 shows that if we consider the four symplectic involutions $\pm\mathrm{id}$, $\pm\sigma$, like in the planar case, a Klein four-group arises, namely as a sub-group of Σ_3. It is generated by $\{\pm\sigma\}$, and we denote it by $\Sigma_3^\omega \cong \mathbb{Z}_2 \times \mathbb{Z}_2$. Hence

$$\Sigma_2 \cong \Sigma_3^\omega \subset \Sigma_3.$$

5.3 Monodromy and reduced monodromy of special symmetric form

5.3.1 For planar symmetric periodic orbits

Suppose that a planar periodic orbit (q, p) is invariant under the anti-symplectic involution

$$\rho_1(q, p) = (q_1, -q_2, q_3, -p_1, p_2, -p_3),$$

which means that it is invariant under reflection about the q_1-axis. Let the starting point

$$q_0 = (q(0), p(0)) \in \mathrm{Fix}(\rho_1).$$

Recall that ρ_1 commutes with the symplectic involution σ, which leaves planar periodic orbits invariant as well. Therefore a Lagrangian basis with respect to the symplectic decomposition

$$T_{q_0}\mathrm{Fix}(\sigma) \oplus E_{-1}\big(d\sigma(q_0)\big)$$

into the 4-dimensional planar and 2-dimensional spatial components is given by

$$\left\{ \begin{pmatrix} 1 \\ 0 \\ 0 \\ 0 \end{pmatrix}, \begin{pmatrix} 0 \\ 0 \\ 0 \\ 1 \end{pmatrix}, \begin{pmatrix} 0 \\ 0 \\ -1 \\ 0 \end{pmatrix}, \begin{pmatrix} 0 \\ 1 \\ 0 \\ 0 \end{pmatrix} \right\} \text{ and } \left\{ \begin{pmatrix} 1 \\ 0 \end{pmatrix}, \begin{pmatrix} 0 \\ -1 \end{pmatrix} \right\}.$$

Then in view of Lemma 4.4.1 the monodromy with respect to these bases is of the form

$$d\varphi_H^{T_q}(q_0) = \begin{pmatrix} A_p & 0 \\ 0 & A_s \end{pmatrix}, \quad A_p \in \widetilde{\mathrm{Sp}}(2), \quad A_s \in \widetilde{\mathrm{Sp}}(1).$$

For the planar reduced monodromy $\overline{A}_p$, we need a basis of the form

$$T_{q_0}\mathrm{Fix}(\sigma|_\Sigma) = \langle \tilde{v}, \tilde{w} \rangle_{\mathbb{R}} \oplus \langle X_H|_\Sigma(q_0) \rangle_{\mathbb{R}}$$

such that $\omega_{q_0}(\tilde{v}, \tilde{w}) = 1$. Note that $\omega_{q_0}\big(\tilde{v}, X_H|_\Sigma(q_0)\big) = \omega_{q_0}\big(\tilde{w}, X_H|_\Sigma(q_0)\big) = 0$. The Hamiltonian (5.1.2) implies the energy condition

$$\Delta p_2(0) = \frac{1}{p_2(0) - q_1(0)} \left(\frac{-q_1(0)}{|q|^3} + 2q_1(0) + p_2(0) \right) \Delta q_1(0), \tag{5.3.9}$$

hence $\Delta q_1(0)$ and $\Delta p_2(0)$ determine each other such that a first basis vector is given by

$$\tilde{v} = (\Delta q_1(0), 0, 0, \Delta p_2(0)).$$

For simplicity we choose $\Delta q_1(0) = 1$ such that the second basis vector is given by

$$\tilde{w} = (0, 0, -1, 0).$$

The Hamiltonian vector field $X_H|_\Sigma(q_0) \in \langle (0,0,-1,0), (0,1,0,0)\rangle_{\mathbb{R}}$ is of the form

$$\big(0, \Delta q_2(0), \Delta p_1(0), 0\big) = \big(0, \dot{q}_2(0), \dot{p}_1(0), 0\big),$$

which is determined by the initial conditions and the equation (5.1.4). With this basis, the reduced monodromy is of the form

$$\overline{d\varphi_H^{T_q}|_\Sigma(q_0)} = \begin{pmatrix} \overline{A}_p & 0 \\ 0 & A_s \end{pmatrix} = \begin{pmatrix} a & b & 0 & 0 \\ c & a & 0 & 0 \\ 0 & 0 & \tilde{a} & \tilde{b} \\ 0 & 0 & \tilde{c} & \tilde{a} \end{pmatrix}, \quad \overline{A}_p, A_s \in \widetilde{\mathrm{Sp}}(1).$$

Recall that $a^2 - bc = \tilde{a}^2 - \tilde{b}\tilde{c} = 1$ and in view of Proposition 4.3.12 the signatures of $b, c, \tilde{b}$ and $\tilde{c}$ are invariant under the choice of the Lagrangian basis.

5.3.2 For spatial symmetric periodic orbits

Suppose a spatial periodic orbit (q, p) is invariant under the anti-symplectic involution

$$\overline{\rho_1}(q, p) = (q_1, -q_2, -q_3, -p_1, p_2, p_3),$$

which means that it is invariant under the rotation around the q_1-axis by π. Note that the following procedure with respect to the the invariance under any other linear anti-symplectic symmetry is analogous. If we choosing again the starting point $q_0 \in \mathrm{Fix}(\overline{\rho_1})$ and a Lagrangian basis, e.g., in the form

$$\left\{ \begin{pmatrix} 1 \\ 0 \\ 0 \\ 0 \\ 0 \\ 0 \end{pmatrix}, \begin{pmatrix} 0 \\ 0 \\ 0 \\ 0 \\ 1 \\ 0 \end{pmatrix}, \begin{pmatrix} 0 \\ 0 \\ 0 \\ 0 \\ 0 \\ 1 \end{pmatrix}, \begin{pmatrix} 0 \\ 0 \\ 0 \\ -1 \\ 0 \\ 0 \end{pmatrix}, \begin{pmatrix} 0 \\ 1 \\ 0 \\ 0 \\ 0 \\ 0 \end{pmatrix}, \begin{pmatrix} 0 \\ 0 \\ 1 \\ 0 \\ 0 \\ 0 \end{pmatrix} \right\},$$

then in view of Proposition 4.3.2 the monodromy is of the form

$$d\varphi_H^{T_q}(q_0) \in \widetilde{\mathrm{Sp}}(3) = \left\{ \begin{pmatrix} A & B \\ C & A^T \end{pmatrix} : B, C, CA, AB \text{ are symmetric and } A^2 - BC = I_3 \right\}.$$

In view of the Hamiltonian (5.1.2) the energy condition is given by

$$\Delta p_3(0) = \frac{1}{p_3(0)} \left(\left(\frac{-q_1(0)}{|q|^3} + 2q_1(0) + p_2(0) \right) \Delta q_1(0) + \big(q_1(0) - p_2(0)\big) \Delta p_2(0) \right),$$

which means that any two of $\Delta p_3(0), \Delta q_1(0)$ and $\Delta p_2(0)$ determine the thirds. Hence two basis vectors of the five dimensional vector space $T_{q_0}\Sigma$ are of the form

$$\big(\Delta q_1(0), 0, 0, 0, \Delta p_2(0), \Delta p_3(0)\big).$$

For simplicity we choose

$$\tilde{v}_1 = \big(1,0,0,0,0,\Delta p_3(0)\big), \quad \tilde{v}_2 = \big(0,0,0,0,1,\Delta p_3(0)\big).$$

The Hamiltonian vector field $X_H|_\Sigma(q_0) \in E_{-1}\big(d\overline{\rho_1}(q_0)\big)$, which is spanned by the last three Lagrangian basis vectors, is of the form

$$\big(0,\Delta q_2(0),\Delta q_3(0),\Delta p_1(0),0,0\big) = \big(0,\dot{q}_2(0),\dot{q}_3(0),\dot{p}_1(0),0,0\big),$$

determined by the initial conditions and the equation (5.1.4). By choosing

$$\tilde{w}_1 = (0,0,0,-1,0,0), \quad \tilde{w}_2 = (0,1,0,0,0,0)$$

we obtain

$$T_{q_0}\Sigma = \langle \tilde{v}_1,\tilde{v}_2,\tilde{w}_1,\tilde{w}_2,X_H|_\Sigma(q_0)\rangle_{\mathbb{R}}, \quad \omega_{x_0}(\tilde{v}_i,\tilde{w}_j) = \delta_{ij}, \quad i,j = 1,2,$$

and

$$\overline{d\varphi_H^{T_q}(q_0)} \in \widetilde{\mathrm{Sp}}(2) = \left\{ \begin{pmatrix} A & B \\ C & A^T \end{pmatrix} : B,C,CA,AB \text{ are symmetric and } A^2 - BC = I_2 \right\}.$$

6 Proof of Theorem 1.2.3 and 1.2.4

> "*Despite J. Moser's explicit statement that the action functional (1) is useless for finding periodic orbits, [19, p. 731], P. Rabinowitz in [21, p. 161 and (2.7)] used precisely this functional to prove his celebrated existence theorem for periodic orbits on starshaped hypersurfaces in* $\mathbb{R}^{2n}$*, thus pioneering the use of global critical point methods in Hamiltonian mechanics. In [10] and subsequent papers, the functional (1) was therefore called Rabinowitz action functional. Other good names for this functional may be "fixed energy action functional" or "Hamiltonian free period action functional", since it selects solutions on the prescribed energy level* $\{H = 0\}$*, allowing for arbitrary period* $|\eta|$*.*"
>
> - U. Frauenfelder and F. Schlenk in [26, p. 295] (2016)

This chapter is based on "*the averaging method*" from [27, Chapter 8] which describes the bifurcation scenario out of a Morse–Bott critical component in the finite-dimensional set-up:

Let M be a manifold and $f_r = f(\cdot, r) \in C^\infty(M, \mathbb{R})$ be a one-parameter family of smooth functions on M, where $r \in [0, 1)$. Assume that

$$C \subset \operatorname{crit}(f_0)$$

is a Morse–Bott component of f_0, i.e., $C \subset M$ is a closed submanifold which corresponds to a connected component of $\operatorname{crit}(f_0)$ such that for every $x \in C$ we have that

$$T_x C = \ker H_{f_0}(x).$$

Suppose that the restriction of the derivative of f_r with respect to r at $r = 0$, denoted by $\mathring{f}_0$, to C is a Morse function. Then by the implicit function theorem, there exists $\varepsilon > 0$, an open neighborhood U of C in M and a one-parameter family of smooth functions

$$x_r = x(\cdot, r) \colon \operatorname{crit}(\mathring{f}_0|_C) \to U, \quad r \in [0, \varepsilon),$$

such that

i) If $\iota : \operatorname{crit}(\mathring{f}_0|_C) \to U$ is the inclusion, then $x_0 = x(\cdot, 0) = \iota$.

ii) For every $r \in (0, \varepsilon)$ the restriction $\mathring{f}_r|_U$ is Morse and $\operatorname{crit}(\mathring{f}_r|_U) = \operatorname{im}(x_r) = \operatorname{im}(x(\cdot, r))$.

6.1 Regularized energy hypersurface

Planar case. To avoid collision orbits, for given energy $c < 0$, we regularize the Hamiltonian of the planar problem, which is the restriction of (5.1.2) to $\operatorname{Fix}(\sigma) = \{q_3 = p_3 = 0\}$, by

$$\begin{aligned} K_c(-p, q) &= \frac{1}{2}\left(- \frac{|q|}{2c}\left(H|_{\operatorname{Fix}(\sigma)}\Big(- \frac{q}{2c}, \sqrt{-2c}p\Big) - c\right) + 1\right)^2 - \frac{1}{2} \\ &= \frac{1}{2}\left(\frac{1}{2}\big(1 + |p|^2\big) + \frac{p_1 q_2 - p_2 q_1}{(-2c)^{\frac{3}{2}}} + \frac{-q_1^2 + \frac{1}{2}q_2^2}{(-2c)^3}\right)^2 |q|^2 - \frac{1}{2} \end{aligned}$$

satisfying $\Sigma_c := (H|_{\mathrm{Fix}(\sigma)})^{-1}(c) = K_c^{-1}(0)$. Note that the transformation consists of the switch map

$$(-p, q) \mapsto (q, p), \tag{6.1.1}$$

which is a linear symplectomorphism on $\mathbb{R}^4$, and $(q, p) \mapsto (-\frac{q}{2c}, \sqrt{-2c}p)$, which is conformally symplectic with its conformal factor $\frac{1}{\sqrt{-2c}}$. In symplectic geometry, we don't want to change the dynamics and indeed this factor only gives rise to a reparametrization of the Hamiltonian flow.

Now the roles of the positions q and momenta p are switched and $-p$ corresponds to the base coordinate and q to the fiber coordinate. By thinking of the two-sphere as $S^2 = \mathbb{R}^2 \cup \{\infty\}$ via stereographic projection from the north pole N, we obtain the inclusion

$$\iota \colon T^*\mathbb{R}^2 \hookrightarrow T^*S^2, \tag{6.1.2}$$

where by adding N the closure of the regularized energy hypersurface $\overline{\iota(\Sigma_c)}$ is a subset of T^*S^2.

Furthermore, for every $c < 0$, K_c smoothly extends to a Hamiltonian on T^*S^2, and by abuse of notation we denote this canonical smooth extension by the same letter. To study the limit case $c \to -\infty$, we replace the energy parameter by $c = \frac{-1}{2r^{2/3}}$, for a homotopy variable $r \in (0, \infty)$. Hence we obtain

$$K_r(-p, q) := \frac{1}{2}\Big(\frac{1}{2}\big(1 + |p|^2\big) + (p_1q_2 - p_2q_1)r + (-q_1^2 + \frac{1}{2}q_2^2)r^2\Big)^2|q|^2 - \frac{1}{2}. \tag{6.1.3}$$

The Hamiltonian (6.1.3) smoothly extends to $r = 0$, where it becomes just the regularized Kepler Hamiltonian

$$K_0(-p, q) = \frac{1}{2}\Big(\frac{1}{2}(1 + |p|^2)\Big)^2|q|^2 - \frac{1}{2},$$

which is the kinetic energy of the "*momentum*" q with respect to the round metric on S^2, i.e., $g_{ij} = \frac{4\delta_{ij}}{(1+|p|^2)^2}$. In general, the regularization of collision orbits for the Kepler problem in $\mathbb{R}^n$ goes back to Moser [51], where the Kepler flow is just the geodesic flow on S^n in the chart given by stereographic projection from N. To regularize the flow means to add the fiber over N. Going through N (the point at infinity) corresponds precisely to the collisions, where p explodes. In the original picture: By regularizing, the third body moves into the mass at the origin like falling onto some kind of trampoline, i.e., at collision it bounces back. Hence, these bounce orbits become periodic according to the periodic geodesic flows on S^2.

Remark 6.1.1. If $K(q, p)$ is the Hamiltonian of the Kepler problem, then on the energy hypersurface $K_0^{-1}(0) = K^{-1}(0)$ the Hamiltonian vector fields are related by

$$X_{K_0}|_{K^{-1}(0)}(p, q) = |q|X_K|_{K^{-1}(0)}(-q, p), \tag{6.1.4}$$

see for instance [27, pp. 47–48].

Now by adding N, the closure of the regularized energy hypersurface $\Sigma := K_0^{-1}(0)$, i.e., which in view of (6.1.2) is

$$\overline{\iota(\Sigma)} \subset T^*S^2,$$

corresponds to the space of great circles on S^2 parametrized by arc length, i.e., the space of oriented simple closed geodesics on S^2. Topologically, it is the set of pairs $(-p, q)$ formed by

base points $-p$ and unit co-vectors q at $-p$ (see Figure 6.1), meaning that it is diffeomorphic to the unit cotangent bundle of S^2,

$$\overline{\iota(\Sigma)} \cong S^*S^2 = \{(-p, q) : |q|_{-p} = 1\},$$

where $|q|_{-p}$ is the length of q with respect to the round co-metric on S^2. By identifying it with the unit tangent bundle, denoted by SS^2, it is diffeomorphic to

$$\overline{\iota(\Sigma)} \cong S^*S^2 \cong SS^2 \cong SO(3) \cong S^3/\mathbb{Z}_2 \cong \mathbb{R}P^3,$$

see [18, p. 195].

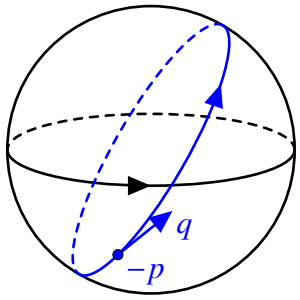

Figure 6.1: The space of parametrized great circles on S^2.

Spatial case. By the same procedure for the spatial system (5.1.2), the closure of the regularized energy hypersurface is the unit cotangent bundle S^*S^3 which is the space of parametrized great circles (parametrized simple closed geodesics) on S^3. The tangent bundle of S^3 is trivial, i.e., $TS^3 \cong S^3 \times \mathbb{R}^3$ (see [33, p. 9]), we therefore have

$$SS^3 \cong S^3 \times S^2.$$

6.2 From the Rabinowitz action functional to Morse–Bott

6.2.1 Rabinowitz action functional

Planar case. We interpret variationally parametrized periodic orbits of K_r (6.1.3) as critical points of the Rabinowitz action functional given by

$$\mathcal{A}_r := \mathcal{A}^{K_r} \colon \mathcal{L} \times \mathbb{R}_{>0} \to \mathbb{R}, \quad (\gamma, \tau) \mapsto \int_{S^1} \gamma^*\lambda - \tau \int_{S^1} K_r(\gamma(t))\, dt, \tag{6.2.5}$$

where $\mathcal{L} = C^\infty(S^1 = \mathbb{R}/\mathbb{Z}, T^*S^2)$ is the free loop space of T^*S^2, λ is the canonical Liouville one-form and where τ can be regarded as the period of γ. This functional can be thought as the Lagrange multiplier functional of the area functional for the constraint given by the mean value of K_r.

For the critical points of $\mathcal{A}_r$ let $(\gamma, \tau) \in \mathcal{L} \times \mathbb{R}_{>0}$ and $(\hat\gamma_1, \hat\tau_1), (\hat\gamma_2, \hat\tau_2) \in T_{(\gamma,\tau)}(\mathcal{L} \times \mathbb{R}_{>0})$ two tangent vectors. For the gradient of $\mathcal{A}_r$ we denote by g the metric on $\mathcal{L}\times\mathbb{R}_{>0}$ which is defined as the product metric of the L^2-metric on $\mathcal{L}$ and the standard metric on $\mathbb{R}_{>0}$. For the L^2-metric we choose a smooth family $\{J_t\}_{t\in S^1}$ of ω-compatible almost complex structures on T^*S^2, meaning that J_t is an automorphism of $T_\gamma T^*S^2$ with $J_t^2 = -\mathrm{id}$ and $\omega(\cdot, J_t\cdot)$ defines a Riemannian metric. Then the metric g is given by

$$g\left(\begin{pmatrix}\hat\gamma_1\\ \hat\tau_1\end{pmatrix}, \begin{pmatrix}\hat\gamma_2\\ \hat\tau_1\end{pmatrix}\right) = \langle\hat\gamma_1, \hat\gamma_2\rangle_{L^2} + \hat\tau_1\hat\tau_2 = \int_{S^1} \omega\big(\hat\gamma_1, J_t(\gamma)\hat\gamma_2\big)dt + \hat\tau_1\hat\tau_2.$$

Pick $(\hat\gamma, \hat\tau) \in T_{(\gamma,\tau)}(\mathcal{L}\times\mathbb{R}_{>0})$, then by following [27, p. 97] we calculate by using Cartan's identity

$$d\mathcal{A}_{r_{(\gamma,\tau)}}(\hat\gamma, \hat\tau) = \int_{S^1} \gamma^*\mathcal{L}_{\hat\gamma}\lambda - \tau\int_{S^1} dK_r(\gamma)\hat\gamma dt - \hat\tau\int_{S^1} K_r(\gamma)dt$$

$$
\begin{aligned}
&= \int_{S^1} \gamma^* d\iota_{\hat\gamma}\lambda + \int_{S^1} \gamma^*\iota_{\hat\gamma} d\lambda - \tau \int_{S^1} \omega\left(\hat\gamma, X_{K_r}(\gamma)\right) dt - \hat\tau \int_{S^1} K_r(\gamma) dt \\
&= \int_{S^1} d\gamma^*\iota_{\hat\gamma}\lambda + \int_{S^1} \gamma^*\iota_{\hat\gamma}\omega - \int_{S^1} \omega\left(\hat\gamma, \tau X_{K_r}(\gamma)\right) dt - \hat\tau \int_{S^1} K_r(\gamma) dt \\
&= \int_{S^1} \frac{d}{dt}\lambda(\hat\gamma) dt + \int_{S^1} \omega(\hat\gamma, \dot\gamma) dt - \int_{S^1} \omega\left(\hat\gamma, \tau X_{K_r}(\gamma)\right) dt - \hat\tau \int_{S^1} K_r(\gamma) dt \\
&= \int_{S^1} \omega\left(\hat\gamma, \dot\gamma - \tau X_{K_r}(\gamma)\right) dt - \hat\tau \int_{S^1} K_r(\gamma) dt \\
&= \int_{S^1} \omega\left(\hat\gamma, J_t(\gamma)\left(-J_t(\gamma)\right)\left(\dot\gamma - \tau X_{K_r}(\gamma)\right)\right) dt - \hat\tau \int_{S^1} K_r(\gamma) dt \\
&= g\left(\begin{pmatrix}\hat\gamma \\ \hat\tau\end{pmatrix}, \begin{pmatrix}-J_t(\gamma)\left(\dot\gamma - \tau X_{K_r}(\gamma)\right) \\ -\int_{S^1} K_r(\gamma) dt\end{pmatrix}\right).
\end{aligned}
$$

Therefore with respect to the metric g the gradient of $\mathcal{A}_r$ reads

$$
\nabla_g \mathcal{A}_r(\gamma, \tau) = \begin{pmatrix}-J_t(\gamma)\left(\dot\gamma(t) - \tau X_{K_r}\left(\gamma(t)\right)\right) \\ -\int_{S^1} K_r\left(\gamma(t)\right) dt\end{pmatrix},
$$

i.e., the critical points of $\mathcal{A}_r$ consist of pairs $(\gamma, \tau) \in \mathcal{L} \times \mathbb{R}_{>0}$ which are solutions of

$$
\begin{cases}\dot\gamma(t) = \tau X_{K_r}\left(\gamma(t)\right) \\ 0 = \int_{S^1} K_r\left(\gamma(t)\right) dt\end{cases} \quad \Leftrightarrow \quad \begin{cases}\dot\gamma(t) = \tau X_{K_r}\left(\gamma(t)\right) \\ 0 = K_r\left(\gamma(t)\right),\end{cases}
$$

where the equivalence follows from preservation of energy. In other words, the critical points of $\mathcal{A}_r$ are parametrized periodic orbits of X_{K_r} of period τ on the fixed energy level set $K_r^{-1}(0)$.

The circle S^1 acts on $\mathcal{L}$ by rotating the loop γ. This S^1-action extends to an action on $\mathcal{L} \times \mathbb{R}_{>0}$, where S^1 acts trivially on $\mathbb{R}_{>0}$, that is

$$
s_*\left(\gamma(t), \tau\right) = \left(\gamma(t + s), \tau\right), \quad t, s \in S^1. \tag{6.2.6}
$$

Note that for every r the Rabinowitz action functional $\mathcal{A}_r$ is invariant under (6.2.6). By the Morse Lemma (see for instance [50, pp. 6–8]) non-degenerate critical points are isolated. Since the critical points of $\mathcal{A}_r$ come in S^1-families, $\mathcal{A}_r$ is never a Morse function, i.e., the kernel of its Hessian at a critical point is never just the zero vector space. Further, the geodesic flow on S^2 is invariant under rotation, thus closed geodesics are not isolated.

The critical points of $\mathcal{A}_0$ correspond to parametrized periodic geodesics on S^2. Note that the minimal period, parametrized by arc length, is 2π, and in particular, $\mathcal{A}_0$ is Morse–Bott, where each connected Morse–Bott submanifold is given by

$$
\operatorname{crit}(\mathcal{A}_0) = \bigsqcup_{k \geq 1} C_k, \quad C_k := \{(\gamma(t), 2k\pi) : \ (\gamma(t), 2k\pi) \in \operatorname{crit}(\mathcal{A}_0)\} \cong \mathbb{R}P^3.
$$

We refer to [24, pp. 431–433] for details. Let denote the Morse–Bott index of every simple closed geodesic on C_1 by ind_{C_1}. By the Morse index theorem (see [50, §15]), the index of a geodesic on the round n-sphere equals the number of conjugate points which are passed by such a geodesic. Therefore,

$$
\operatorname{ind}_{C_1} = 1, \quad C_1 \cong \mathbb{R}P^3 \subset \operatorname{crit}(\mathcal{A}_0).
$$

For the derivative of $\mathcal{A}_r$ with respect to r at $r = 0$ at $(\gamma, 2\pi) = (-p, q, 2\pi) \in C_1$ we compute

$$\begin{aligned}\frac{\partial K_r}{\partial r}\bigg|_{r=0}(-p,q) &= \frac{1}{2}\big(1+|p|^2\big)(p_1q_2 - p_2q_1)|q|^2 \\ &= \sqrt{\big(2K_0(-p,q)+1\big)}|q|(p_1q_2 - p_2q_1).\end{aligned}$$

Note that the original angular momentum (5.1.1) is invariant under the switch map (6.1.1), i.e.,

$$L(q,p) = p_1q_2 - p_2q_1 = L(-p,q).$$

For $(\gamma, 2\pi) \in C_1$ we have that $K_0(\gamma) = 0$ and since L is constant along periodic orbits of the Kepler problem we obtain

$$\begin{aligned}\mathring{\mathcal{A}}_0(\gamma,2\pi) := \frac{\partial \mathcal{A}_r}{\partial r}\bigg|_{r=0}(\gamma,2\pi) &= -2\pi\int_{S^1}\frac{\partial K_r}{\partial r}\bigg|_{r=0}\big(\gamma(t)\big) \\ &= -2\pi\int_{S^1}|q|L\big(\gamma(t)\big)dt \\ &= -2\pi L\big(\gamma(0)\big)\int_{S^1}|q|dt \\ &= -2\pi L(-p,q). \qquad (6.2.7)\end{aligned}$$

The last integral is 1 and independent of the orbit, since by (6.1.4) it determines the ratio of a Kepler ellipse's period of energy 0 before and after regularization, which is 2π in this two cases.

Spatial case. All connected Morse–Bott submanifolds C_k are diffeomorphic to $S^3 \times S^2$, for all $k \geq 1$. The analogous procedure gives the same equation and function (6.2.7) of the same form, i.e., $\mathring{\mathcal{A}}_0(\gamma, 2\pi) = -2\pi(p_1q_2 - p_2q_1)$, where $(\gamma, 2\pi) \in C_1$ is a simple closed geodesic on S^3 with

$$\operatorname{ind}_{C_1} = 2, \quad C_1 \cong S^3 \times S^2 \subset \operatorname{crit}(\mathcal{A}_0).$$

6.2.2 Critical points of $-L$ on SS^2 and SS^3 and their Morse–Bott indices

Recall that if x is a critical point of a Morse–Bott function f, then the Morse–Bott index $\operatorname{ind}_f(x)$ of f at x is the number of negative eigenvalues of the Hessian of f at x. Therefore in view of (6.2.7) we wish to compute the critical points of

$$-L\colon C_1 \cong SS^2 \to \mathbb{R}, \quad (-p,q) \mapsto q_1p_2 - q_2p_1 \qquad (6.2.8)$$

and of

$$-L\colon C_1 \cong SS^3 \to \mathbb{R}, \quad (-p,q) \mapsto q_1p_2 - q_2p_1. \qquad (6.2.9)$$

Lemma 6.2.1 (**Planar case**). *The critical points of (6.2.8) are exactly two circles over the equator moving in opposite direction and (6.2.8) is Morse–Bott along them. Furthermore, one is a maximum and the other one is a minimum, and*

crit$(-L)$	*Morse–Bott index*	*corresponding periodic orbit in the original picture*
maximum	*2*	*circular direct motion*
minimum	*0*	*circular retrograde motion*

Proof. Given the switch (6.1.1), let $S^2 = \{(-p_1, -p_2, -p_3) \mid p_1^2 + p_2^2 + p_3^2 = 1\} \subset \mathbb{R}^3$ be the unit sphere. Then view T^*S^2 as a subset of $\mathbb{R}^6 = \{-p_1, -p_2, -p_3, q_1, q_2, q_3\}$ and the unit tangent bundle $SS^2 \subset TS^2$, which is the closure of the regularized energy hypersurface

$$\mathbb{R}P^3 \cong S^*S^2 \cong SS^2 = \{(-p, q) \in \mathbb{R}^3 \times \mathbb{R}^3 \mid \|p\|^2 = \|q\|^2 = 1, \langle -p, q\rangle = 0\} \subset \mathbb{R}^6.$$

To find the critical points of (6.2.8) we parametrize S^2 by

$$\Phi\colon [0, 2\pi) \times (-\frac{\pi}{2}, \frac{\pi}{2}) \to \mathbb{R}^3, \quad (\varphi, \theta) \mapsto \begin{pmatrix} \cos\theta\cos\varphi \\ \cos\theta\sin\varphi \\ \sin\theta \end{pmatrix},$$

hence the north and south poles are not parametrized. This does not matter since one can check that the same calculation with a chart including the north and south poles shows that there are no critical points of (6.2.8) at the two circles there. However, the tangent plane $T_{-p}S^2$ at a point $-p \in S^2$ is spanned by the two orthogonal vectors

$$\frac{\partial\Phi}{\partial\varphi} = \begin{pmatrix} -\cos\theta\sin\varphi \\ \cos\theta\cos\varphi \\ 0 \end{pmatrix}, \quad \frac{\partial\Phi}{\partial\theta} = \begin{pmatrix} -\sin\theta\cos\varphi \\ -\sin\theta\sin\varphi \\ \cos\theta \end{pmatrix}$$

with $\|\frac{\partial\Phi}{\partial\varphi}\| = \cos\theta$ and $\|\frac{\partial\Phi}{\partial\theta}\| = 1$, whence we can take the orthonormal basis $\left\{(\cos\theta)^{-1}\frac{\partial\Phi}{\partial\varphi}, \frac{\partial\Phi}{\partial\theta}\right\}$. Any unit tangent vector q at $-p$ is given by

$$q = \cos\alpha(\cos\theta)^{-1}\frac{\partial\Phi}{\partial\varphi} + \sin\alpha\frac{\partial\Phi}{\partial\theta} = \cos\alpha\begin{pmatrix} -\sin\varphi \\ \cos\varphi \\ 0 \end{pmatrix} + \sin\alpha\begin{pmatrix} -\sin\theta\cos\varphi \\ -\sin\theta\sin\varphi \\ \cos\theta \end{pmatrix},$$

for $\alpha \in [0, 2\pi)$, and we can parametrize SS^2 away from the circles at the two poles by $(\varphi, \theta, \alpha)$. With this we readily find that (6.2.8) becomes

$$-L(\varphi, \theta, \alpha) = \cos\theta\cos\alpha.$$

Hence the gradient $\nabla(-L) = (0, -\sin\theta\cos\alpha, -\cos\theta\sin\alpha)^{\mathrm{T}}$ vanishes exactly for $\theta = 0$ and $\alpha \in \{0, \pi\}$, i.e., at the circles over the equator. For each φ, the two critical points

$$\begin{aligned} c_1 &:= (\cos\varphi, \sin\varphi, 0, -\sin\varphi, \cos\varphi, 0), \quad -L(\varphi, 0, 0) = 1 \\ c_2 &:= (\cos\varphi, \sin\varphi, 0, \sin\varphi, -\cos\varphi, 0), \quad -L(\varphi, 0, \pi) = -1 \end{aligned}$$

give the initial conditions at $\varphi_0 := \varphi \in [0, 2\pi)$. The corresponding trajectories in the loop space $C^\infty(S^1, SS^2)$ are, respectively,

$$\begin{aligned} \gamma_1(t) &= \big(\cos(\varphi_0 + t), \sin(\varphi_0 + t), 0, -\sin(\varphi_0 + t), \cos(\varphi_0 + t), 0\big) \\ \gamma_2(t) &= \big(\cos(\varphi_0 - t), \sin(\varphi_0 - t), 0, \sin(\varphi_0 - t), -\cos(\varphi_0 - t), 0\big), \end{aligned}$$

for $t \in [0, 2\pi)$. The Hessian of $-L$ at these two circles $\gamma_1(t)$ and $\gamma_2(t)$ is, respectively:

$$\mathrm{H}_{-L}(\varphi_0 + t, 0, 0) = \begin{pmatrix} 0 & 0 & 0 \\ 0 & -1 & 0 \\ 0 & 0 & -1 \end{pmatrix}, \quad \mathrm{H}_{-L}(\varphi_0 - t, 0, \pi) = \begin{pmatrix} 0 & 0 & 0 \\ 0 & 1 & 0 \\ 0 & 0 & 1 \end{pmatrix}.$$

Therefore $-L$ is Morse–Bott along these two circles. In other words, all critical points are transverse Morse and its Hessian is non-degenerate in the direction normal to C_1. The maximum is attained along $\gamma_1(t)$ and the minimum along $\gamma_2(t)$ and their Morse–Bott indices are

$$\mathrm{ind}_{-L}\big(\gamma_1(t)\big) = 2, \quad \mathrm{ind}_{-L}\big(\gamma_2(t)\big) = 0.$$

Note that $\gamma_1(t)$ and $\gamma_2(t)$ are two circles over the equator moving in opposite direction, of Figure 6.1. To see them in the original picture, we consider the stereographic projection

$$\sigma_N \colon S^2 \setminus \{N\} \to \mathbb{R}^2, \quad (x_1, x_2, x_3) \mapsto \left(\frac{x_1}{1 - x_3}, \frac{x_2}{1 - x_3} \right),$$

and its cotangent lift

$$T^*\big(S^2 \setminus \{N\}\big) \to T^*\mathbb{R}^2, \quad (x, y) \mapsto \big(\sigma_N(x), (d\sigma_N(x)^{\mathrm{T}})^{-1}(y)\big),$$

where $(d\sigma_N(x)^{\mathrm{T}})^{-1}(y) = \big(y_1(1 - x_3) + x_1 y_3, y_2(1 - x_3) + x_2 y_3\big)$. Together with the switch (6.1.1) we obtain that the maximum γ_1 corresponds to

$$\big(q_1(t), q_2(t), p_1(t), p_2(t)\big) = \big(-\sin(\varphi_0 + t), \cos(\varphi_0 + t), -\cos(\varphi_0 + t), -\sin(\varphi_0 + t)\big),$$

which rotates in a direct motion, and the minimum γ_2 to

$$\big(q_1(t), q_2(t), p_1(t), p_2(t)\big) = \big(\sin(\varphi_0 - t), -\cos(\varphi_0 - t), -\cos(\varphi_0 - t), -\sin(\varphi_0 - t)\big),$$

which rotates in a retrograde motion. Their angular momentum is -1 resp. 1. □

Lemma 6.2.2 (Spatial case). *The critical points of (6.2.9) are exactly four circles, and (6.2.9) is Morse–Bott along them. There are one maximum, two saddle points and one minimum. The maximum and minimum are two critical points inherited from the planar case, and the two saddle points are two circles moving through the north pole. Moreover,*

crit$(-L)$	*Morse–Bott index*	*corresponding periodic orbit in the original picture*
maximum	*4*	*circular direct motion (planar)*
saddle point	*2*	*collision orbit bouncing back (spatial)*
saddle point	*2*	*collision orbit bouncing back (spatial)*
minimum	*0*	*circular retrograde motion (planar)*

Proof. By using a parametrization of S^3 where the north and south poles are not parametrized, one obtains two critical points inherited from the planar problem, namely

$$\begin{aligned} c_1 &:= (\cos\varphi, \sin\varphi, 0, 0, -\sin\varphi, \cos\varphi, 0, 0), & -L(c_1) &= 1, & \mathrm{ind}_{-L}(c_1) &= 4, \\ c_2 &:= (\cos\varphi, \sin\varphi, 0, 0, \sin\varphi, -\cos\varphi, 0, 0), & -L(c_2) &= -1, & \mathrm{ind}_{-L}(c_2) &= 0. \end{aligned}$$

Therefore we parametrize S^3 by

$$\Phi\colon [0,2\pi)\times(-\frac{\pi}{2},\frac{\pi}{2})\times(-\frac{\pi}{2},\frac{\pi}{2})\to\mathbb{R}^4,\quad (\varphi,\theta_1,\theta_2)\mapsto\begin{pmatrix}\sin\theta_2\\ \sin\theta_1\cos\theta_2\\ \cos\theta_1\cos\theta_2\cos\varphi\\ \cos\theta_1\cos\theta_2\sin\varphi\end{pmatrix}.$$

At a point $-p\in S^3$ we choose $\left\{(\cos\theta_1)^{-1}(\cos\theta_2)^{-1}\frac{\partial\Phi}{\partial\varphi},(\cos\theta_2)^{-1}\frac{\partial\Phi}{\partial\theta_1},\frac{\partial\Phi}{\partial\theta_2}\right\}$ as the orthonormal basis of the tangent plane $T_{-p}S^3$. Then every unit tangent vector q at $-p$ is written as

$$q=\cos\alpha_1\cos\alpha_2\begin{pmatrix}0\\0\\-\sin\varphi\\\cos\varphi\end{pmatrix}+\cos\alpha_1\sin\alpha_2\begin{pmatrix}0\\\cos\theta_1\\-\sin\theta_1\cos\varphi\\-\sin\theta_1\sin\varphi\end{pmatrix}+\sin\alpha_1\begin{pmatrix}\cos\theta_2\\-\sin\theta_1\sin\theta_2\\-\cos\theta_1\sin\theta_2\cos\varphi\\-\cos\theta_1\sin\theta_2\sin\varphi\end{pmatrix},$$

for $\alpha_1\in(-\frac{\pi}{2},\frac{\pi}{2})$, $\alpha_2\in[0,2\pi)$. Moreover, we parametrize SS^3 away from circles on S^3 with only first and second coordinates by $(\varphi,\theta_1,\theta_2,\alpha_1,\alpha_2)$. Then (6.2.9) becomes

$$-L(\varphi,\theta_1,\theta_2,\alpha_1,\alpha_2)=\cos\theta_1\sin\theta_2\cos\alpha_1\sin\alpha_2-\sin\theta_1\sin\alpha_1.$$

For the critical points, the third component of the gradient

$$\nabla(-L)=\begin{pmatrix}0\\-\sin\theta_1\sin\theta_2\cos\alpha_1\sin\alpha_2-\cos\theta_1\sin\alpha_1\\\cos\theta_1\cos\theta_2\cos\alpha_1\sin\alpha_2\\-\cos\theta_1\sin\theta_2\sin\alpha_1\sin\alpha_2-\sin\theta_1\cos\alpha_1\\\cos\theta_1\sin\theta_2\cos\alpha_1\cos\alpha_2\end{pmatrix}$$

implies that $\sin\alpha_2=0$, hence $\alpha_2\in\{0,\pi\}$. Moreover, by the fifth component we obtain that $\sin\theta_2=0$, i.e., $\theta_2=0$. The two cases for α_2 together with the second and fourth component give the further solutions $\alpha_1=0$ and $\theta_1=0$. Therefore in addition there are for every φ two critical points

$$\begin{aligned}c_3&:=(0,0,\cos\varphi,\sin\varphi,0,0,-\sin\varphi,\cos\varphi),&&-L(\varphi,0,0,0,0)=0,\\ c_4&:=(0,0,\cos\varphi,\sin\varphi,0,0,\sin\varphi,-\cos\varphi),&&-L(\varphi,0,0,0,\pi)=0,\end{aligned}$$

giving the initial conditions at $\varphi_0:=\varphi\in[0,2\pi)$ for the corresponding trajectories in the loop space $C^\infty(S^1,SS^3)$, which are respectively

$$\begin{aligned}\gamma_3(t)&=\big(0,0,\cos(\varphi+t),\sin(\varphi+t),0,0,-\sin(\varphi+t),\cos(\varphi+t)\big)\\ \gamma_4(t)&=\big(0,0,\cos(\varphi-t),\sin(\varphi-t),0,0,\sin(\varphi-t),-\cos(\varphi-t)\big).\end{aligned}$$

The Hessian at $(\varphi+t,0,0,0,0)$ and $(\varphi-t,0,0,0,\pi)$ is given respectively by

$$\mathrm{H}_{-L}=\begin{pmatrix}0&0&0&0&0\\0&0&0&-1&0\\0&0&0&0&1\\0&-1&0&0&0\\0&0&1&0&0\end{pmatrix},\quad \mathrm{H}_{-L}=\begin{pmatrix}0&0&0&0&0\\0&0&0&-1&0\\0&0&0&0&-1\\0&-1&0&0&0\\0&0&-1&0&0\end{pmatrix}.$$

Hence $-L$ is Morse–Bott along γ_3 and γ_4, and in each case there are besides the zero eigenvalue the eigenvalues 1 and -1 with double multiplicity, thus $\gamma_3(t)$ and $\gamma_4(t)$ are saddle points with

$$\operatorname{ind}_{-L}\big(\gamma_3(t)\big) = \operatorname{ind}_{-L}\big(\gamma_4(t)\big) = 2.$$

These two circles move trough the north pole for $\varphi_0 \pm t = \frac{\pi}{2}$ in opposite direction, i.e. in the original picture, these two great circles correspond to collision orbits moving into the mass at the origin with only the spatial coordinates bouncing back. More precisely, analogous to the planar case, by using the stereographic projection from the north pole

$$\sigma_N \colon S^3 \setminus \{N\} \to \mathbb{R}^3, \quad (x_1, x_2, x_3, x_4) \mapsto \left(\frac{x_1}{1-x_4}, \frac{x_2}{1-x_4}, \frac{x_3}{1-x_4}\right),$$

its cotangent lift

$$T^*\big(S^3 \setminus \{N\}\big) \to T^*\mathbb{R}^3, \quad (x, y) \mapsto \big(\sigma_N(x), y_1(1-x_4) + x_1 y_4, y_2(1-x_4) + x_2 y_4, y_3(1-x_4) + x_3 y_4\big)$$

and the switch (6.1.1), γ_3 resp. γ_4 become

$$\left(0, 0, 1 - \sin(\varphi_0 + t), 0, 0, \frac{\cos(\varphi_0 + t)}{\sin(\varphi_0 + t) - 1}\right), \quad \left(0, 0, \sin(\varphi_0 - t) - 1, 0, 0, \frac{\cos(\varphi_0 - t)}{\sin(\varphi_0 - t) - 1}\right).$$

The first one collides with the origin from above and the second one from below. Their angular momentum is zero. □

6.3 Morse case and bifurcation of family g and f from the geodesic flow

In each case, the S^1-action obtained by rotating the loop corresponds to the zero eigenvalue of the Hessian. By taking the quotient by this action we obtain the space of oriented unparametrized great circles on S^2 (planar case), and the same is true for all $n \geq 2$, see for instance [15], [43]. Since an oriented great circle on S^n corresponds to an oriented 2-plane through the origin of $\mathbb{R}^{n+1}$, the space of oriented unparametrized great circles on S^n is diffeomorphic to the oriented Grassmannian $G^+(2, n+1)$ of oriented 2-planes through the origin of $\mathbb{R}^{n+1}$. For instance,

$$G^+(2, 3) \cong S^2$$

by associating to an oriented 2-plane its unit normal vector. Furthermore,

$$G^+(2, 4) \cong S^2 \times S^2,$$

see [15, p. 55].

Planar case. By the invariance of the functionals $\mathcal{A}_r$ under the circle action (6.2.6), they induce action functionals

$$\overline{\mathcal{A}_r} : (\mathcal{L} \times \mathbb{R}_{>0})/S_1 \to \mathbb{R}.$$

Note that the quotient $(\mathcal{L} \times \mathbb{R}_{>0})/S_1$ is an orbifold. Since the S^1-action on $C_1 \subset \mathcal{L} \times \mathbb{R}_{>0}$ is free, the quotient space

$$C_1/S^1 \cong S^2 \subset \operatorname{crit}(\overline{\mathcal{A}_0})$$

is a submanifold of $(\mathcal{L} \times \mathbb{R}_{>0})/S^1$, which is the space of oriented unparametrized great circles on S^2. Hence in view of (6.2.7) the restriction

$$\overline{\overset{\circ}{\mathcal{A}_0}}|_{S^2} = \overline{-2\pi L(-p,q)}|_{S^2} \colon S^2 \to \mathbb{R}$$

is a Morse function on S^2 having one maximum and one minimum with Morse indices 2 and 0, respectively. In particular, $\overline{\overset{\circ}{\mathcal{A}_0}}|_{S^2}$ is diffeomorphic to the standard height function on S^2. Hence two families of periodic orbits bifurcate like the critical points on S^2. This bifurcation is generated by a small perturbation of $\overline{\overset{\circ}{\mathcal{A}_0}}|_{S^2}$, as follows from the implicit function theorem which we mentioned in the beginning of this chapter.

Therefore, there exists $\varepsilon > 0$, an open neighborhood U of S^2 in $(\mathcal{L} \times \mathbb{R}_{>0})/S^1$ and a one-parameter family of smooth functions

$$x_r = x(\cdot, r) : \operatorname{crit}(\overline{\overset{\circ}{\mathcal{A}_0}}|_{S^2}) \to U, \quad r \in [0, \varepsilon)$$

with the following two properties:

i) If $\iota : \operatorname{crit}(\overline{\overset{\circ}{\mathcal{A}_0}}|_{S^2}) \to U$ is the inclusion, then $x_0 = x(\cdot, 0) = \iota$.

ii) For every $r \in (0, \varepsilon)$ the restriction $\overline{\overset{\circ}{\mathcal{A}_r}}|_U$ is Morse and $\operatorname{crit}(\overline{\overset{\circ}{\mathcal{A}_r}}|_U) = \operatorname{im}(x_r) = \operatorname{im}(x(\cdot, r))$.

The family bifurcating from the circular direct one (corresponding to the maximum) is referred to as **direct periodic orbits**, and the family bifurcating from the circular retrograde orbit (corresponding to the minimum) as **retrograde periodic orbits**. We call them **family g and f**, respectively. The bifurcation scenario is shown in Figure 6.2.

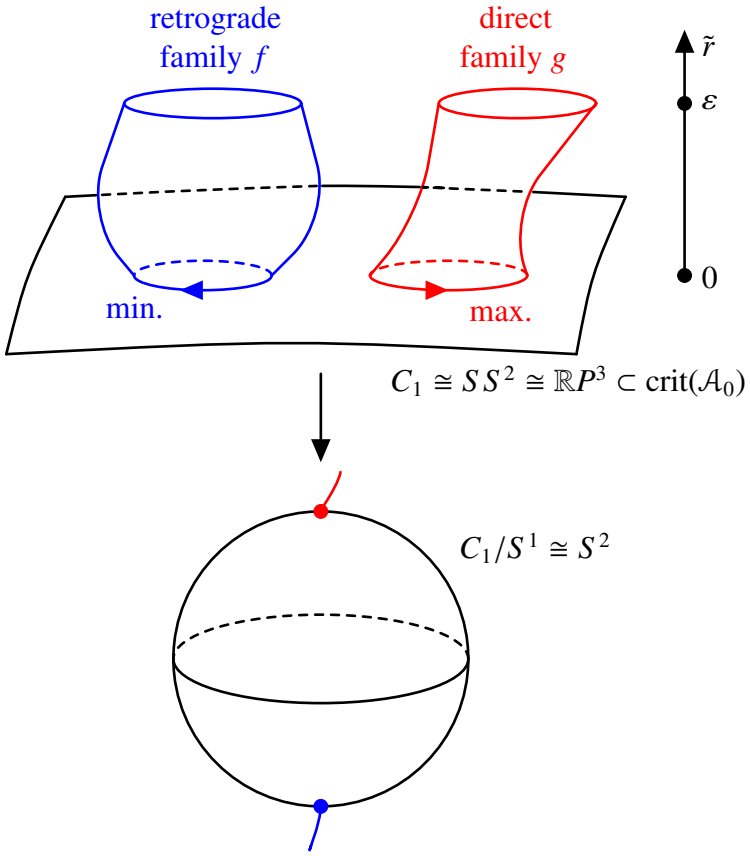

Figure 6.2: Periodic orbits bifurcate like critical points of the height function on S^2.

The Conley–Zehnder indices. In our transversally non-degenerate setting the transversal Conley–Zehnder index of each bifurcating family from the geodesic flow equals the sum of the Morse–Bott index ind_{C_1} and the Morse index $\mathrm{ind}_{\overline{\mathcal{A}_0}|_{S^2}}$. Therefore we have

$$\mu_{CZ} = \mathrm{ind}_{C_1} + \mathrm{ind}_{\overline{\mathcal{A}_0}|_{S^2}} = \begin{cases} 1+2=3 & \text{for family } g \\ 1+0=1 & \text{for family } f, \end{cases}$$

which proves Theorem 1.2.3.

Spatial case. Recall that the space of oriented unparametrized great circles on S^3 is diffeomorphic to $S^2 \times S^2$. Thus the restriction

$$\overline{\mathcal{A}_0}|_{S^2\times S^2} = \overline{-2\pi L(-p,q)}|_{S^2\times S^2} \colon S^2 \times S^2 \to \mathbb{R}$$

is a Morse function on $S^2 \times S^2$ having one maximum, two saddle points and one minimum with Morse indices 4, 2, 2, and 0, respectively. The planar direct orbit, two collision spatial orbits and planar retrograde periodic orbit bifurcate now like these critical points on $S^2 \times S^2$, which is illustrated in Figure 6.3.

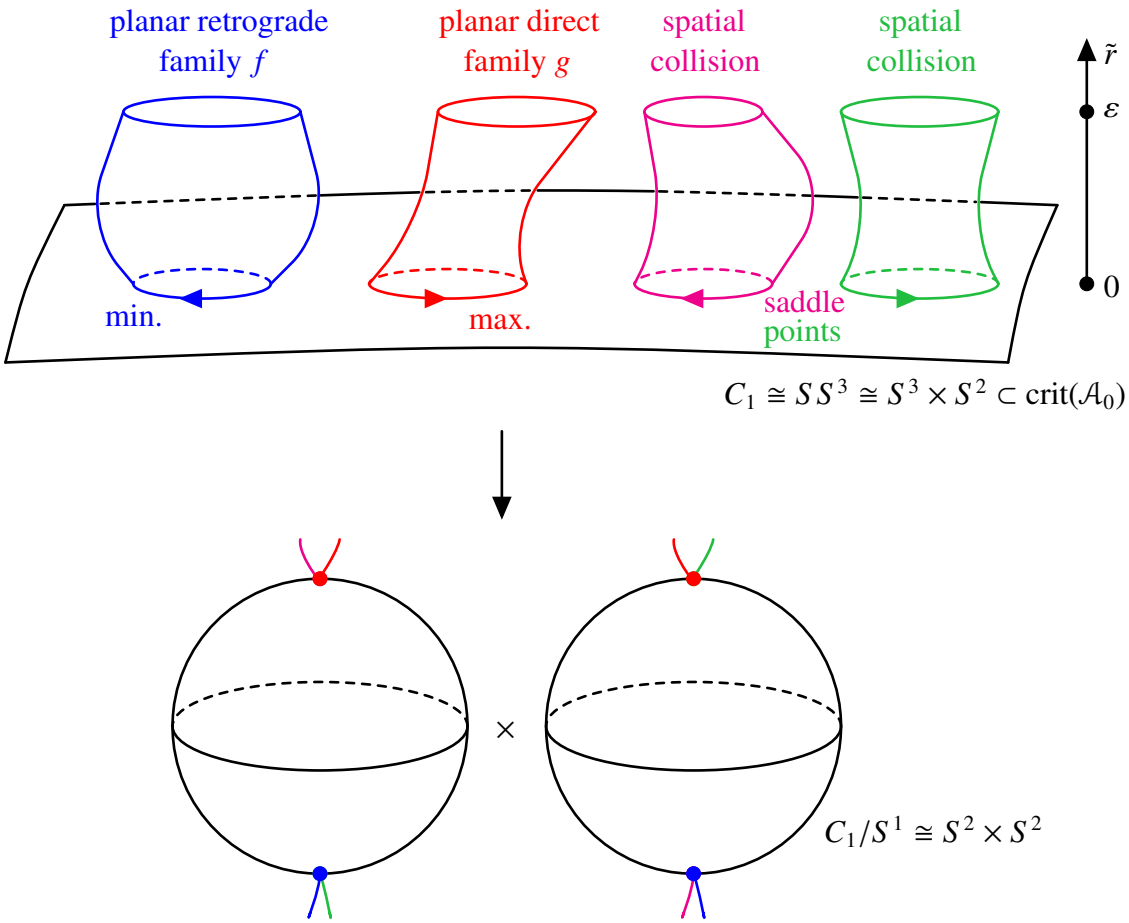

Figure 6.3: Bifurcation picture in the spatial case.

Now Theorem 1.2.4 follows by the indices given by

$$\mu_{CZ} = \operatorname{ind}_{C_1} + \operatorname{ind}_{\frac{\circ}{\mathcal{A}_0}|_{S^2\times S^2}} = \begin{cases} 2+4=6 & \text{for family } g \text{ (planar)} \\ 2+2=4 & \text{for collision orbits (spatial)} \\ 2+2=4 & \text{for collision orbits (spatial)} \\ 2+0=2 & \text{for family } f \text{ (planar).} \end{cases}$$

6.4 General Hamiltonians

Proposition 6.4.1. The bifurcation picture of this chapter holds for all Hamiltonians of the form

$$T^*\big(\Omega \setminus \{(0,0,0)\}\big) \to \mathbb{R}, \quad (q,p) \mapsto \frac{1}{2}|p|^2 - \frac{\mu}{|q|} + p_1q_2 - p_2q_1 + V(q), \tag{6.4.10}$$

where $\Omega \subset \mathbb{R}^3$ is an open subset containing the origin, $V\colon \Omega \to \mathbb{R}$ is a smooth function such that $(0,0,0) \in \operatorname{crit}(V)$ and $\mu > 0$.

Remark 6.4.2. These forms of Hamiltonians consist of the rotating Kepler problem plus some velocity independent forces given by $V(q)$.

Proof of Proposition 7.4.1. For the proof one needs to verify the same steps as in [27, pp. 138–140] where the analog statement of the planar case is shown.

For given $c < 0$, the regularization of (6.4.10) is given by

$$\begin{aligned} K_c(-p,q) &= \frac{1}{2}\left(-\frac{|q|}{2c}\Big(H\big(-\frac{q}{2c}, \sqrt{-2c}p\big) - c - V(0)\Big) + \mu\right)^2 - \frac{\mu^2}{2} \\ &= \frac{1}{2}\left(\frac{1}{2}\big(1+|p|^2\big) + \frac{p_1q_2 - p_2q_1}{(-2c)^{\frac{3}{2}}} - \frac{V(-\frac{q}{2c}) - V(0)}{2c}\right)^2 |q|^2 - \frac{\mu^2}{2}. \end{aligned}$$

As in the spatial Hill three-body problem, we change the energy parameter to $c = \frac{-1}{2r^{2/3}}$ and obtain

$$K_r(-p,q) := \frac{1}{2}\left(\frac{1}{2}\big(1+|p|^2\big) + (p_1q_2 - p_2q_1)r + \big(V(qr^{\frac{2}{3}}) - V(0)\big)r^{\frac{2}{3}}\right)^2 |q|^2 - \frac{\mu^2}{2}.$$

We see immediately that the Hamiltonian

$$K_0(-p,q) = \frac{1}{2}\left(\frac{1}{2}(1+|p|^2)\right)^2 |q|^2 - \frac{\mu^2}{2}$$

is independent from the choice of V. Moreover, its flow on $K_0^{-1}(0)$ is the geodesic flow on S^3 up to reparametrization.

The same calculation as in [27, pp. 138–140] shows that K_r is twice continuously differentiable in $r \in [0,\infty)$ and

$$\left.\frac{\partial K_r}{\partial r}\right|_{r=0}(-p,q) = \sqrt{\big(2K_0(-p,q) + \mu^2\big)}|q|(p_1q_2 - p_2q_1),$$

which does not depend on V as well. Hence, exactly as in the spatial Hill three-body problem, the geodesic flow bifurcates at $r = 0$ into the four known periodic orbits. □

Remark 6.4.3. The further assumption that the Hamiltonian (6.4.10) is invariant under the symplectic involution σ from (1.2.3) implies the additive splitting of the Conley–Zehnder indices for planar periodic orbits, such as in the spatial Hill three-body problem.

7 Local Floer homology and good & bad orbits

"Floer homology is today an essential technique in symplectic topology. Inspired by ideas of Witten and Gromov in the 1980s, it has made possible the resolution of many difficult problems, and continues to do so."

- M. Audin and M. Damian in [7, p. vii] (2014)

We now work locally near a family of non-degenerate periodic orbits. The crossing of the eigenvalue 1, and thereby the index jump, generates bifurcations of new families of planar or spatial periodic orbits, respectively. For details on the existence and properties of such bifurcations we refer to the book of Abraham–Marsden [1, pp. 597–604]. The Conley–Zehnder index leads to a grading on the local Floer homology. At a bifurcation point, the local Floer homology and its Euler characteristic stay invariant. We refer the curious reader for details on local Floer homology to the article by Ginzburg [29] (2010). Moreover, we consider unparametrized periodic orbits, hence we need to use the equivariant Floer homology, whose local version is described by Ginzburg–Gürel [30] (2020).

In our set-up, we need to use the local version of the S^1-equivariant Floer homology of the Rabinowitz action functional (6.2.5), since we mod out the circle S^1-action given by reparametrization of the free loop space. The Floer homology for the Rabinowitz action functional was introduced by Cieliebak–Frauenfelder [21] (2009) and the S^1-equivariant Rabinowitz–Floer homology was discussed by Frauenfelder–Schlenk [26] (2016), whose local version is our tool.

Notice that for every $\tilde{k}$-th cover of a periodic orbit there is a local S^1-equivariant Rabinowitz–Floer homology associated to this $\tilde{k}$-th cover. Given a family $\tilde{\gamma}$ of non-degenerate unparametrized periodic orbits, we denote by

$$RFH_*^{S^1}(\tilde{\gamma})$$

its local S^1-equivariant Rabinowitz–Floer homology and by

$$\chi(\tilde{\gamma}) = \sum_{m\in\mathbb{Z}} (-1)^m \dim RFH_m^{S^1}(\tilde{\gamma})$$

its Euler characteristic. The following two important examples are analogous to those given in [30, p. 540].

Example 7.0.1. Let $\tilde{\gamma}$ be a family of simple closed non-degenerate periodic orbits. Then, $RFH_*^{S^1}(\tilde{\gamma})$ has rank one when $*$ equals the Conley–Zehnder index of $\tilde{\gamma}$ and zero otherwise.

Example 7.0.2 (Good and bad orbits). Assume that an iterated planar periodic orbit $q^{\tilde{k}}$ is non-degenerate for all $\tilde{k} \geq 1$. Its indices we denote by $\mu_{CZ}^p(q^{\tilde{k}})$ and $\mu_{CZ}^s(q^{\tilde{k}})$ which are determined by the index iteration in Table 2.1. Let $\mu_{CZ}^p(q)$ and $\mu_{CZ}^s(q)$ be the indices of the underlying simple closed periodic orbit q, then if

$$\mu_{CZ}^p(q^{\tilde{k}}) \equiv \mu_{CZ}^p(q) \bmod 2, \quad \mu_{CZ}^s(q^{\tilde{k}}) \equiv \mu_{CZ}^s(q) \bmod 2, \tag{7.0.1}$$

or both equations in (7.0.1) are not simultaneously satisfied, then $q^{\tilde{k}}$ is called a **good orbit**. Otherwise, $q^{\tilde{k}}$ is called a **bad orbit**. Therefore, all simple closed periodic orbits are good. Furthermore, bad orbits occur as $\tilde{k}$-th cover of planar periodic orbits which are either planar or spatial negative hyperbolic, where $\tilde{k}$ is even. If $\tilde{\gamma}$ is a family of good orbits, then

$$RFH_*^{S^1}(\tilde{\gamma}\,;\,\mathbb{Q}) = \begin{cases} \mathbb{Q}, & * = \mu_{CZ} \\ 0, & \text{otherwise.} \end{cases}$$

If $\tilde{\gamma}$ is a family of bad orbits, then

$$RFH_*^{S^1}(\tilde{\gamma}\,;\,\mathbb{Q}) = 0$$

in all degrees. Hence bad orbits contribute nothing to the local homology and the Euler characteristic.

Family g and f for very low energies. For planar families we have two local homologies, namely one viewed in the planar problem and one in the spatial problem. They differ only by the index shift given by μ_{CZ}^s and we denote them by

$$pRFH_*^{S^1}(\tilde{\gamma}\,;\,\mathbb{Q}), \quad \chi_p(\tilde{\gamma}), \qquad\qquad sRFH_*^{S^1}(\tilde{\gamma}\,;\,\mathbb{Q}), \quad \chi_s(\tilde{\gamma}).$$

Note that a planar periodic orbit can be a good orbit viewed in the planar system but a bad orbit considered in the spatial system, and vice versa. Therefore in view of the last chapter, for very low energies we have

$$pRFH_*^{S^1}(g\,;\,\mathbb{Q}) = \begin{cases} \mathbb{Q}, & * = 3 \\ 0, & \text{otherwise} \end{cases} \qquad \chi_p(g) = (-1)^3 = -1$$

$$sRFH_*^{S^1}(g\,;\,\mathbb{Q}) = \begin{cases} \mathbb{Q}, & * = 6 \\ 0, & \text{otherwise} \end{cases} \qquad \chi_s(g) = (-1)^6 = 1$$

$$pRFH_*^{S^1}(f\,;\,\mathbb{Q}) = \begin{cases} \mathbb{Q}, & * = 1 \\ 0, & \text{otherwise} \end{cases} \qquad \chi_p(f) = (-1)^1 = -1$$

$$sRFH_*^{S^1}(f\,;\,\mathbb{Q}) = \begin{cases} \mathbb{Q}, & * = 2 \\ 0, & \text{otherwise} \end{cases} \qquad \chi_s(f) = (-1)^2 = 1.$$

8 Numerical data and detailed results

> "*Consider a complex system (say, the restricted problem) and investigate the behavior of this system, regarding periodic motion. If a family of periodic orbits of this system exists, then often numerical integration must be used to find the family when the system is of any difficulty. On the other hand there are large classes of periodic orbits which defy the application of presently existing analytical existence proofs. Nevertheless, one may be able to find orbits which, within the limitations of numerical accuracies, show periodicity. Such experimental findings then may suggest that analytical attempts be made to show the actual existence of these orbits.*"
>
> - V. Szebehely in [56, p. 443] (1967)

8.1 Planar direct periodic orbits

8.1.1 The family g

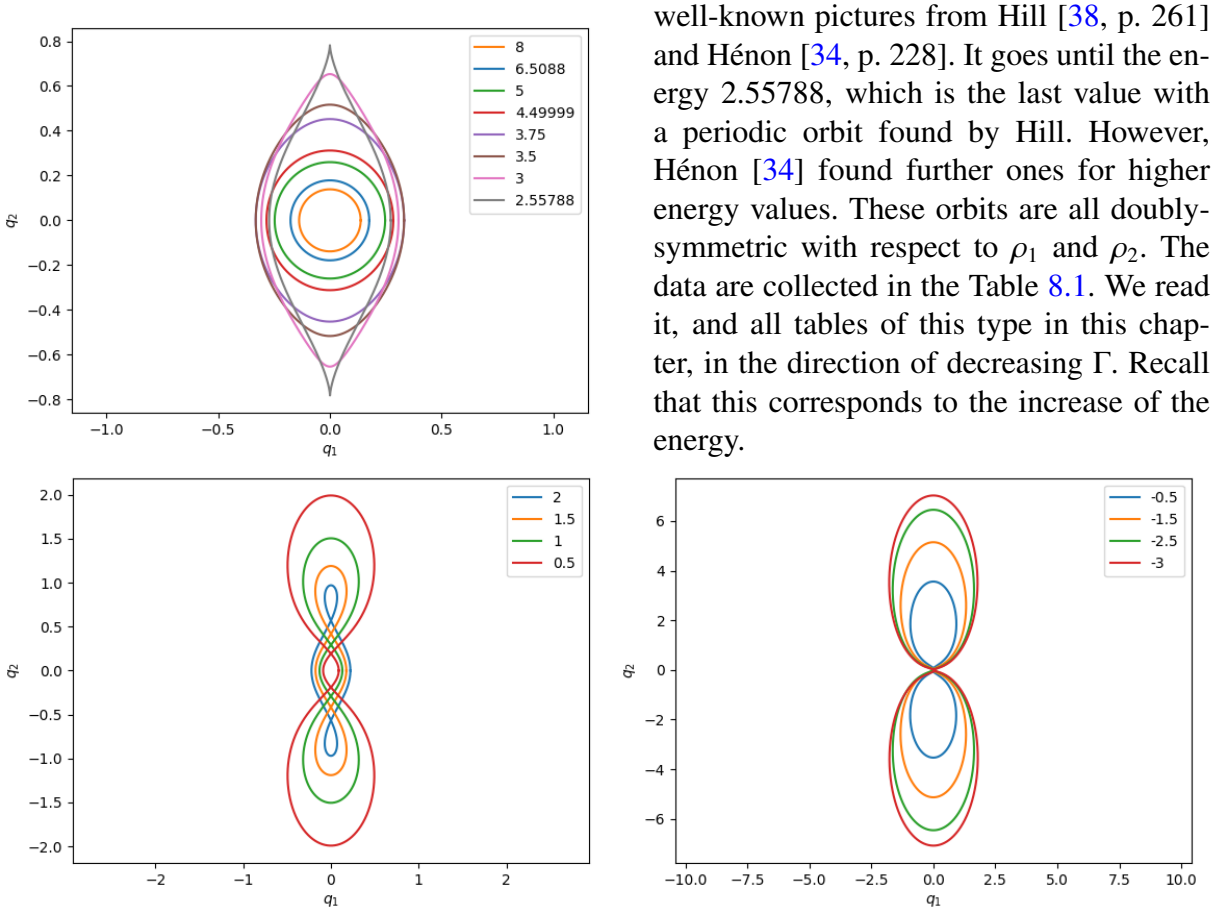

Figure 8.1: The family g.

Our first plot in Figure 8.1 is similar to the well-known pictures from Hill [38, p. 261] and Hénon [34, p. 228]. It goes until the energy 2.55788, which is the last value with a periodic orbit found by Hill. However, Hénon [34] found further ones for higher energy values. These orbits are all doubly-symmetric with respect to ρ_1 and ρ_2. The data are collected in the Table 8.1. We read it, and all tables of this type in this chapter, in the direction of decreasing Γ. Recall that this corresponds to the increase of the energy.

Γ	$q_1(0)$	$\dot{q}_2(0)$	T_s	$\mathrm{tr}(\overline{A}_p)$	$\mathrm{sign}_{c/b}(\varphi_p/\lambda_p)$	T_a	$\mathrm{tr}(A_s)$	$\mathrm{sign}_{\tilde{c}/\tilde{b}}(\varphi_s/\lambda_s)$	T_d	$\mu^p_{CZ}/\mu^s_{CZ}/\mu_{CZ}$
8	0.13772	2.56	19.78	1.89	$(+/-)\ \varphi_p = 0.31$	18.82	1.87	$(+/-)\ \varphi_s = 0.35$	18.73	3 / 3 / 6
6.5088	0.176097	2.22	29.52	1.80	$(+/-)\ \varphi_p = 0.44$	27.55	1.72	$(+/-)\ \varphi_s = 0.53$	27.21	3 / 3 / 6
5	0.247	1.81	53.64	1.65	$(+/-)\ \varphi_p = 0.59$	49.01	1.07	$(+/-)\ \varphi_s = 1.01$	46.27	3 / 3 / 6
4.49999	0.283500	1.67	71.25	1.99	$(+/-)\ \varphi_p = 0.03$	70.91	0.43	$(+/-)\ \varphi_s = 1.34$	58.66	3 / 3 / 6
4.278924	0.301158	1.62	82.44	2.71	$(-/-)\ \lambda_p = 2.26$		≈ 0	$(+/-)\ \varphi_s = 1.57$	65.95	2 / 3 / 5
3.876616	0.327645	1.59	109.5	8.64	$(-/-)\ \lambda_p = 8.53$		−1.0	$(+/-)\ \varphi_s = 2.09$	82.15	2 / 3 / 5
3.75	0.33178	1.61	119.3	14.1	$(-/-)\ \lambda_p = 14.04$		−1.3	$(+/-)\ \varphi_s = 2.27$	87.63	2 / 3 / 5
3.5	0.331730	1.69	139.9	37.5	$(-/-)\ \lambda_p = 37.48$		−1.7	$(+/-)\ \varphi_s = 2.62$	98.05	2 / 3 / 5
3.057471	0.310843	1.91	171.2	154.3	$(-/-)\ \lambda_p = 154.3$		−2	$(+/-)\ \varphi_s = 3.14$	114.1	2 / 3 / 5
3	0.306900	1.94	175.1	178.9	$(-/-)\ \lambda_p = 178.9$		−1.9	$(-/+)\ \varphi_s = 3.20$	116.0	2 / 3 / 5
2.55788	0.271795	2.24	204.8	453.9	$(-/-)\ \lambda_p = 453.9$		−1.7	$(-/+)\ \varphi_s = 3.64$	129.7	2 / 3 / 5
2.073537	0.228450	2.61	238.9	932.6	$(-/-)\ \lambda_p = 932.6$		−0.9	$(-/+)\ \varphi_s = 4.18$	143.3	2 / 3 / 5
2	0.221683	2.67	244.5	1034	$(-/-)\ \lambda_p = 1034$		−0.8	$(-/+)\ \varphi_s = 4.29$	145.2	2 / 3 / 5
1.746370	0.198221	2.90	264.9	1356	$(-/-)\ \lambda_p = 1356$		≈ 0	$(-/+)\ \varphi_s = 4.71$	151.4	2 / 3 / 5
1.5	0.175446	3.16	287.1	1746	$(-/-)\ \lambda_p = 1746$		1.22	$(-/+)\ \varphi_s = 5.37$	154.8	2 / 3 / 5
1.383094	0.164715	3.35	298.6	1916	$(-/-)\ \lambda_p = 1916$		2.00	$(+/+)\ \lambda_s = 1.01$		2 / 4 / 6
1	0.130319	3.79	341.7	2601	$(-/-)\ \lambda_p = 2601$		5.86	$(+/+)\ \lambda_s = 5.69$		2 / 4 / 6
0.5	0.089019	4.68	412.1	4913	$(-/-)\ \lambda_p = 4913$		13.4	$(+/+)\ \lambda_s = 13.3$		2 / 4 / 6
−0.5	0.033920	7.71	550.5	9830	$(-/-)\ \lambda_p = 9830$		26.5	$(+/+)\ \lambda_s = 26.4$		2 / 4 / 6
−1.5	0.013560	12.2	620.5	27860	$(-/-)\ \lambda_p = 27860$		16.2	$(+/+)\ \lambda_s = 16.2$		2 / 4 / 6
−2.5	0.006313	17.8	653.8	63560	$(-/-)\ \lambda_p = 63560$		6.07	$(+/+)\ \lambda_s = 5.90$		2 / 4 / 6
−3	0.004523	21.1	665.7	90300	$(-/-)\ \lambda_p = 90300$		3.69	$(+/+)\ \lambda_s = 3.39$		2 / 4 / 6

Table 8.1: The family g.

The maximum of $q_1(0)$ is reached at about $\Gamma = 3.75$ and the orbits come closer and closer to the earth. According to [34, pp. 230–234], based on numerical results, the distance $q_1(0)$ converges to 0 if the energy Γ goes to $-\infty$. Hence in the limit there is a collision. In that case the period is 4π, thus the synodic month T_s takes 730.5 days. In addition, by [36, p. 319], $\mathrm{tr}(A_s)$ converges to 2 from above. Notice that the speed of the orbit increases if it is closer to the earth.

Very shortly above $\Gamma = 4.49999$ the planar index μ^p_{CZ} jumps from 3 to 2 since the rotation by φ_p goes to zero at that point. From then on the orbits are planar pos. hyperb. I. Slightly before this transition the anomalistic period is almost the synodic period. At this transition a new family of planar periodic orbits bifurcates (see the family g' in the next Subsection 8.1.2). This bifurcation arises below the critical value $3^{4/3}$ and above the energy value for the Moon (from the second row in Table 8.1).

Furthermore, these orbits are all spatial elliptic until shortly before the energy value $\Gamma = 1.383094$ where they become spatial pos. hyperb. II and φ_s goes through 2π. Thus μ^s_{CZ} jumps from 3 to 4, and shortly before this change, the draconitic period is almost half of the synodic period. At this transition a new family of spatial periodic orbits bifurcates from the planar (see the family g_{2v} in the Subsection 8.3.1).

We note that all initial data are from Hénon [34], [36] and Hill [38], except the ones for the energy values 4.278924, 3.876616, 2.073537 and 1.746370, where φ_s is a 3th resp. 4th root of unity, which are from Kalantonis [44].

8.1.2 The family g'

The family g' branches out from the family g at the energy value $\Gamma = 4.49999$ (see Table 8.1), which was discovered by Hénon [34]. At this bifurcation the double-symmetry breaks, meaning that the orbits are only symmetric with respect to ρ_1 (see Figure 8.3). By using ρ_2, i.e., the reflection on the q_2-axis, these orbits appear twice. The data of the family g' are collected in the Table 8.2. The family g' and its symmetric family start being planar as well as spatial elliptic and its both indices start with 3.

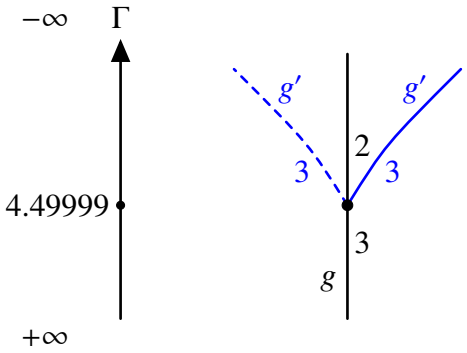

In Table 1.7 we checked that the Euler characteristics before and after bifurcation coincide, which can be seen in Figure 8.2 as well.

Figure 8.2: The bifurcation graph between g and g' with planar indices. The horizontal symmetry corresponds to the reflection about the q_2-axis.

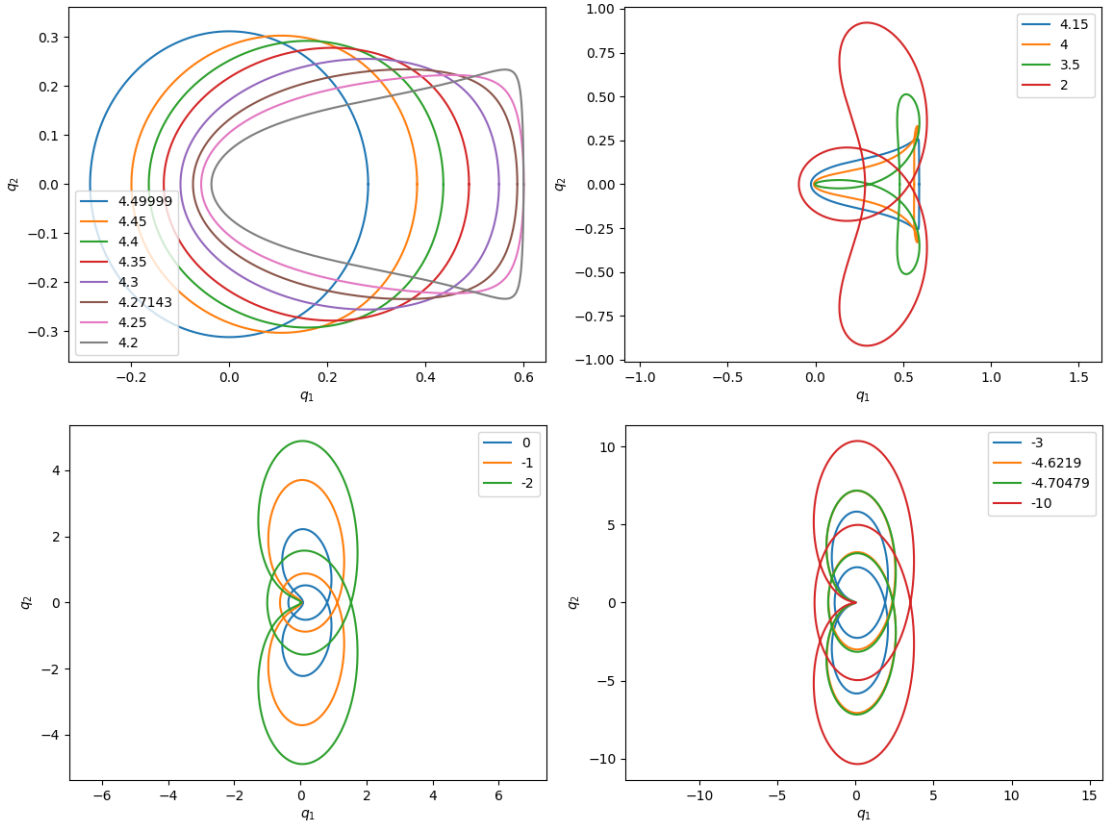

Figure 8.3: The family g'.

In view of Table 8.2, we see the same behaviour as for the family g of the distances $q_1(0)$, namely there is a collision in the limit.

Note that we have found the initial conditions for the Γ value -4.69849 by ourselves. Since at this Γ we have $\varphi_p = 4.75$, we can imply that the planar index jumps from 3 to 4 in which we can see that φ_p goes through 2π and hence μ_{CZ}^p jumps from 3 to 4.

The initial data for the energy values 4.435711, 4.347942, 4.242877, 4.200105, 0.063099 and -0.081977, where φ_s is a 3rd resp. 4th root of unity, are from Kalantonis [44] and the others from Hénon [34], [36].

Γ	$q_1(0)$	$\dot{q}_2(0)$	T_s	$\mathrm{tr}(\overline{A}_p)$	$\mathrm{sign}_{c/b}(\varphi_p/\lambda_p)$	T_a	$\mathrm{tr}(A_s)$	$\mathrm{sign}_{\tilde{c}/\tilde{b}}(\varphi_s/\lambda_s)$	T_d	$\mu^p_{CZ}/\mu^s_{CZ}/\mu_{CZ}$
4.49999	0.283500	1.67	71.25	1.99	$(+/-)\ \varphi_p = 0.03$	70.92	0.43	$(+/-)\ \varphi_s = 1.34$	58.66	3 / 3 / 6
4.45	0.383360	1.09	76.34	1.77	$(+/-)\ \varphi_p = 0.47$	70.96	0.11	$(+/-)\ \varphi_s = 1.51$	61.52	3 / 3 / 6
4.435711	0.399433	1.02	78.07	1.69	$(+/-)\ \varphi_p = 0.55$	71.72	≈ 0	$(+/-)\ \varphi_s = 1.57$	62.45	3 / 3 / 6
4.4	0.436840	0.86	83.11	1.45	$(+/-)\ \varphi_p = 0.75$	74.18	−0.3	$(+/-)\ \varphi_s = 1.73$	65.11	3 / 3 / 6
4.35	0.489180	0.67	93.16	0.95	$(+/-)\ \varphi_p = 1.07$	79.57	−0.9	$(+/-)\ \varphi_s = 2.07$	70.02	3 / 3 / 6
4.347942	0.491443	0.66	93.70	0.93	$(+/-)\ \varphi_p = 1.08$	79.88	−1.0	$(+/-)\ \varphi_s = 2.09$	70.27	3 / 3 / 6
4.3	0.550290	0.49	112.1	0.04	$(+/-)\ \varphi_p = 1.54$	90.01	−1.8	$(+/-)\ \varphi_s = 2.73$	78.18	3 / 3 / 6
4.285183	0.570854	0.44	122.2	−0.5	$(+/-)\ \varphi_p = 1.86$	94.28	−1.9	$(+/-)\ \varphi_s = 3.13$	81.54	3 / 3 / 6
4.282893	0.573907	0.43	124.0	−0.7	$(+/-)\ \varphi_p = 1.94$	94.73	−2.0	$(+/+)\ \lambda_s = -1.06$		3 / 3 / 6
4.280603	0.576960	0.42	125.9	−0.9	$(+/-)\ \varphi_p = 2.04$	95.05	−1.9	$(-/+)\ \varphi_s = 3.14$	83.95	3 / 3 / 6
4.27143	0.587690	0.41	133.8	−1.9	$(+/-)\ \varphi_p = 3.11$	89.47	−1.8	$(-/+)\ \varphi_s = 3.47$	86.15	3 / 3 / 6
4.25	0.600900	0.40	150.0	−8.1	$(+/+)\ \lambda_p = -8.0$		−1.2	$(-/+)\ \varphi_s = 4.04$	91.25	3 / 3 / 6
4.242877	0.602371	0.40	154.0	−11.2	$(+/+)\ \lambda_p = -11.1$		−0.9	$(-/+)\ \varphi_s = 4.18$	92.43	3 / 3 / 6
4.200105	0.600418	0.46	169.0	−35.6	$(+/+)\ \lambda_p = -35.6$		≈ 0	$(-/+)\ \varphi_s = 4.71$	96.58	3 / 3 / 6
4.2	0.600400	0.46	169.0	−35.6	$(+/+)\ \lambda_p = -35.6$		≈ 0	$(-/+)\ \varphi_s = 4.71$	96.58	3 / 3 / 6
4.15	0.59171	0.52	177.8	−67.2	$(+/+)\ \lambda_p = -67.2$		0.6	$(-/+)\ \varphi_s = 5.07$	98.86	3 / 3 / 6
4	0.562913	0.70	190.1	−150	$(+/+)\ \lambda_p = -150$		1.3	$(-/+)\ \varphi_s = 5.43$	102.0	3 / 3 / 6
3.5	0.480802	1.16	207.9	−305	$(+/+)\ \lambda_p = -304$		1.9	$(-/+)\ \varphi_s = 6.02$	106.1	3 / 3 / 6
3.390159	0.464697	1.24	211.0	−313	$(+/+)\ \lambda_p = -313$		2.0	$(+/+)\ \lambda_s = 1.00$		3 / 4 / 7
2	0.283653	2.30	262.1	−421	$(+/+)\ \lambda_p = -421$		2.6	$(+/+)\ \lambda_s = 2.16$		3 / 4 / 7
1.5	0.224220	2.75	293.2	−439	$(+/+)\ \lambda_p = -439$		2.7	$(+/+)\ \lambda_s = 2.36$		3 / 4 / 7
1	0.167780	3.31	337.7	−465	$(+/+)\ \lambda_p = -465$		2.7	$(+/+)\ \lambda_s = 2.35$		3 / 4 / 7
0.5	0.116370	4.08	401.6	−511	$(+/+)\ \lambda_p = -511$		2.1	$(+/+)\ \lambda_s = 1.32$		3 / 4 / 7
0.477157	0.114196	4.13	405.1	−514	$(+/+)\ \lambda_p = -514$		2.0	$(+/+)\ \lambda_s = 1.03$		3 / 4 / 7
0.063099	0.078843	5.03	474.4	−596	$(+/+)\ \lambda_p = -596$		≈ 0	$(+/-)\ \varphi_s = 1.57$	210.8	3 / 5 / 8
0	0.074220	5.19	485.8	−614	$(+/+)\ \lambda_p = -614$		−0.4	$(+/-)\ \varphi_s = 1.78$	212.6	3 / 5 / 8
−0.081977	0.068564	5.40	500.2	−639	$(+/+)\ \lambda_p = -639$		−0.9	$(+/-)\ \varphi_s = 2.09$	214.4	3 / 5 / 8
−0.219528	0.059949	5.79	524.6	−686	$(+/+)\ \lambda_p = -686$		−1.9	$(+/-)\ \varphi_s = 3.13$	209.9	3 / 5 / 8
−1	0.029281	8.32	643.0	−880	$(+/+)\ \lambda_p = -880$		−6.6	$(-/-)\ \lambda_s = -6.5$		3 / 5 / 8
−2	0.014641	11.7	743.8	−732	$(+/+)\ \lambda_p = -732$		−11.8	$(-/-)\ \lambda_s = -11.7$		3 / 5 / 8
−3	0.008613	15.3	796.6	−499	$(+/+)\ \lambda_p = -499$		−14.9	$(-/-)\ \lambda_s = -14.8$		3 / 5 / 8
−4.69219	0.004302	21.6	835.1	−2	$(+/+)\ \lambda_p = -1.0$		−18.3	$(-/-)\ \lambda_s = -18.2$		3 / 5 / 8
−4.69849	0.004292	21.6	836.2	0.07	$(-/+)\ \varphi_p = 4.75$	476.2	−18.9	$(-/-)\ \lambda_s = -18.8$		3 / 5 / 8
−4.70479	0.004283	21.7	836.3	2	$(-/-)\ \lambda_p = 1.0$		−19.5	$(-/-)\ \lambda_s = -19.4$		4 / 5 / 9
−5	0.003870	22.8	840.4	96.8	$(-/-)\ \lambda_p = 96.8$		−20.3	$(-/-)\ \lambda_s = -20.2$		4 / 5 / 9
−6	0.002837	26.6	850.9	432	$(-/-)\ \lambda_p = 432$		−22.9	$(-/-)\ \lambda_s = -22.8$		4 / 5 / 9
−10	0.001162	41.6	870.8	1989	$(-/-)\ \lambda_p = 1989$		−59.5	$(-/-)\ \lambda_s = -59.5$		4 / 5 / 9
−20	0.000363	74.2	876.6	7190	$(-/-)\ \lambda_p = 7190$		−3727	$(-/-)\ \lambda_s = -3727$		4 / 5 / 9

Table 8.2: The family g'.

8.2 Planar retrograde periodic orbits

8.2.1 The family f

Some of its orbits are plotted in Figure 8.4 and its data are given in Table 8.3. We observe that the retrograde periodic orbits are all planar and spatial elliptic and are at larger and larger distance from the earth. Therefore the index of the simple closed orbits does not change.

Moreover, the planar rotation angle φ_p as well as the spatial one φ_s decrease and then increase. The orbits for the Γ values from -0.2154 to -0.5269 we have found ourselves. They show that φ_s never becomes a 4th root of unity, hence the smallest one is a 5th one. Both rotation angles approach 2π for higher energy values. In other words, all three periods approach 365.25 days, which is the period of the Earth around the Sun.

The initial data for the Γ values 1.359293 and 0.755141, where φ_s is a 6th resp. 5th root of unity, are from the data provided on request by Kalantonis [44]. All the others are from Hénon [37], [34].

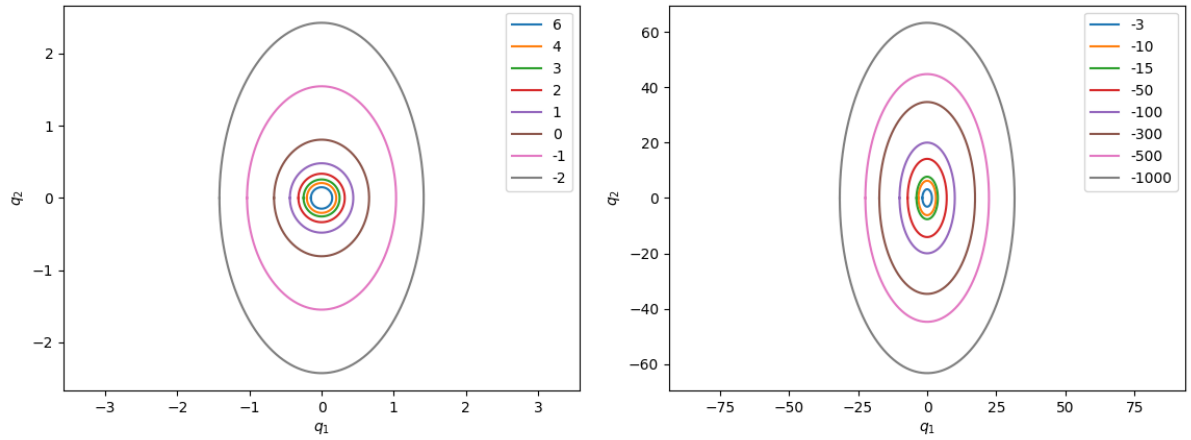

Figure 8.4: The family f.

Γ	$q_1(0)$	$\dot{q}_2(0)$	T_s	$\mathrm{tr}(\overline{A}_p)$	$\mathrm{sign}_{c/b}(\varphi_p)$	T_a	$\mathrm{tr}(A_s)$	$\mathrm{sign}_{\bar{c}/\bar{b}}(\varphi_s)$	T_d	$\mu^p_{CZ}/\mu^s_{CZ}/\mu_{CZ}$
6	−0.147790	2.75	19.72	1.88	(−/+) $\varphi_p = 5.93$	20.87	1.89	(−/+) $\varphi_s = 5.97$	20.80	1 / 1 / 2
4	−0.204210	2.43	31.19	1.70	(−/+) $\varphi_p = 5.73$	34.19	1.75	(−/+) $\varphi_s = 5.78$	33.89	1 / 1 / 2
3	−0.250710	2.27	41.49	1.48	(−/+) $\varphi_p = 5.55$	47.40	1.59	(−/+) $\varphi_s = 5.63$	46.24	1 / 1 / 2
2	−0.321630	2.12	58.28	1.05	(−/+) $\varphi_p = 5.27$	69.48	1.30	(−/+) $\varphi_s = 5.42$	67.52	1 / 1 / 2
1.359293	−0.389537	2.05	75.25	0.57	(−/+) $\varphi_p = 5.00$	94.5	0.99	(−/+) $\varphi_s = 5.23$	90.35	1 / 1 / 2
1	−0.439910	2.03	88.25	0.20	(−/+) $\varphi_p = 4.81$	115.1	0.78	(−/+) $\varphi_s = 5.11$	108.4	1 / 1 / 2
0.755141	−0.481217	2.02	99.10	−0.08	(−/+) $\varphi_p = 4.66$	133.4	0.61	(−/+) $\varphi_s = 5.02$	123.8	1 / 1 / 2
0.015388	−0.655072	2.07	145.5	−0.99	(−/+) $\varphi_p = 4.18$	218.3	0.18	(−/+) $\varphi_s = 4.80$	190.3	1 / 1 / 2
0	−0.659660	2.08	146.7	−1.01	(−/+) $\varphi_p = 4.18$	220.6	0.18	(−/+) $\varphi_s = 4.80$	192.0	1 / 1 / 2
−0.2154	−0.72779	2.13	165.0	−1.24	(−/+) $\varphi_p = 4.03$	256.8	0.14	(−/+) $\varphi_s = 4.78$	216.7	1 / 1 / 2
−0.2538	−0.74179	2.14	168.3	−1.23	(−/+) $\varphi_p = 4.04$	261.4	0.14	(−/+) $\varphi_s = 4.78$	221.1	1 / 1 / 2
−0.2681	−0.74679	2.14	169.6	−1.24	(−/+) $\varphi_p = 4.04$	263.7	0.14	(−/+) $\varphi_s = 4.78$	222.8	1 / 1 / 2
−0.2847	−0.75279	2.15	171.1	−1.24	(−/+) $\varphi_p = 4.03$	266.2	0.14	(−/+) $\varphi_s = 4.78$	224.7	1 / 1 / 2
−0.3152	−0.76259	2.16	174.0	−1.30	(−/+) $\varphi_p = 4.00$	273.1	0.15	(−/+) $\varphi_s = 4.78$	228.3	1 / 1 / 2
−0.5269	−0.84189	2.24	196.9	−1.37	(−/+) $\varphi_p = 3.95$	308.1	0.22	(−/+) $\varphi_s = 4.82$	252.4	1 / 1 / 2
−1	−1.034000	2.47	237.1	−1.29	(−/+) $\varphi_p = 4.01$	372.4	0.62	(−/+) $\varphi_s = 5.02$	296.2	1 / 1 / 2
−1.411618	−1.199879	2.71	267.3	−0.99	(−/+) $\varphi_p = 4.18$	401.1	1.02	(−/+) $\varphi_s = 5.25$	319.7	1 / 1 / 2
−2	−1.416810	3.07	296.5	−0.46	(−/+) $\varphi_p = 4.47$	416.8	1.44	(−/+) $\varphi_s = 5.52$	337.6	1 / 1 / 2
−3	−1.731950	3.62	323.2	0.28	(−/+) $\varphi_p = 4.85$	418.3	1.76	(−/+) $\varphi_s = 5.79$	350.3	1 / 1 / 2
−10	−3.162278	6.37	357.4	1.64	(−/+) $\varphi_p = 5.67$	395.8	1.99	(−/+) $\varphi_s = 6.18$	362.8	1 / 1 / 2
−15	−3.872983	7.77	360.9	1.80	(−/+) $\varphi_p = 5.83$	388.8	1.99	(−/+) $\varphi_s = 6.23$	363.9	1 / 1 / 2
−50	−7.071067	14.1	364.5	1.96	(−/+) $\varphi_p = 6.09$	375.4	1.99	(−/+) $\varphi_s = 6.27$	365.0	1 / 1 / 2
−100	−10	20.0	364.9	1.98	(−/+) $\varphi_p = 6.17$	371.4	1.99	(−/+) $\varphi_s = 6.28$	365.1	1 / 1 / 2
−300	−17.320508	34.6	365.2	1.99	(−/+) $\varphi_p = 6.23$	368.0	1.99	(−/+) $\varphi_s = 6.28$	365.2	1 / 1 / 2
−500	−22.360679	44.7	365.2	1.99	(−/+) $\varphi_p = 6.25$	367.1	1.99	(−/+) $\varphi_s = 6.28$	365.2	1 / 1 / 2
−1000	−31.622776	63.2	365.2	1.99	(−/+) $\varphi_p = 6.26$	366.3	1.99	(−/+) $\varphi_s = 6.28$	365.2	1 / 1 / 2

Table 8.3: The family f.

The limit case. Like Hénon [34, p. 227] for $\Gamma \to -\infty$ in the planar problem, we can neglect the gravitational force of the smaller primary at the origin for a first approximation, since $q_1(0)$ increases for higher energies. Then a short calculation yields a planar solution given by

$$q_1(t) = c\cos t, \quad q_2(t) = -2c\sin t, \quad p_1(t) = c\sin t, \quad p_2(t) = -c\cos t, \quad c \in \mathbb{R}, \tag{8.2.1}$$

which is in q-variables an ellipse in a retrograde motion with the origin as its center, semi-major axis c and semi-minor axis $-2c$. Through the Jacobi integral Γ one obtains the relation

$$q_1(0) = c = -\sqrt{-\Gamma}, \tag{8.2.2}$$

which we use for Table 8.3, from $\Gamma = -15$ on. To obtain the Hamiltonian in the limit, for a

constant $\gamma < 0$ we zoom out by the coordinate transformation

$$\phi_\gamma \colon T^*\mathbb{R}^3 \to T^*\mathbb{R}^3, \quad (q,p) \mapsto \big(\sqrt{(-2\gamma)}q,\ \sqrt{(-2\gamma)}p\big),$$

which is conformally symplectic, i.e., $\phi_\gamma^*\omega = -2\gamma\omega$. We introduce the family of Hamiltonians

$$H_\gamma \colon T^*\big(\mathbb{R}\setminus\{(0,0,0)\}\big) \to \mathbb{R}, \quad (q,p) \mapsto -\frac{1}{2\gamma}(H\circ\phi_\gamma)(q,p),$$

and compute

$$H_\gamma(q,p) = \frac{1}{2}\big((p_1+q_2)^2 + (p_2-q_1)^2 + p_3^2\big) - \frac{3}{2}q_1^2 + \frac{1}{2}q_3^2 - \frac{1}{|q|2\gamma\sqrt{(-2\gamma)}}.$$

For $\gamma \to -\infty$, H_γ converges uniformly in the C^∞-topology on each compact subset to

$$\widetilde{H} \colon T^*\mathbb{R}^3 \to \mathbb{R}, \quad (q,p) \mapsto \frac{1}{2}\big((p_1+q_2)^2 + (p_2-q_1)^2 + p_3^2\big) - \frac{3}{2}q_1^2 + \frac{1}{2}q_3^2.$$

Note that this limit Hamiltonian does not contain the gravitational force of the Earth, in contrast to the spatial Hill three-body problem (5.1.2).

We restrict to the planar case and consider the energy hypersurface $\Sigma := \widetilde{H}^{-1}(\frac{1}{2})$. Hence by the relation (8.2.2) and the limit solution (8.2.1) we obtain

$$c = -1, \quad q_1(t) = -\cos t, \quad q_2(t) = 2\sin t, \quad p_1(t) = -\sin t, \quad p_2(t) = \cos t,$$

with the first return time $T_q = 2\pi$, which corresponds to the synodic period of 365.25 days. The linearized equation is given by

$$\begin{cases} \Delta q_1(t) = c_1\cos t + c_2\sin t + 2c_3 \\ \Delta q_2(t) = -2c_1\sin t + 2c_2\cos t - 3c_3 t + c_4 \\ \Delta p_1(t) = c_1\sin t - c_2\cos t + 3c_3 t - c_4 \\ \Delta p_2(t) = -c_1\cos t - c_2\sin t - c_3, \end{cases}$$

where c_1, c_2, c_3 and c_4 are constants. Note that these solutions are not periodic along the flow if $c_3 \neq 0$. The basis vectors of the tangent space at q_0 are of the form

$$\big(\Delta q_1(0), \Delta q_2(0), \Delta p_1(0), \Delta p_2(0)\big) = (c_1 + 2c_3, 2c_2 + c_4, -c_2 - c_4, -c_1 - c_3).$$

The energy condition (5.3.9) implies

$$\Delta q_1(0) = -\Delta p_2(0),$$

and hence $c_3 = 0$. Therefore the linearized solutions on the energy hypersurface are 2π periodic, which means that

$$\overline{A}_p = \begin{pmatrix} 1 & 0 \\ 0 & 1 \end{pmatrix},$$

where the eigenvalue 1 has algebraic and geometric multiplicity 2.

A real fundamental system for the spatial equation is given by $\{\cos t, \sin t\}$, hence the 2π-

periodic solutions are of the form

$$\begin{cases} \Delta q_3(t) = c_1 \cos t + c_2 \sin t \\ \Delta p_3(t) = -c_1 \sin t + c_2 \cos t, \end{cases}$$

where c_1 and c_2 are constants. In particular, we have

$$A_s = \begin{pmatrix} 1 & 0 \\ 0 & 1 \end{pmatrix},$$

where the eigenvalue 1 has algebraic and geometric multiplicity 2 as well. Therefore the limit orbit is planar and spatial degenerate, and the planar and spatial neighbouring orbits make exactly one complete rotation during T_q, which corresponds to 365.25 days.

8.2.2 Family g_3: Bifurcation from a 3rd cover of f to a 3rd cover of f

At the Γ values 0.015388 and -1.411618 for the family f, where φ_p is a 3th root of unity (see Table 8.3), the planar index of each 3rd cover jumps from 5 to 3 resp. from 3 to 5. Before and after each transition of each 3rd cover of these two retrograde orbits, new families of planar retrograde periodic orbits bifurcate. These families were discovered by Hénon [35], [37] in which he named them family g_3. The orbits in these families do not lose the symmetry from f, i.e., they are also doubly-symmetric with respect to ρ_1 and ρ_2 (see Figure 8.5). Their data are collected in Table 8.4.

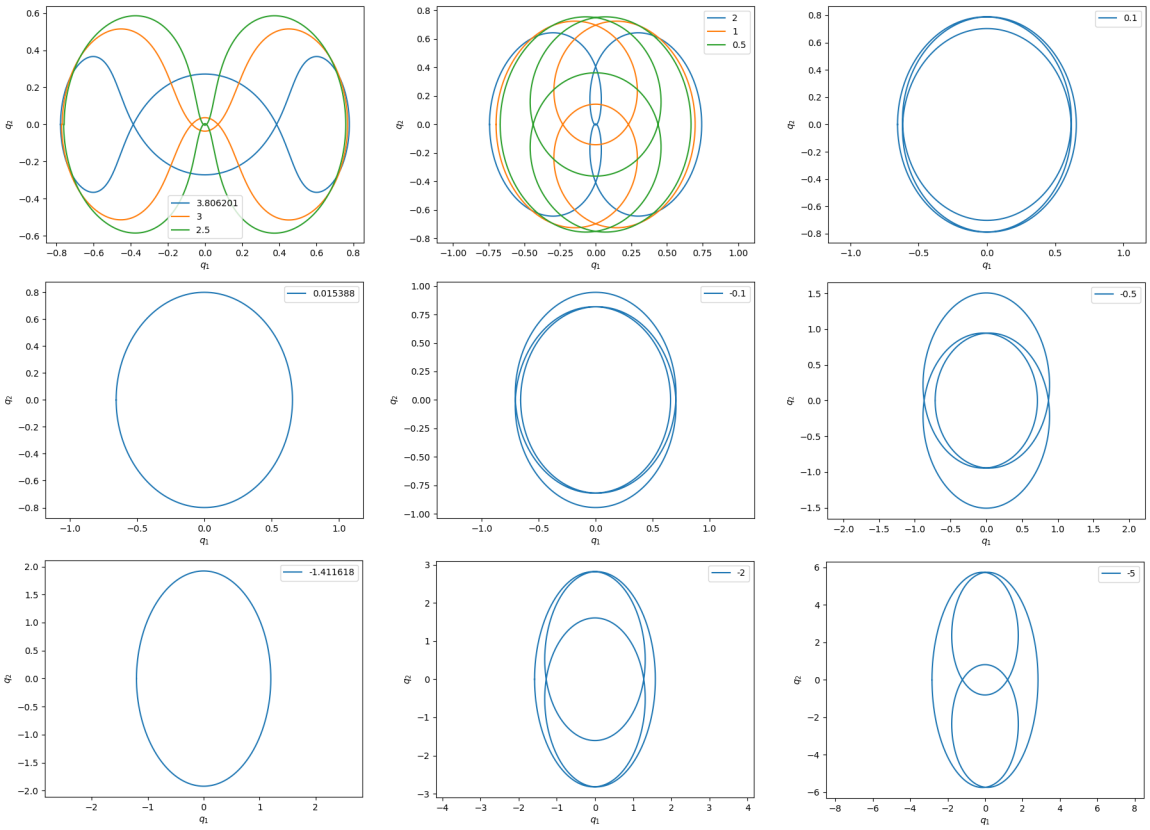

Figure 8.5: The family g_3.

Γ	$q_1(0)$	$\dot{q}_2(0)$	T_s	$\mathrm{tr}(\overline{A}_p)$	$\mathrm{sign}_{c/b}(\varphi_p/\lambda_p)$	T_a	$\mathrm{tr}(A_s)$	$\mathrm{sign}_{\bar{c}/\bar{b}}(\varphi_s/\lambda_s)$	T_d	$\mu^p_{CZ}/\mu^s_{CZ}/\mu_{CZ}$
										birth-death
3.806201	−0.77896	0.76	386.1	2.01	$(-/-)\ \lambda_p = 1.01$		2.10	$(+/+)\ \lambda_s = 1.37$		4 / 6 / 10
3.2	−0.77176	1.08	279.2	5921	$(-/-)\ \lambda_p = 5921$		−1.7	$(-/+)\ \varphi_s = 3.62$	108.36	4 / 5 / 9
3	−0.76939	1.17	271.6	3665	$(-/-)\ \lambda_p = 3665$		−1.9	$(-/+)\ \varphi_s = 3.45$	106.5	4 / 5 / 9
2.5	−0.75961	1.36	262.7	1649	$(-/-)\ \lambda_p = 1649$		−1.9	$(-/+)\ \varphi_s = 3.20$	104.6	4 / 5 / 9
2	−0.74453	1.53	263.5	367	$(-/-)\ \lambda_p = 367$		−1.9	$(+/-)\ \varphi_s = 3.03$	106.1	4 / 5 / 9
1	−0.69838	1.82	298.0	26.4	$(-/-)\ \lambda_p = 26.3$		−1.7	$(+/-)\ \varphi_s = 2.62$	123.2	4 / 5 / 9
0.5	−0.66969	1.95	346.9	5.40	$(-/-)\ \lambda_p = 5.21$		−1.2	$(+/-)\ \varphi_s = 2.26$	147.0	4 / 5 / 9
0.1	−0.65482	2.05	417.3	2.07	$(-/-)\ \lambda_p = 1.31$		−0.6	$(+/-)\ \varphi_s = 1.90$	181.2	4 / 5 / 9
0.015388	−0.655072	2.07	436.5	2.00	$\lambda_p^3 = 1.00$		−0.5	$(+/-)\ \varphi_s = 1.84$	190.3	5↛3 / 5 / 10↛8
−0.1	−0.65866	2.10	465.3	2.12	$(+/+)\ \lambda_p = 1.41$		−0.4	$(+/-)\ \varphi_s = 1.81$	203.3	4 / 5 / 9
−0.5	−0.7161	2.19	575.5	3.50	$(+/+)\ \lambda_p = 3.19$		−0.8	$(+/-)\ \varphi_s = 2.03$	247.6	4 / 5 / 9
−1	−0.92602	2.39	709.6	2.92	$(+/+)\ \lambda_p = 2.53$		−1.7	$(+/-)\ \varphi_s = 2.58$	294.2	4 / 5 / 9
−1.3	−1.1221	2.61	779.7	2.1	$(+/+)\ \lambda_p = 1.32$		−1.9	$(+/-)\ \varphi_s = 3.01$	314.3	4 / 5 / 9
−1.411618	−1.199879	2.71	801.9	2.00	$\lambda_p^3 = 1.00$		−1.9	$(-/+)\ \varphi_s = 3.19$	319.7	3↛5 / 5 / 8↛10
−1.6	−1.32953	2.89	834.0	2.24	$(-/-)\ \lambda_p = 1.63$		−1.8	$(-/+)\ \varphi_s = 3.48$	326.5	4 / 5 / 9
−2	−1.58227	3.28	882.4	4.63	$(-/-)\ \lambda_p = 4.41$		−1.3	$(-/+)\ \varphi_s = 4.00$	334.6	4 / 5 / 9
−3	−2.0889	4.11	941.8	27.1	$(-/-)\ \lambda_p = 27.0$		0.25	$(-/+)\ \varphi_s = 4.84$	339.9	4 / 5 / 9
−4	−2.49041	4.83	967.9	84.7	$(-/-)\ \lambda_p = 84.7$		1.37	$(-/+)\ \varphi_s = 5.46$	337.2	4 / 5 / 9
−5	−2.49041	5.45	982.2	188	$(-/-)\ \lambda_p = 188$		2.25	$(-/-)\ \lambda_s = 1.64$		4 / 6 / 10
−9	−3.90443	7.43	1005	1223	$(-/-)\ \lambda_p = 1223$		5.40	$(-/-)\ \lambda_s = 5.21$		4 / 6 / 10

Table 8.4: The family g_3.

Since the planar index of the 3rd cover of the f-orbit at 0.015388 jumps from 5 to 3 and the one of the f-orbit at −1.411618 from 3 to 5, and at each transition each new family is planar positive hyperbolic, at each transition each new family has $\mu^p_{CZ} = 4$. Thereby the Euler characteristics before and after each bifurcation are zero, see Table 8.5.

energy value	before bifurcation	after bifurcation
$\Gamma = 0.015388$	$(-1)^5 + (-1)^4 = 0$	$(-1)^4 + (-1)^3 = 0$
$\Gamma = -1.411618$	$(-1)^4 + (-1)^3 = 0$	$(-1)^5 + (-1)^4 = 0$

Table 8.5: Planar Euler characteristics for the bifurcation points between f^3 and g_3.

Furthermore, the family starting at 0.015388 and ending at −1.411618 has constant Conley–Zehnder index, thus it forms a planar bridge between these 3rd covers. Note that this bridge is planar pos. hyperb. II and spatial elliptic.

If the energy decreases, then the family g_3 ends at a degenerate periodic orbit which is of birth-death type. In other words, the family g_3 starts from one branch of a degenerate planar periodic orbit which is of birth-death type. Recall from the introduction that a periodic orbit of birth-death type is a degenerate orbit from which two families bifurcate with an index difference of 1 and into the same energy direction. Its local Floer homology and its Euler characteristic are therefore zero.

8.3 Spatial periodic orbits bifurcating from planar ones

8.3.1 From the spatial index jump of g

From the family g at the Γ value 1.383094, where μ^s_{CZ} jumps from 3 to 4 (see Table 8.1), a new family of spatial periodic orbits bifurcates, which was found by Batkhin–Batkhina [13] and called family g_{2v}. Some of its orbits are plotted in Figure 8.6 and their data are collected in Table 8.6. Its initial data was provided on personal request by the first author of [13].

These spatial orbits are doubly-symmetric with respect to ρ_1 and ρ_2, hence they start perpendicularly and hit perpendicularly the Lagrangian submanifolds

$$\mathrm{Fix}(\rho_1) = \{(q_1, 0, q_3, 0, p_2, 0)\}, \quad \mathrm{Fix}(\rho_2) = \{(0, q_2, q_3, p_1, 0, 0)\}.$$

In view of

$$\rho_1 \circ \rho_2 = \rho_2 \circ \rho_1 = -\sigma,$$

the orbits are invariant under the symplectic involution $-\sigma$, but by using σ, these spatial orbits give raise to yet another family of spatial orbits. Since the relation

$$\sigma \circ \rho_i = \rho_i \circ \sigma = \overline{\rho_i}, \quad i \in \{1, 2\},$$

the orbits of the symmetric family are doubly-symmetric with respect to $\overline{\rho_1}$ and $\overline{\rho_2}$ (see the last row in Figure 8.6). The bifurcation graph is shown in Figure 8.7.

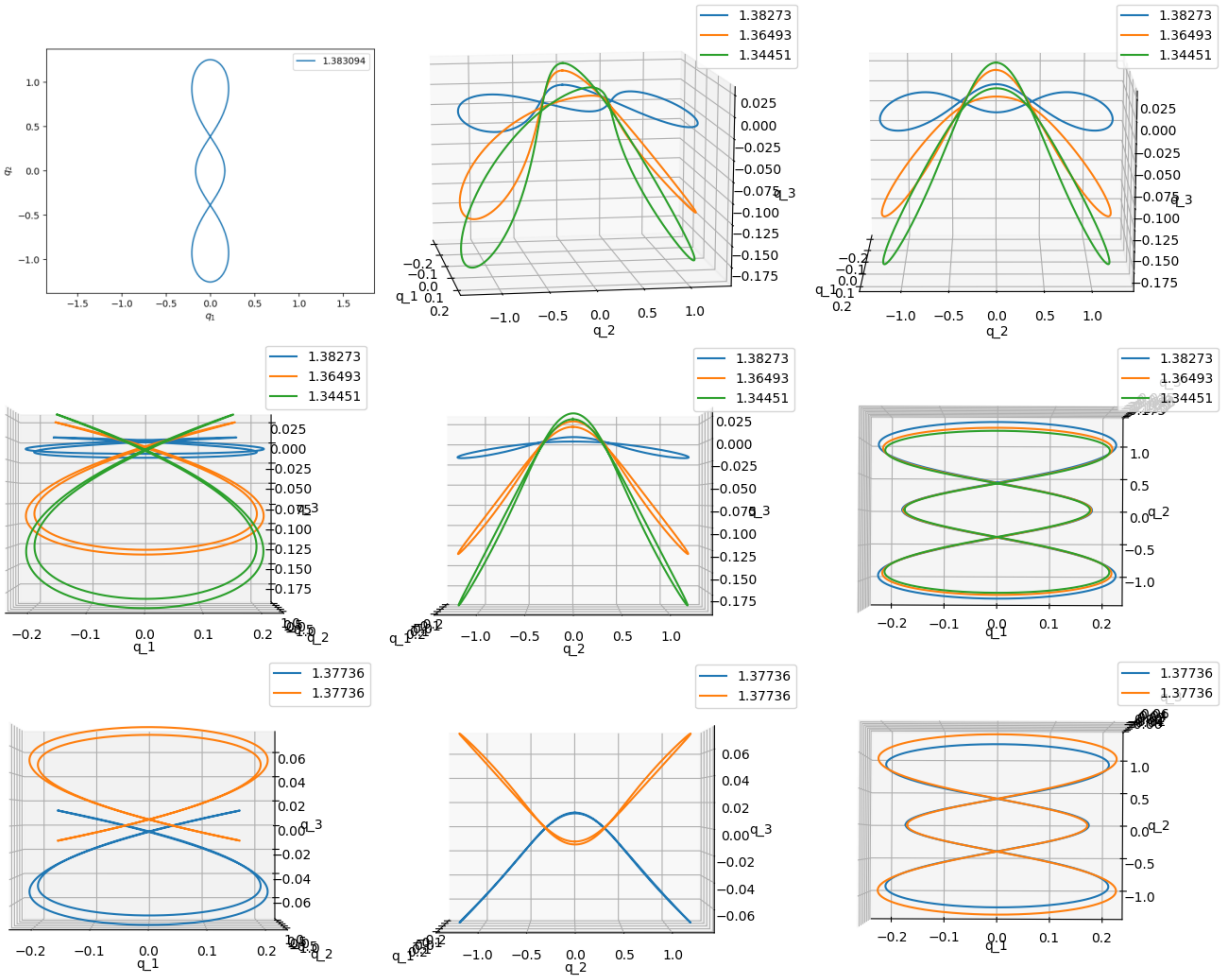

Figure 8.6: From the spatial index jump of g (family g_{2v}).

Γ	$q_1(0)$	$q_3(0)$	$\dot{q}_2(0)$	$T_q/2$	$\text{sign}_{C/B}$ and Floquet multipliers	μ_{CZ}
1.383094	−0.164715	0	−3.2924	2.56855	$(-/-)$ $\lambda = 1916.4$ & $\varphi_s = 0$	$2 + (3 \to 4) = 5 \to 6$
1.38273	−0.164661	0.002986	−3.2928	2.56857	$(-/-)$ $\lambda = 1881.2$ & $(-/+)$ $\varphi = 6.180$	5
1.37736	−0.16386	0.011810	−3.2980	2.5678	$(-/-)$ $\lambda = 1906.7$ & $(-/+)$ $\varphi = 5.993$	5
1.36493	−0.162007	0.020887	−3.3101	2.566	$(-/-)$ $\lambda = 2013.8$ & $(-/+)$ $\varphi = 5.791$	5
1.34451	−0.158974	0.030092	−3.3304	2.563	$(-/-)$ $\lambda = 1853.9$ & $(-/+)$ $\varphi = 5.531$	5
1.30865	−0.153669	0.040951	−3.3669	2.55756	$(-/-)$ $\lambda = 1816.1$ & $(-/+)$ $\varphi = 5.241$	5

Table 8.6: From the spatial index jump of g (family g_{2v}).

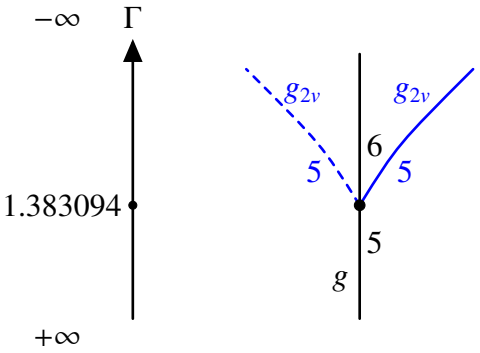

Figure 8.7: The bifurcation graph between g and g_{2v}. The horizontal symmetry corresponds to σ.

At the bifurcation point (see Figure 8.7) the index of g jumps from 5 to 6, and the family g_{2v} and its symmetric family begin with the index 5. Therefore the Euler characteristics before and after bifurcation are $(-1)^5 = -1$ and $2 \cdot (-1)^5 + (-1)^6 = -1$.

8.3.2 The 2nd cover of g and the 2nd cover of g'

From the double cover of the g-orbits at the Γ value 3.057471 the spatial index jumps from 9 to 11 (see Table 8.1), and from the double cover of the g'-orbits at the Γ value 4.285183 the spatial index jumps from 10 to 11 (see Table 8.2). In view of Example 7.0.2, in the latter there exist bad orbits, which are the double covers of the g'-orbits after the index jump. Recall that the bad orbits do not contribute to the local Floer homology groups nor to the Euler characteristics. The underlying simple closed orbits are plotted in Figure 8.8.

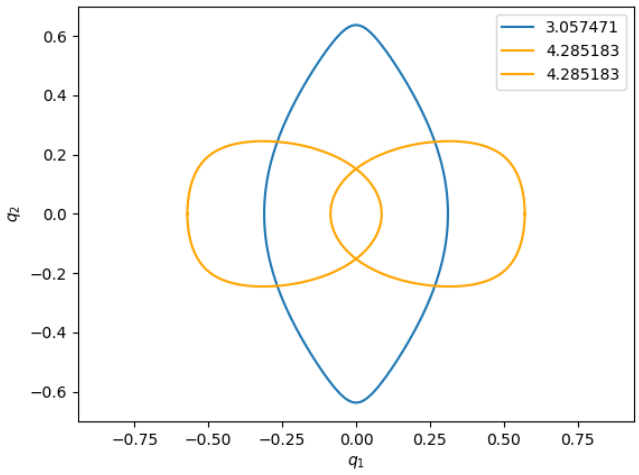

Figure 8.8: g-orbit (blue) at the Γ value 3.057471 and g'-orbits (orange) at the Γ value 4.285183.

The underlying simple closed orbits of g' are planar elliptic, and the spatial behaviour changes from elliptic to neg. hyperb. II with the indices $\mu^p_{CZ}(g') = \mu^s_{CZ}(g') = 3$. The indices of the double cover g'^2 before and after this transition are

$$\mu^p_{CZ}(g'^2) = \mu^s_{CZ}(g'^2) = 5, \qquad \mu^p_{CZ}(g'^2) = 5, \quad \mu^s_{CZ}(g'^2) = 6,$$

hence the index jumps from 10 to 11.

At these transitions new families of spatial symmetric periodic orbits bifurcate. In particular, two families bifurcate from the double cover of g and one family from the double cover of g'. All these families bifurcate after the index jump. Using the same notation as in Figure 1.7 of the

introduction, the bifurcation graph for this scenario is shown in Figure 8.9. Note that we draw the families of bad orbits by dashed black edges.

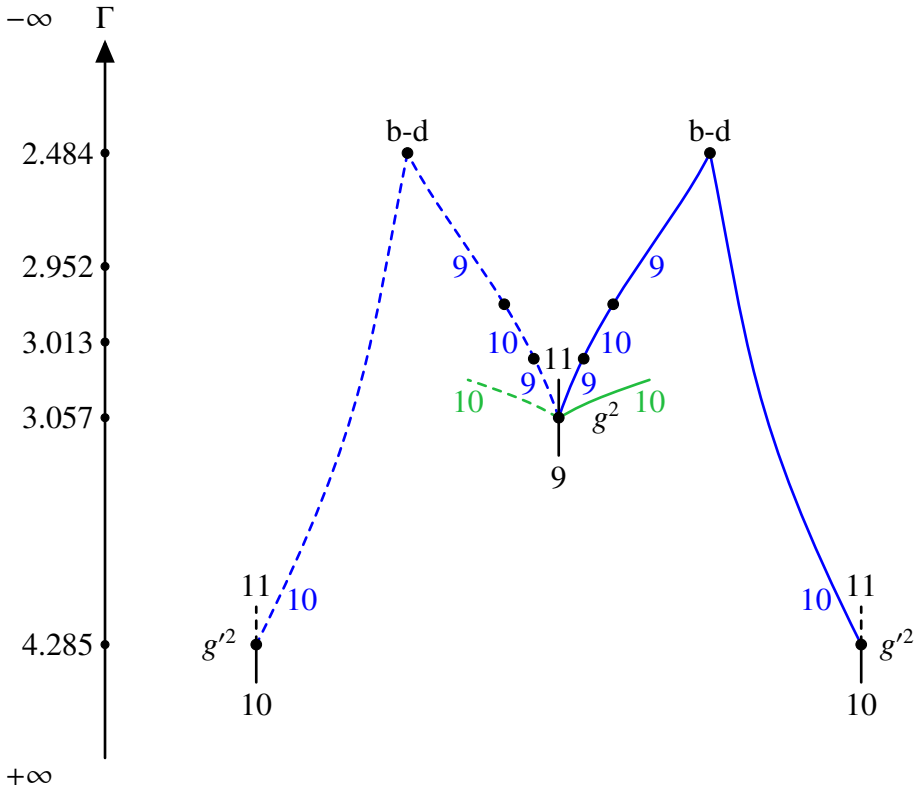

Figure 8.9: The bifurcation graph between the 2nd cover of g' and the 2nd cover of g with the families $g1v$ and g_{1v}^{YOZ}.

To the family $g1v$: This family bifurcates from the double cover of g. It was found by Michalodimitrakis [49] where the initial conditions for our data given in Table 8.7 are from. Some of its orbits are plotted in Figure 8.10. If the energy increases, then the orbits end at a degenerate periodic orbit of birth-death type. The other branch bifurcation of this birth-death type periodic orbit is the branch bifurcation from the double cover of g'. All the orbits of the family $g1v$ are doubly-symmetric with respect to $\overline{\rho_1}$ and ρ_1, therefore they start perpendicularly and hit perpendicularly

$$\mathrm{Fix}(\overline{\rho_1}) = \{(q_1, 0, 0, 0, p_2, p_3)\}, \quad \mathrm{Fix}(\rho_1) = \{(q_1, 0, q_3, 0, p_2, 0)\}.$$

Moreover, they are invariant under σ, but the symmetry $-\sigma$ yields the symmetrical family (dashed in the bifurcation graph), whose orbits are also symmetric with respect to ρ_2 and $\overline{\rho_2}$ (see the last row in Figure 8.10).

To the family g_{1v}^{YOZ}: This family bifurcating from the double cover of g was discovered by Batkhin–Batkhina [13]. The orbits are doubly-symmetric with respect to $\overline{\rho_2}$ and ρ_2. Note that we have not studied them further, but since at the value $\Gamma = 3.057$ the index of the double cover of g jumps from 9 to 11 and the family $g1v$ and its symmetric family start with index 9, the family g_{1v}^{YOZ} and its symmetric family have to start with index 10.

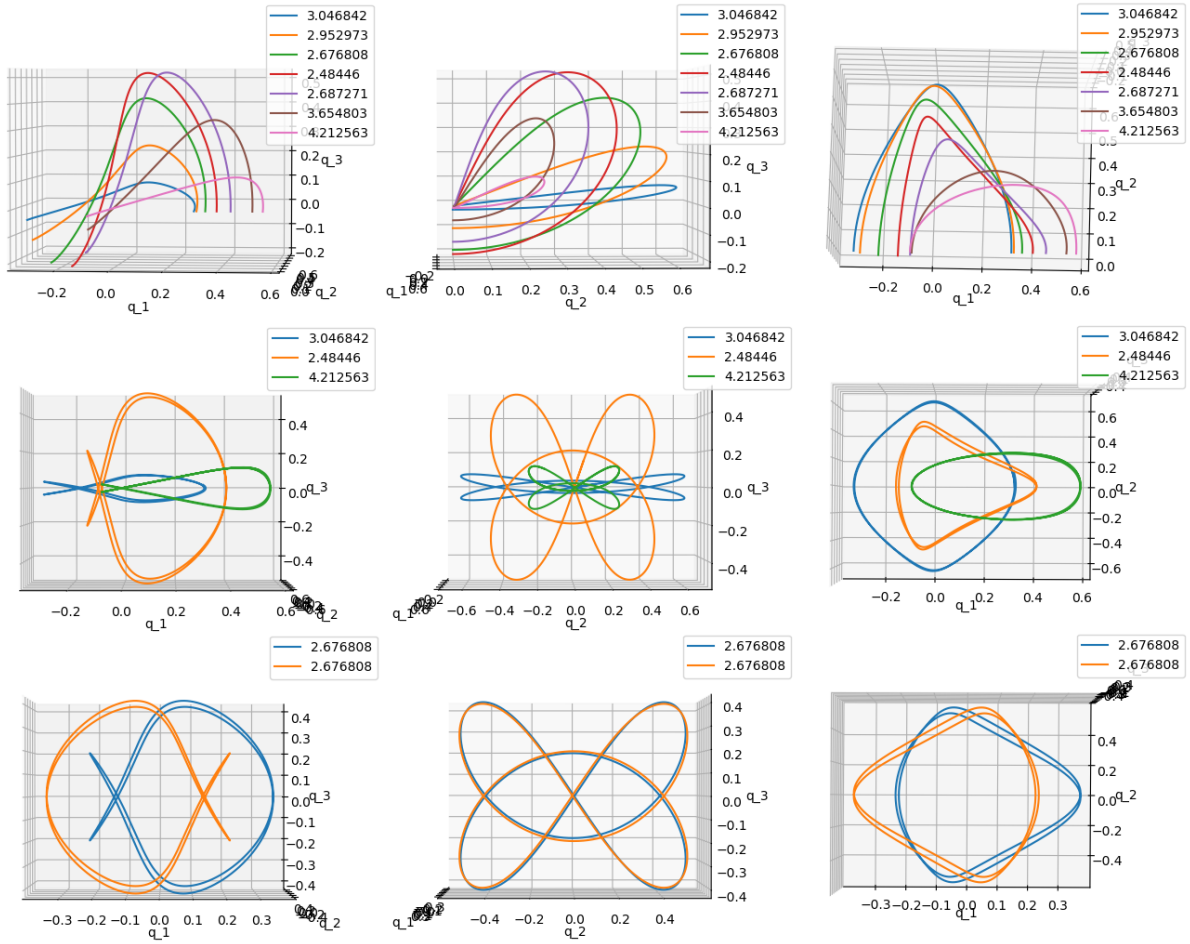

Figure 8.10: From the 2nd cover of g to the 2nd cover of g' (family $g1v$).

Γ	$q_1(0)$	$\dot{q}_2(0)$	$\dot{q}_3(0)$	$T_q/4$	$\text{sign}_{C/B}$ and Floquet multipliers	μ_{CZ}
3.057471	0.310843	1.9148	0	1.4727	$(-/-)$ $\lambda_p^2 = 24713.62$ & $\varphi_s^2 = 0$	$4 + (5 \to 7) = 9 \to 11$
3.046842	0.311905	1.88871	0.299	1.4733	$(-/-)$ $\lambda = 22211$ & $(-/+)$ $\varphi = 5.847$	9
3.013637	0.31526	1.807899	0.600	1.4751	$(-/-)$ $\lambda_1 = 20289$ & $(-/-)$ $\lambda_2 = 1.250$	10
2.952973	0.321529	1.663566	0.899	1.4783	$(-/-)$ $\lambda = 15610$ & $(-/+)$ $\varphi = 6.117$	9
2.852855	0.332366	1.43388	1.199	1.4833	$(-/-)$ $\lambda = 10175$ & $(-/+)$ $\varphi = 6.013$	9
2.676808	0.353928	1.048739	1.500	1.4895	$(-/-)$ $\lambda = 3938.3$ & $(-/+)$ $\varphi = 5.772$	9
2.48446	0.396	0.561861	1.649	1.4675	$(-/-)$ $\lambda = 300.99$ & $(-/+)$ $\varphi = 5.661$	9
						birth-death
2.687271	0.44745	0.364873	1.500	1.3488	-8.925 ± 3.401i & -0.097 ± 0.037i	10
3.202673	0.49409	0.370874	1.199	1.2151	-3.433 ± 6.225i & -0.067 ± 0.123i	10
3.654803	0.52756	0.401491	0.899	1.1343	-4.565 ± 2.778i & -0.159 ± 0.097i	10
3.998524	0.551501	0.424737	0.600	1.0857	-2.900 ± 0.096i & -0.344 ± 0.011i	10
4.212563	0.565996	0.438274	0.300	1.0596	$(-/+)$ $\varphi_1 = 3.507$ & $(-/+)$ $\varphi_2 = 4.757$	10
4.285183	0.570854	0.4426	0	1.0513	$(-/+)$ $\varphi_p^2 = 3.72$ & $\varphi_s^2 = 0$	$5 + (5 \to 6) = 10 \to 11$

Table 8.7: From the 2nd cover of g to the 2nd cover of g' (family $g1v$).

8.3.3 The 3rd cover of g, the 5th cover of f and the 3rd cover of g'

In this subsection we collect the underlying data for the bifurcation graph in Figure 1.7 and its discussion from the introduction with the families $f_g^{(2,3)}$, $f_g^{(2cut,3)}$, $f_{g'}^{(2,3)}$ and $f_{g'}^{(2cut,3)}$. All the initial data are provided on personal request from Kalantonis [44].

To the family $f_g^{(2,3)}$: The orbits are doubly-symmetric with respect to $\overline{\rho_1}$ and $\overline{\rho_2}$. Some of its orbits are plotted in Figure 8.11. Its symmetric family is obtained by using σ (see the last row in Figure 8.11). The data for the orbits are given in Table 8.8.

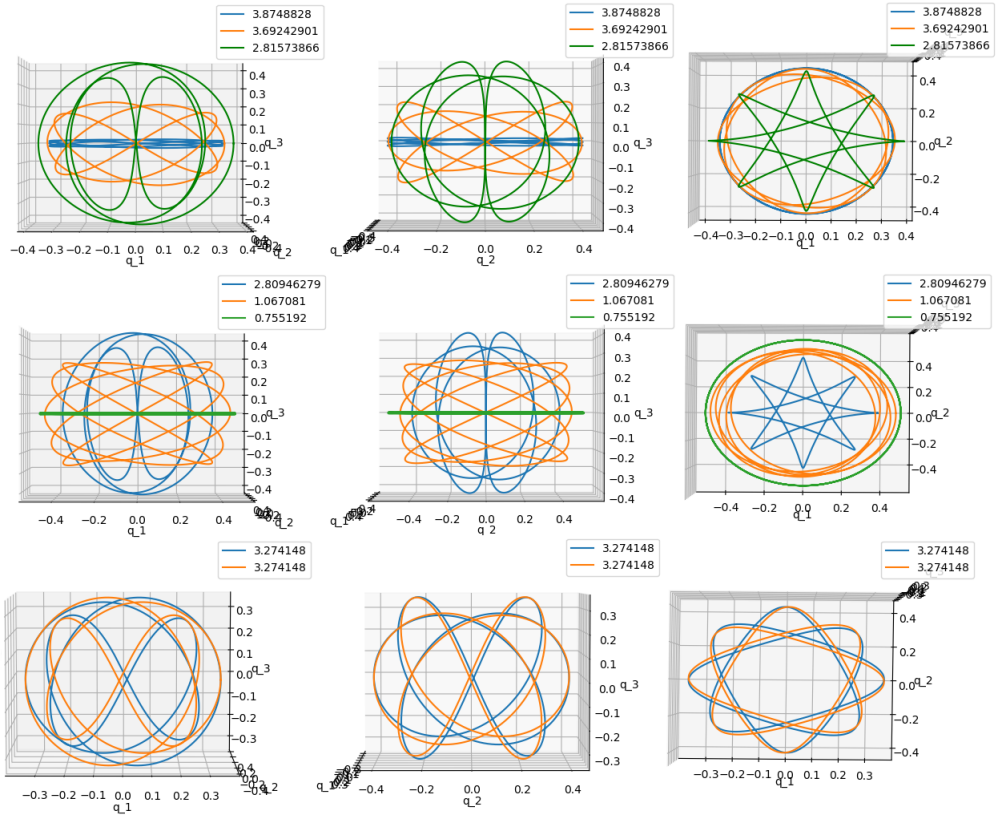

Figure 8.11: From g^3 to f^5 (family $f_g^{(2,3)}$).

Γ	$q_1(0)$	$\dot{q}_2(0)$	$\dot{q}_3(0)$	$T_q/2$	$\text{sign}_{C/B}$ and Floquet multipliers	μ_{CZ}
3.876616	0.327645	1.596748	0	2.82652	$(-/-)$ $\lambda_p^3 = 619.96$ & $\varphi_s^3 = 0$	$6 + (7 \to 9) = 13 \to 15$
3.876404	0.327652	1.596390	0.034	2.82665	$(-/-)$ $\lambda_1 = 620.39$ & $(-/-)$ $\lambda_2 = 1.003$	14
3.874882	0.327708	1.593827	0.100	2.82688	$(-/-)$ $\lambda_1 = 615.97$ & $(-/-)$ $\lambda_2 = 1.010$	14
3.866582	0.328011	1.579855	0.239	2.82811	$(-/-)$ $\lambda_1 = 592.21$ & $(-/-)$ $\lambda_2 = 1.008$	14
3.692429	0.334427	1.292631	0.975	2.85507	$(-/-)$ $\lambda_1 = 238.02$ & $(-/-)$ $\lambda_2 = 1.023$	14
3.274148	0.350335	0.647245	1.544	2.92956	$(-/-)$ $\lambda_1 = 1.228$ & $(-/-)$ $\lambda_2 = 1.053$	14
3.274118	0.350344	0.647179	1.544	2.92982	$(-/-)$ $\lambda_1 = 1.231$ & $\lambda_2 = 1$	$14 \to 15$
3.272832	0.350387	0.645310	1.545	2.92982	$(-/-)$ $\lambda = 1.229$ & $(+/-)$ $\varphi = 0.334$	15
3.239877	0.351673	0.597055	1.569	2.93637	$(-/-)$ $\lambda = 1.270$ & $(+/-)$ $\varphi = 1.750$	15
3.171140	0.354373	0.497587	1.612	2.95039	$(-/-)$ $\lambda = 1.402$ & $(-/+)$ $\varphi = 3.154$	15
3.088817	0.357637	0.380540	1.656	2.96784	$(-/-)$ $\lambda = 1.852$ & $(-/+)$ $\varphi = 4.538$	15
2.815738	0.368722	0.008233	1.736	3.03160	$(-/-)$ $\lambda = 17.24$ & $(-/+)$ $\varphi = 5.876$	15
2.809462	0.368982	−0.000038	1.737	3.03319	$(-/-)$ $\lambda = 17.64$ & $(-/+)$ $\varphi = 5.879$	15
2.659074	0.375277	−0.194503	1.747	3.07285	$(-/-)$ $\lambda = 25.89$ & $(-/+)$ $\varphi = 5.922$	15
1.783658	0.415479	−1.185880	1.463	3.39795	$(-/-)$ $\lambda = 20.95$ & $(-/+)$ $\varphi = 6.051$	15
1.067081	0.456943	−1.812982	0.805	3.89795	$(-/-)$ $\lambda = 2.986$ & $(-/+)$ $\varphi = 6.213$	15
0.939632	0.466113	−1.904426	0.613	4.03095	$(-/-)$ $\lambda = 1.035$ & $(-/+)$ $\varphi = 5.563$	15
0.813156	0.476186	−1.988018	0.338	4.18381	$(-/-)$ $\lambda = 1.015$ & $(-/+)$ $\varphi = 4.764$	15
0.755192	0.481212	−2.023751	0.010	4.26211	$(-/-)$ $\lambda = 1.008$ & $(-/+)$ $\varphi = 4.503$	15
0.755141	0.481217	−2.02378	0	4.26215	$\varphi_s^5 = 0$ & $(-/+)$ $\varphi_p^5 = 4.503$	$7 + (9 \to 7) = 16 \to 14$

Table 8.8: From the 3rd cover of g to the 5th cover of f (family $f_g^{(2,3)}$).

To the family $f_{g'}^{(2,3)}$: The orbits are simply-symmetric with respect to $\overline{\rho_1}$. Some of its orbits are plotted in Figure 8.12. The 3rd row in Figure 8.12 shows the symmetric orbit obtained by using $\overline{\rho_2}$, which bifurcates from the planar orbit which is symmetric to g'. The symmetry σ yields the symmetric family bifurcation from the same planar orbit of g' (see the last row in Figure 8.12). The data for the orbits are given in Table 8.9.

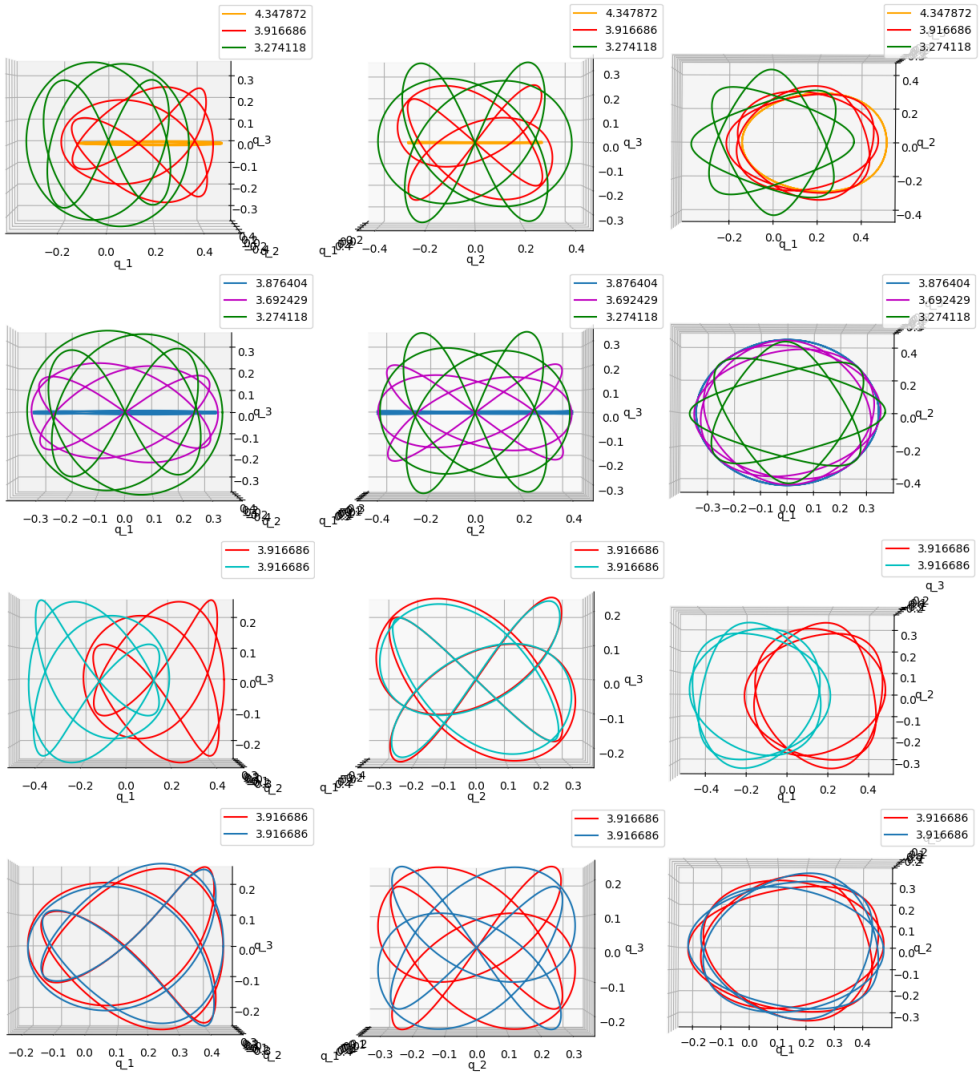

Figure 8.12: From the 3rd cover of g' to the index jump (14 → 15) in Table 8.8 (family $f_{g'}^{(2,3)}$).

Γ	$q_1(0)$	$\dot{q}_2(0)$	$\dot{q}_3(0)$	$T_q/2$	$\text{sign}_{C/B}$ and Floquet multipliers	μ_{CZ}
4.347942	0.491443	0.668022	0	2.41792	$(-/+)$ $\varphi_p^3 = 3.260$ & $\varphi_s^3 = 0$	7 + (7 → 9) = 14 → 16
4.347872	0.491437	0.668012	0.010	2.41797	$(-/+)$ $\varphi = 3.261$ & $(-/-)$ $\lambda = 1.014$	15
4.332819	0.490248	0.666260	0.154	2.42320	$(-/+)$ $\varphi = 3.238$ & $(-/-)$ $\lambda = 1.006$	15
4.308139	0.488286	0.663388	0.251	2.43186	$(-/-)$ $\lambda_1 = -1.008$ & $(-/-)$ $\lambda_2 = 1.012$	15
3.916686	0.454659	0.618385	0.848	2.58670	$(-/-)$ $\lambda_2 = -1.591$ & $(-/-)$ $\lambda_2 = 1.390$	15
3.720467	0.435295	0.597320	1.042	2.67843	$(+/-)$ $\varphi = 3.126$ & $(-/-)$ $\lambda = 1.705$	15
3.419999	0.397616	0.577871	1.322	2.84056	$(+/-)$ $\varphi = 1.622$ & $(-/-)$ $\lambda = 2.049$	15
3.274124	0.350644	0.646271	1.542	2.92956	$(+/-)$ $\varphi = 0.030$ & $(-/-)$ $\lambda = 1.231$	15
3.274118	0.350344	0.647179	1.544	2.92982	$\lambda_1 = 1$ & $(-/-)$ $\lambda_2 = 1.231$	14 → 15
3.274123	0.350042	0.648097	1.545	2.92956	$(+/-)$ $\varphi = 0.029$ & $(-/-)$ $\lambda = 1.230$	15
3.690961	0.238777	1.376348	1.720	2.69315	$(+/-)$ $\varphi = 2.849$ & $(-/-)$ $\lambda = 1.755$	15
3.917774	0.199644	1.850406	1.672	2.58622	$(-/-)$ $\lambda_1 = -1.592$ & $(-/-)$ $\lambda_2 = 1.389$	15
4.308371	0.137956	3.113046	0.744	2.43178	$(+/-)$ $\varphi = 3.145$ & $(-/-)$ $\lambda = 1.016$	15
4.347515	0.132083	3.292440	0.080	2.41809	$(+/-)$ $\varphi = 3.265$ & $(-/-)$ $\lambda = 1.053$	15
4.347942	0.132020	3.294475	0	2.41792	$(-/+)$ $\varphi_p^3 = 3.260$ & $\varphi_s^3 = 0$	7 + (7 → 9) = 14 → 16

Table 8.9: From the 3rd cover of g' to the index jump (14 → 15) in Table 8.8 (family $f_{g'}^{(2,3)}$).

To the family $f_g^{(2cut,3)}$: The orbits are doubly-symmetric with respect to ρ_1 and ρ_2. Some of these orbits are plotted in Figure 8.13. Its symmetric family is obtained by using σ (see the last row in Figure 8.13). The data for the orbits are given in Table 8.10.

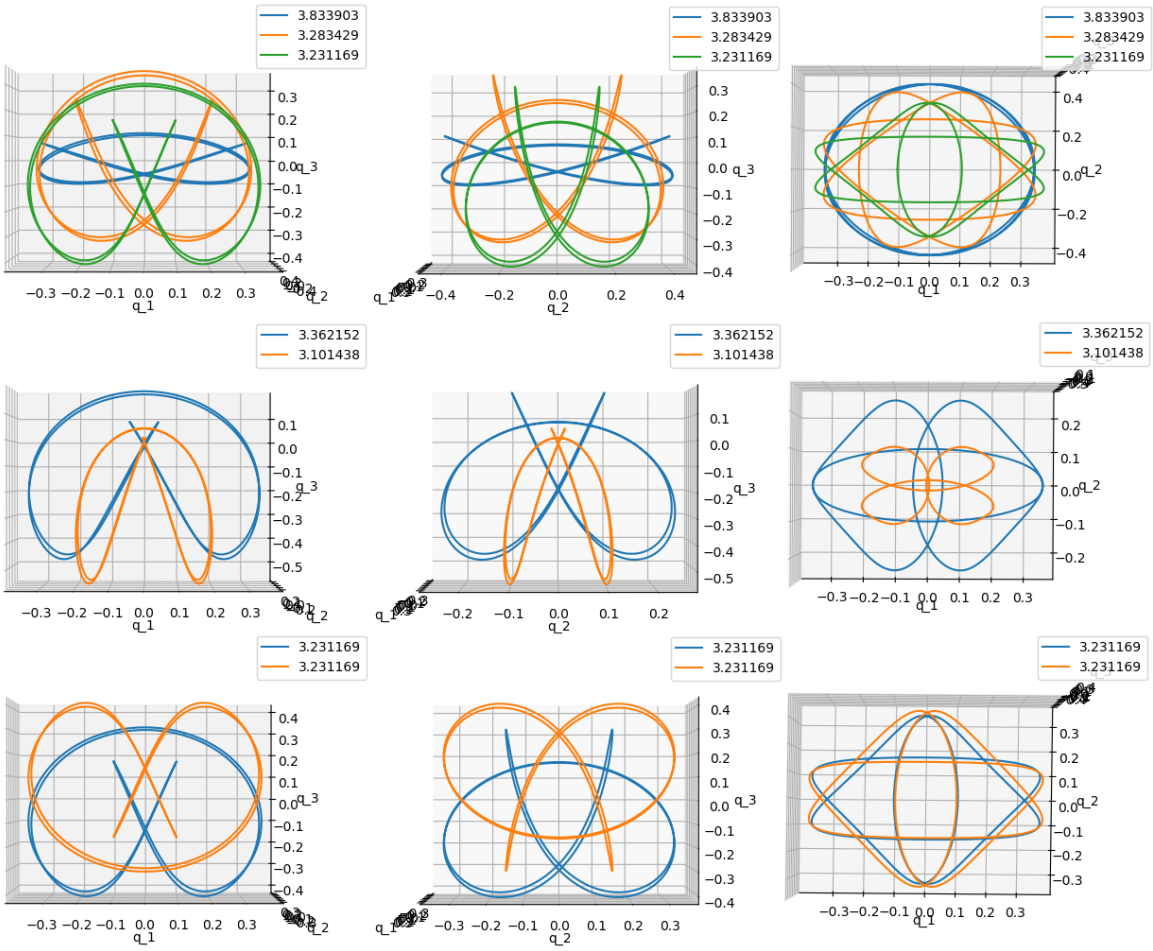

Figure 8.13: From the 3rd cover of g to collision (family $f_g^{(2cut,3)}$).

Γ	$q_1(0)$	$q_3(0)$	$\dot{q}_2(0)$	$T_q/2$	$\text{sign}_{C/B}$ and Floquet multipliers	μ_{CZ}
3.876616	−0.327645	0	−1.596	2.82652	$(-/-)$ $\lambda_p^3 = 619.96$ & $\varphi_s^3 = 0$	$6 + (7 \to 9) = 13 \to 15$
3.833903	−0.320106	0.072500	−1.600	2.83301	$(-/-)$ $\lambda = 505.63$ & $(-/+)$ $\varphi = 6.278$	13
3.283429	−0.212345	0.250499	−1.696	2.92604	$(-/-)$ $\lambda = 1.725$ & $(-/+)$ $\varphi = 6.048$	13
3.280180	−0.211571	0.250950	−1.698	2.92662	$\lambda = 1$ & $(-/+)$ $\varphi = 6.081$	$13 \to 14$
3.279799	−0.211477	0.250999	−1.698	2.92669	$(+/-)$ $\varphi_1 = 0.186$ & $(-/+)$ $\varphi_2 = 6.080$	14
3.189269	−0.186389	0.258719	−1.766	2.94124	$(+/-)$ $\varphi_1 = 3.129$ & $(-/+)$ $\varphi_2 = 5.968$	14
3.136701	−0.150862	0.240737	−1.978	2.92889	$(-/+)$ $\varphi_1 = 6.277$ & $(-/+)$ $\varphi_2 = 4.689$	14
3.136701	−0.150811	0.24068	−1.978	2.92882	$\lambda = 1$ & $(-/+)$ $\varphi = 4.691$	birth-death
3.231169	−0.097655	0.166387	−2.671	2.77297	$(+/+)$ $\lambda = 3.712$ & $(-/+)$ $\varphi = 4.346$	15
3.362152	−0.042376	0.077137	−4.400	2.43258	$\lambda = 1$ & $(-/+)$ $\varphi = 3.498$	birth-death
3.362152	−0.042344	0.077087	−4.401	2.43234	$(-/+)$ $\varphi_1 = 6.249$ & $(-/+)$ $\varphi_2 = 3.497$	14
3.329430	−0.024918	0.050537	−5.671	2.29164	$(-/+)$ $\varphi_1 = 5.662$ & $(-/+)$ $\varphi_2 = 3.143$	14
3.101438	−0.004205	0.014387	−11.41	2.06718	$(-/+)$ $\varphi_1 = 6.012$ & $(-/+)$ $\varphi_2 = 2.426$	14

Table 8.10: From the 3rd cover of g to collision (family $f_g^{(2cut,3)}$).

To the family $f_{g'}^{(2cut,3)}$: The orbits are simply-symmetric with respect to ρ_1. Some of these orbits are plotted in Figure 8.14. The 3rd row in Figure 8.14 shows the symmetric orbits obtained by using ρ_2, which bifurcate from the planar orbit which is symmetric to g'. The symmetry σ yields the symmetric family bifurcation from the same planar orbit of g' (see the last row in Figure 8.14). The data for the orbits are given in Table 8.11.

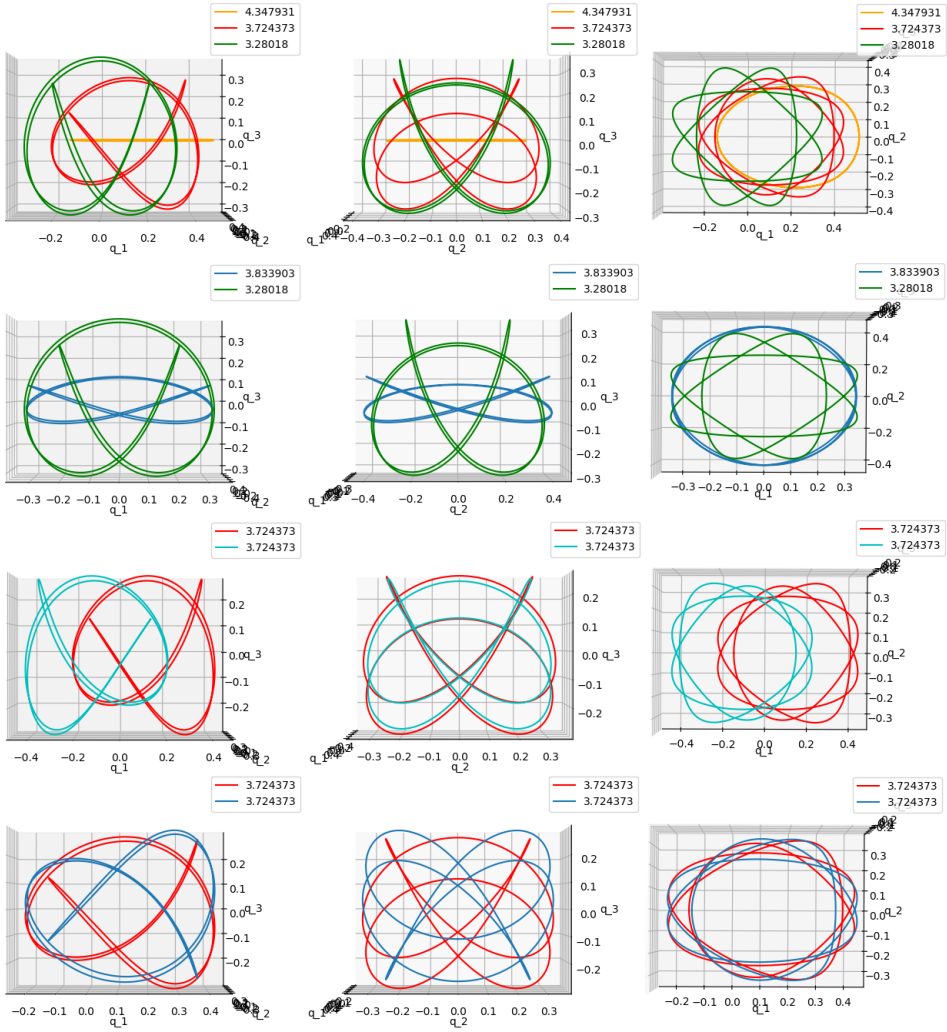

Figure 8.14: From the 3rd cover of g' to the index jump $(13 \to 14)$ in Table 8.10 (family $f_{g'}^{(2cut,3)}$).

Γ	$q_1(0)$	$q_3(0)$	$\dot{q}_2(0)$	$T_q/2$	$\text{sign}_{C/B}$ and Floquet multipliers	μ_{CZ}
4.347942	−0.132020	0	−3.294	2.41792	$(-/+)$ $\varphi_p^3 = 3.260$ & $\varphi_s^3 = 0$	$7 + (7 \to 9) = 14 \to 16$
4.347931	−0.132019	0.000400	−3.294	2.41795	$(-/+)$ $\varphi_1 = 3.261$ & $(-/+)$ $\varphi_2 = 6.275$	14
4.307008	−0.131939	0.024999	−3.261	2.43226	$(-/-)$ $\lambda = -1.020$ & $(-/+)$ $\varphi = 5.858$	14
3.724373	−0.138067	0.120000	−2.692	2.67594	$(+/-)$ $\varphi_1 = 3.051$ & $(-/+)$ $\varphi_2 = 5.741$	14
3.381250	−0.165321	0.192269	−2.133	2.86377	$(+/-)$ $\varphi_1 = 1.013$ & $(-/+)$ $\varphi_2 = 5.311$	14
3.381167	−0.165336	0.192296	−2.133	2.86382	0.551 ± 0.816i & 0.541 ± 0.858i	14
3.329148	−0.177357	0.211699	−1.990	2.89575	0.973 ± 0.919i & 0.543 ± 0.511i	14
3.280274	−0.209888	0.249451	−1.710	2.92656	1.039 ± 0.161i & 0.939 ± 0.145i	14
3.280237	−0.210257	0.249782	−1.707	2.92659	$(+/-)$ $\varphi_1 = 0.131$ & $(-/+)$ $\varphi_2 = 6.127$	14
3.280180	−0.211571	0.250950	−1.698	2.92662	$\lambda = 1$ & $(-/+)$ $\varphi = 6.081$	$13 \to 14$
3.280236	−0.212874	0.252084	−1.689	2.92659	$(+/-)$ $\varphi_1 = 0.122$ & $(-/+)$ $\varphi_2 = 6.121$	14
3.280241	−0.212932	0.252134	−1.688	2.92658	1.002 ± 0.146i & 0.976 ± 0.142i	14
3.357252	−0.266603	0.281661	−1.390	2.87838	0.773 ± 0.967i & 0.504 ± 0.630i	14
3.380289	−0.275442	0.283788	−1.350	2.86435	0.571 ± 0.871i & 0.527 ± 0.801i	14
3.381154	−0.275758	0.283852	−1.349	2.86383	$(+/-)$ $\varphi_1 = 1.006$ & $(-/+)$ $\varphi_2 = 5.304$	14
3.454933	−0.300084	0.286253	−1.247	2.82013	$(+/-)$ $\varphi_1 = 1.663$ & $(-/+)$ $\varphi_2 = 5.497$	14
3.727521	−0.370162	0.266224	−0.999	2.67439	$(+/+)$ $\lambda = -1.025$ & $(-/+)$ $\varphi_2 = 5.744$	14
4.347932	−0.491441	0.001213	−0.668	2.41795	$(-/+)$ $\varphi_1 = 3.261$ & $(-/+)$ $\varphi_2 = 6.279$	14
4.347942	−0.491443	0	−0.668	2.41792	$(-/+)$ $\varphi_p^3 = 3.260$ & $\varphi_s^3 = 0$	$7 + (7 \to 9) = 14 \to 16$

Table 8.11: From the 3rd cover of g' to the index jump $(13 \to 14)$ in Table 8.10 (family $f_{g'}^{(2cut,3)}$).

8.3.4 The 4th cover of g, the 6th cover of f and the 4th cover of g'

At the value $\Gamma = 4.435711$ the spatial index of the 4th cover of the orbit of the family g' jumps from 18 to 20 (see Table 8.2). Moreover, at the value $\Gamma = 4.278924$ the spatial index of the 4th cover of g jumps from 17 to 19 (see Table 8.1). The bifurcation graph for this case is illustrated in Figure 8.15.

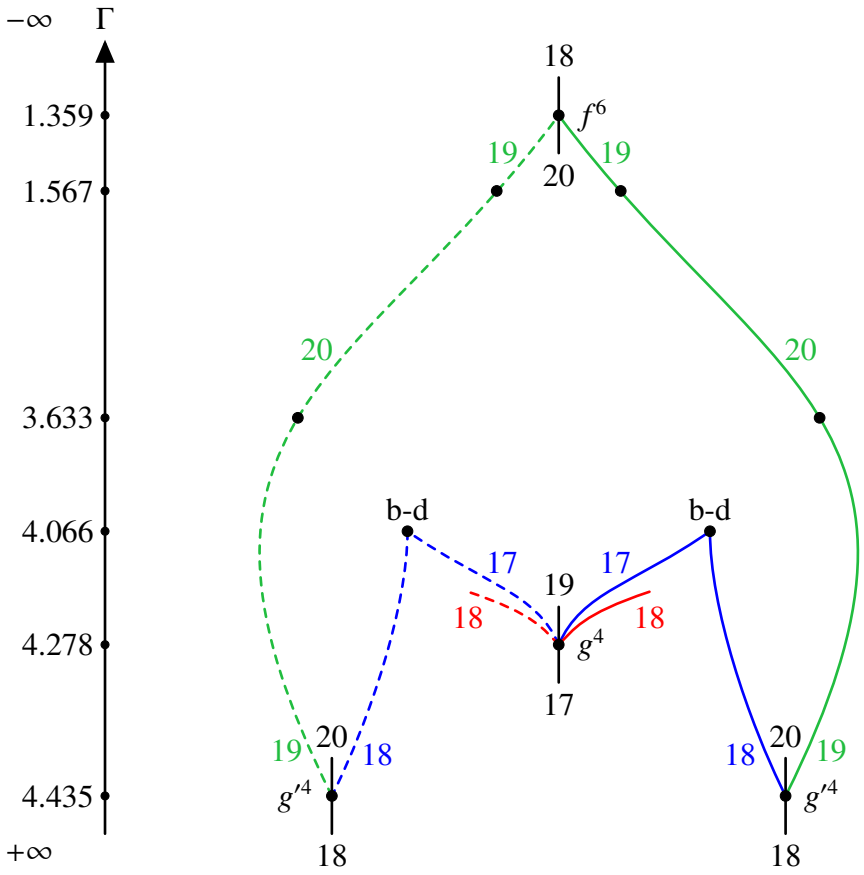

Figure 8.15: The bifurcation graph between the 4th cover of g', the 4th cover of g and the 6th cover of f with the families $f_{g'}^{(1,4)}$, $f_{g'}^{(1cut,4)}$ and $f_{g}^{(1,4)}$.

The three families $f_{g'}^{(1,4)}$, $f_{g'}^{(1cut,4)}$ and $f_{g}^{(1,4)}$ were found by Kalantonis [44], who provided on personal request the initial data. All orbits are doubly-symmetric with respect to $\overline{\rho_1}$ and ρ_1, hence they are invariant under σ. Each symmetric family (dashed) is obtained by using the symmetry $-\sigma$. Note that the orbits of each symmetric family are doubly-symmetric with respect to $\overline{\rho_2}$ and ρ_2.

To the family $f_{g'}^{(1,4)}$: It consists of two branches bifurcating respectively from the 4th cover of g' at the value $\Gamma = 4.435$ and from the 4th cover of g at the value $\Gamma = 4.278$. The two branches meet at the value $\Gamma = 4.066$ at a degenerate orbit of birth-death type. Some orbits of the family $f_{g'}^{(1,4)}$ are plotted in Figure 8.16, where the last row shows a symmetric orbit. The data for the orbits are collected in Table 8.12.

To the family $f_{g'}^{(1cut,4)}$: This family bifurcating from the 4th cover of g' at the value $\Gamma = 4.435$ ends planar at the 6th cover of the retrograde orbit at the value $\Gamma = 1.359$. Note that inbetween there are two index jumps. In view of Table 8.3, the index of f^6 at the value $\Gamma = 1.359$ jumps from 20 to 18. At this transition, the Euler characteristics show that there are still undiscovered families branching out from f^6. Some of the orbits of the family $f_{g'}^{(1cut,4)}$ are plotted in Figure

8.17, where the last row shows a symmetric orbit, and the data are collected in Table 8.13.

To the family $f_g^{(1,4)}$: We have not studied it further, but since at the value $\Gamma = 4.278$ the index of the 4th cover of g jumps from 17 to 19 and the family $f_{g'}^{(1,4)}$ and its symmetric family start with index 17, the family $f_g^{(1,4)}$ and its symmetric family have to start with index 18.

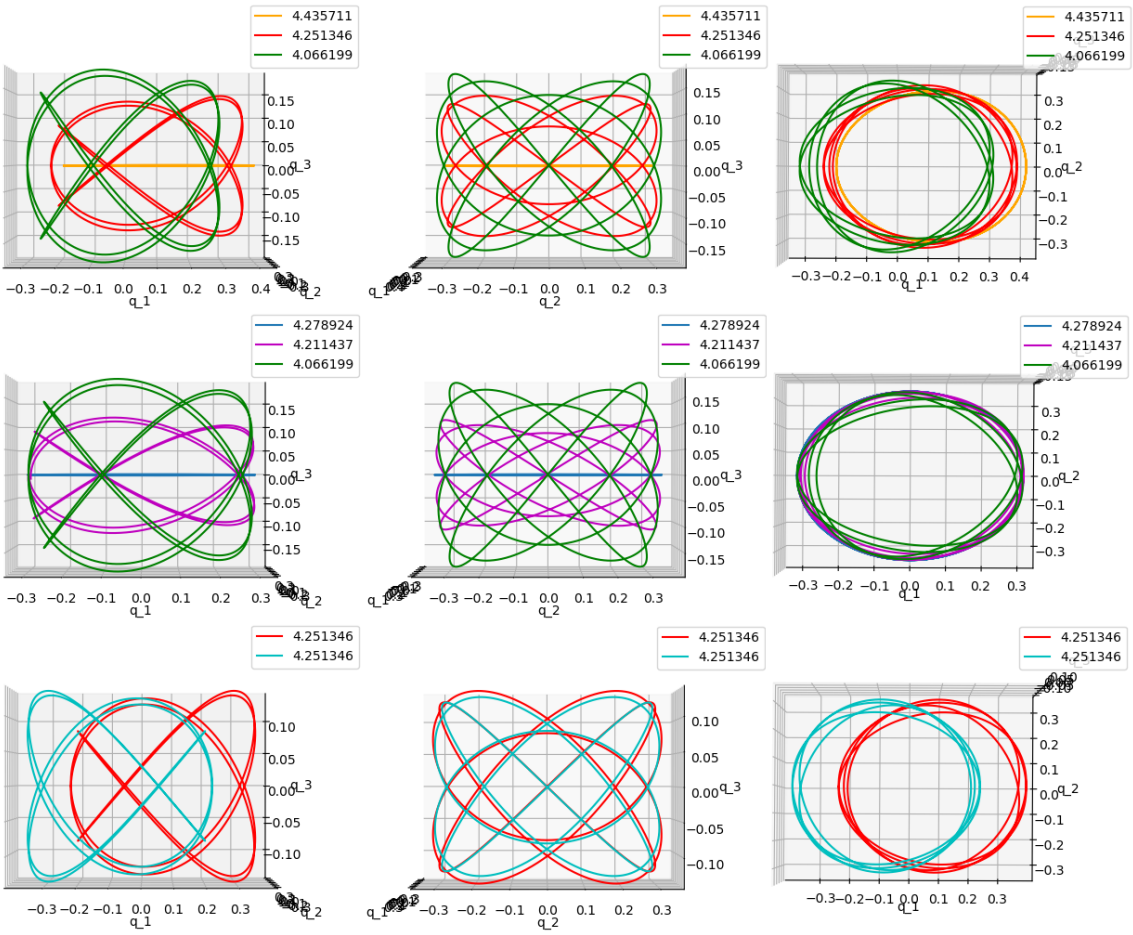

Figure 8.16: From the 4th cover of g' to the 4th cover of g (family $f_{g'}^{(1,4)}$).

Γ	$q_1(0)$	$\dot{q}_2(0)$	$\dot{q}_3(0)$	$T_q/4$	$\text{sign}_{C/B}$ and Floquet multipliers	μ_{CZ}
4.435711	−0.188043	−2.511218	0	1.34304	$(+/-)\ \varphi_p^4 = 2.224$ & $\varphi_s^4 = 0$	$9 + (9 \to 11) = 18 \to 20$
4.435711	−0.188043	−2.511218	−0.0004	1.34305	$(+/-)\ \varphi_1 = 2.232$ & $(-/+)\ \varphi_2 = 6.261$	18
4.384342	−0.198011	−2.339590	−0.6000	1.35458	$(+/-)\ \varphi_1 = 2.079$ & $(-/+)\ \varphi_2 = 6.210$	18
4.251346	−0.226833	−1.933856	−0.9900	1.38612	$(+/-)\ \varphi_1 = 1.616$ & $(-/+)\ \varphi_2 = 6.196$	18
4.068814	−0.294711	−1.340590	−1.0866	1.43386	$(+/-)\ \varphi_1 = 0.143$ & $(-/+)\ \varphi_2 = 6.195$	18
4.068801	−0.294728	−1.340490	−1.0866	1.43386	$1.000 \pm 0.087i$ & $0.986 \pm 0.141i$	18
4.067084	−0.297534	−1.324490	−1.0798	1.43439	$1.094 \pm 0.018i$ & $0.913 \pm 0.016i$	18
4.066595	−0.298720	−1.317990	−1.0766	1.43456	$(-/-)\ \lambda_1 = 1.119$ & $(+/+)\ \lambda_2 = 1.064$	18
4.066199	−0.300790	−1.307190	−1.0703	1.43477	$(-/-)\ \lambda_1 = 1.321$ & $(+/+)\ \lambda_2 = 1.001$	18
4.066199	−0.300810	−1.307090	−1.0702	1.43477	$(-/-)\ \lambda_1 = 1.322$ & $\lambda_2 = 1$	birth-death
4.066199	−0.300851	−1.306890	−1.0701	1.43478	$(-/-)\ \lambda = 1.325$ & $\varphi = 6.276$	17
4.083662	−0.304840	−1.312317	−1.0167	1.43352	$(-/-)\ \lambda = 2.779$ & $\varphi = 6.275$	17
4.211437	−0.302530	−1.514041	−0.6178	1.42338	$(-/-)\ \lambda = 15.30$ & $\varphi = 6.275$	17
4.278924	−0.301158	−1.623019	−0.0003	1.41824	$(-/-)\ \lambda = 26.32$ & $\varphi = 6.276$	17
4.278924	−0.301158	−1.623018	0	1.41824	$\lambda_p^4 = 26.26$ & $\varphi_s^4 = 0$	$8 + (9 \to 11) = 17 \to 19$

Table 8.12: From the 4th cover of g' to the 4th cover of g (family $f_{g'}^{(1,4)}$).

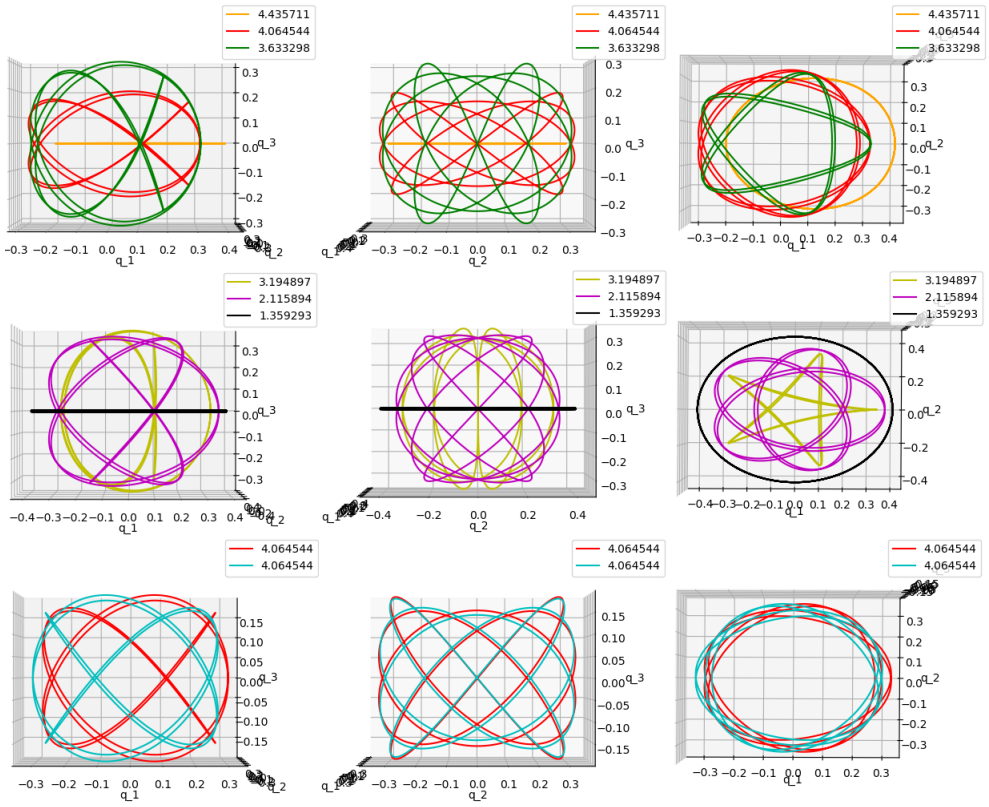

Figure 8.17: From the 4th cover of g' to the 6th cover of f (family $f_{g'}^{(1cut,4)}$).

Γ	$q_1(0)$	$\dot{q}_2(0)$	$\dot{q}_3(0)$	$T_q/4$	$\text{sign}_{C/B}$ and Floquet multipliers	μ_{CZ}
4.435711	0.399433	1.024708	0	1.34304	$(+/-)\ \varphi_p^4 = 2.224$ & $\varphi_s^4 = 0$	$9 + (9 \to 11) = 18 \to 20$
4.435711	0.399433	1.024704	0.001	1.34305	$(+/-)\ \varphi = 2.225$ & $(-/-)\ \lambda = 1.009$	19
4.358078	0.388745	1.036921	0.405	1.36065	$(+/-)\ \varphi = 1.998$ & $(-/-)\ \lambda = 1.045$	19
4.064544	0.313078	1.240223	1.039	1.43467	$(+/-)\ \varphi = 0.298$ & $(-/-)\ \lambda = 1.035$	19
3.721469	0.313247	0.753339	1.546	1.46539	$(-/+)\ \varphi = 4.711$ & $(-/-)\ \lambda = 1.007$	19
3.634638	0.315238	0.624474	1.617	1.47381	$(-/+)\ \varphi = 6.123$ & $(-/-)\ \lambda = 1.010$	19
3.633298	0.315269	0.622499	1.618	1.47394	$(-/-)\ \lambda_1 = 1.088$ & $(-/-)\ \lambda_2 = 1.010$	20
3.194897	0.325968	−0.000610	1.805	1.52212	$(-/-)\ \lambda_1 = 11.37$ & $(-/-)\ \lambda_2 = 1.009$	20
3.039053	0.330063	−0.210854	1.817	1.54192	$(-/-)\ \lambda_1 = 13.01$ & $(-/-)\ \lambda_2 = 1.009$	20
2.115894	0.358524	−1.326885	1.444	1.70332	$(-/-)\ \lambda_1 = 7.647$ & $(-/-)\ \lambda_2 = 1.006$	20
1.567391	0.380122	−1.874481	0.783	1.86052	$(-/-)\ \lambda_1 = 1.026$ & $(-/-)\ \lambda_2 = 1.006$	20
1.567110	0.380135	−1.874738	0.782	1.86062	$(-/-)\ \lambda = 1.007$ & $(-/+)\ \varphi = 6.240$	19
1.411644	0.387099	−2.012299	0.393	1.91992	$(-/-)\ \lambda = 1.007$ & $(-/+)\ \varphi = 5.085$	19
1.359329	0.389535	−2.056719	0.010	1.94188	$(-/-)\ \lambda = 1.014$ & $(-/+)\ \varphi = 4.888$	19
1.359293	0.389537	−2.05674	0	1.94179	$\varphi_s^6 = 0$ & $(-/+)\ \varphi_p^6 = 4.886$	$9 + (11 \to 9) = 20 \to 18$

Table 8.13: From the 4th cover of g' to the 6th cover of f (family $f_{g'}^{(1cut,4)}$).

Bibliography

[1] Abraham R.,Marsden J. E.: *Foundations of Mechanics*. Second Edition. Addison-Wesley Publishing Company (1978)

[2] Adams. J. C.: *On the Motion of the Moon's Node in the case when the Orbits of the Sun and Moon are supposed to have no Eccentricities, and when their mutual Inclination is supposed to be indefinitely small*. Monthly Notices Roy. Astron. Soc. **38**(1), 43–53 (1877)

[3] Albers P., Frauenfelder U.: *The space of linear anti-symplectic involutions is a homogenous space*. Arch. Math. (Basel) **99**(6), 531–536 (2012)

[4] Albers P., Frauenfelder U., van Koert O., Paternain G.: *Contact geometry of the restricted three-body problem*. Comm. Pure Appl. Math. **65**(2), 229–263 (2012)

[5] Arnold V. I.: *Mathematical methods of classical mechanics*. Second Edition. Graduate Texts in Mathematics **60**. Springer-Verlag (1989)

[6] Arnold V. I.: *Polymathematics: is mathematics a single science or a set of arts?* Mathematics: frontiers and perspectives, Amer. Math. Soc., Providence, RI, 403–416 (2000)

[7] Audin M., Damian M.: *Morse Theory and Floer Homology*. Universitext. Springer (2014)

[8] Aydin C.: *From Babylonian lunar observations to Floquet multipliers and Conley–Zehnder Indices*. Submitted for publication (2023)

[9] Aydin C.: *Symplectic splitting of Hamiltonian structures and reduced monodromy matrices*. To appear in Linear Algebra Appl. (2023)

[10] Aydin C.: *The Conley–Zehnder Indices of the spatial Hill three-body problem*. Celest. Mech. Dyn. Astron. **135**(32) (2023)

[11] Aydin C.: *The linear symmetries of Hill's lunar problem*. Arch. Math. (Basel) **120**(3), 321–330 (2023)

[12] Banyaga A., Hurtubise D.: *Lectures on Morse Homology.* Kluwer Academic Publishers (2004)

[13] Batkhin A. B., Batkhina N. V.: *Hierarchy of periodic solutions families of spatial Hill's problem*. Sol. Syst. Res. **43**, 178–183 (2009)

[14] Belbruno E., Frauenfelder U., van Koert O.: *A family of periodic orbits in the three-dimensional lunar problem*. Celest. Mech. Dyn. Astron. **131**(7), 1–22 (2019)

[15] Besse A. L.: *Manifolds all of whose Geodesics are Closed*. Springer (1978)

[16] Birkhoff G. D.: *The restricted problem of three bodies.* Rend. Circ. Mat. Palermo **39**, 265–334 (1915)

[17] Bott R.: *Nondegenerate critical manifolds.* Ann. of Math. **60**(2), 248–261 (1954)

[18] Bott R., Tu L. W.: *Differential Forms in Algebraic Topology.* Springer (1982)

[19] Brown E. W.: *Tables of the motion of the moon*. New Haven, Yale University Press (1919)

[20] Cho W., Jung H., Kim G.: *The contact geometry of the spatial circular restricted 3-body problem*. Abh. Math. Semin. Univ. Hambg. **90**(2), 161–181 (2020)

[21] Cieliebak K., Frauenfelder U.: *A Floer homology for exact contact embedding*. Pacific J. Math. **239**(2), 251–316 (2009)

[22] Conley C., Zehnder E.: *Morse type index theory for flows and periodic solutions for Hamiltonian Equations.* Comm. Pure Appl. Math. **37**(2), 207–253 (1984)

[23] Frauenfelder U.: *The Arnold-Givental conjecture and moment Floer homology.* Int. Math. Res. Not. **2004**(42), 2179–2269 (2004)

[24] Frauenfelder U., Labrousse C., Schlenk F.: *Slow volume growth for Reeb flows on spherizations and contact Bott–Samelson theorems*. J. Topol. Anal. **7**(3), 407–451 (2015)

[25] Frauenfelder U., Moreno A.: *On GIT quotients of the symplectic group, stability and bifurcations of symmetric orbits*. To appear in J. Symplectic Geom. (2023)

[26] Frauenfelder U., Schlenk F.: *S^1-equivariant Rabinowitz-Floer homology*. Hokkaido Math. J. **45**(3), 293–323 (2016)

[27] Frauenfelder U., van Koert O.: *The Restricted Three-Body Problem and Holomorphic Curves*. Birkhäuser, Basel (2018)

[28] Ginsburg J., Smith D. E.: *A History of Mathematics in America before 1990*. Carus Mathematical Monograph **5**, The Mathematical Association of America (1934)

[29] Ginzburg V. L.: *The Conley conjecture*. Ann. of Math. (2) **172**(2), 1127–1180 (2010)

[30] Ginzburg V. L., Gürel B. Z.: *Lusternik–Schnirelmann theory and closed Reeb orbits*. Math. Z. **295**(1-2), 515–582 (2020)

[31] Goldstein B. R.: *On the Babylonian discovery of the periods of lunar motion*. J. Hist. Astronom. **33**(110), 1–13 (2002)

[32] Gutzwiller M. C.: *Moon-Earth-Sun: The oldest three-body problem*. Rev. Modern Phys. **70**(2), 589–639 (1998)

[33] Hatcher A.: *Vector Bundles and K-Theory*. Version 2.2 (2017)

[34] Hénon M.: *Numerical Exploration of the Restricted Problem. V. Hill's Case: Periodic Orbits and Their Stability*. Astron. Astrophys. **1**, 223–238 (1969)

[35] Hénon M.: *Numerical Exploration of the Restricted Problem. VI. Hill's Case: Non-Periodic Orbits*. Astron. Astrophys. **9** , 24–36 (1970)

[36] Hénon M.: *Vertical stability of periodic orbits in the restricted problem II. Hill's case*. Astron. Astrophys. **30**, 317–321 (1974)

[37] Hénon M.: *New families of periodic orbits in Hill's problem of three bodies*. Celest. Mech. Dyn. Astron. **85**, 223–246 (2003)

[38] Hill G. W.: *Researches in the Lunar Theory*. Amer. J. Math. **1**(3), 245–260 (1878)

[39] Hill. G. W.: *On the part of the motion of the lunar perigee which is a function of the mean motions of the sun and moon*. Acta Math. **8**, 1–36 (1886)

[40] Hofer H., Wysocki K., Zehnder E.: *The Dynamics on Three-Dimensional Strictly Convex Energy Surfaces*. Ann. of Math. (2) **148**(1), 197–289 (1998)

[41] Hofer H., Wysocki K., Zehnder E.: *Finite Energy Foliations of Tight Three-Spheres and Hamiltonian Dynamics*. Ann. of Math. (2) **157**(1), 125–255 (2003)

[42] Hofer H., Zehnder E.: *Symplectic Invariants and Hamiltonian Dynamics*. Birkhäuser, Basel (1994)

[43] Klingenberg W.: *Lectures on Closed Geodesics*. Springer (1978)

[44] Kalantonis V. S.: *Numerical Investigation for Periodic Orbits in the Hill Three-Body Problem*. Universe **6**(72) (2020)

[45] Lang K. R.: *Astrophysical Data: Planets and Stars*. Springer-Verlang New York (1992)

[46] Linton C. M.: *From Eudoxus to Einstein. A History of Mathematical Astronomy*. Cambridge University Press (2004)

[47] McDuff D., Salamon D.: *Introduction to Symplectic Topology*. Second Edition. Oxford University Press (1998)

[48] Meyer K. R., Hall G. R., Offin D.: *Introduction to Hamiltonian Dynamical Systems and the N-Body Problem*. Second Edition. Springer (2009)

[49] Michalodimitrakis M.: *Hill's Problem: Families of Three-Dimensional Periodic Orbits (Part I)*. Astrophys. Space Sci. **68**, 253–268 (1980)

[50] Milnor. J.: *Morse Theory*. Princeton University Press (1963)

[51] Moser. J.: *Regularization of kepler's problem and the averaging method on a manifold*. Comm. Pure Appl. Math. **23**(4), 609–636 (1970)

[52] Neugebauer O.: *A History of Ancient Mathematical Astronomy*. Springer-Verlag Berlin Heidelberg (1975)

[53] Schultz L.: *Planetologie: eine Einführung*. Birkhäuser (1993)

[54] Smart. W. M.: *Textbook on Spherical Astronomy*. Cambridge University Press (1977)

[55] Swerdlow N. M., Neugebauer O.: *Mathematical Astronomy in Copernicus's De Revolutionibus*. Springer-Verlag (1984)

[56] Szebehely V.: *Theory of Orbits - The Restricted Problem of Three Bodies*. Academic Press, New York (1967)

[57] Toomer. G. J.: *Ptolemy's Almagest. Translated and annotated by G. J. Toomer*. Duckworth (1984)

[58] Weyl H.: *Symmetry*. Princeton University Press (1952)

[59] Wilson. C.: *The Hill-Brown Theory of the Moon's Motion - Its Coming-to-be and Short-lived Ascendancy (1877-1984)*. Springer (2010)

[60] Wonenburger M.: *Transformations which are products of two involutions.* J. Math. Mech. **16**, 327–338 (1966)

[61] Zhou B.: *Iteration formulae for brake orbit and index inequalities for real pseudoholomorphic curves.* J. Fixed Point Theory Appl. **24**(15), 1–30 (2022)